HARD PROTECTIVE COATINGS

ON

MAGNETIC RECORDING HEADS

BY

MARTIN Y.M. NG

A THESIS SUBMITTED FOR THE DEGREE
OF MASTER OF PHILOSOPHY IN PHYSICS

THE HONG KONG POLYTECHNIC UNIVERSITY

SEPTEMBER 1997

This thesis is dedicated to my dear shepherd, Jesus Christ,

my dear parents, my family and all my friends.

Acknowledgments

I am grateful to be offered as Teaching Company Associate on a scheme operated by The Hong Kong Polytechnic University in collaboration with SAE Magnetics (H.K) Ltd.

I would first like to acknowledge Dr. C.W.Ong, my chief supervisor in university, for his close supervision and fruitful discussions within appointment period. I express gratitude to Prof. X.-A. Zhao for his enlightening suggestions and recommendation in my scientific research life.

I would like to extend my special thanks to Dr. Mike Wu and Dr. Mike Chan (SAE magnetics Ltd.) for understanding the advanced magnetic recording heads. Finally, I wish to thank Dr. R. W. M. Kwok (C.U.H.K.) for his assistance in XPS analyses, Mr. K.F. Chan for his assistance in some hard coating deposition and all staff of our department for their technical support.

Abstract

Recently, carbon nitride (CN_x) has already emerged as a new material of both fundamental and application interest. In particular application of protective coatings on magnetic recording heads, CN_x has potential to replace diamondlike carbon (DLC) which has been widely employed. In this study, the nitrogen content dependence of the structure and the mechanical properties of ion beam deposited CN_x films was investigated. Results showed that when the nitrogen content increased from 0 to 22.8 at.%, a diamondlike-to-polymeric transition in the film structure occurred. Related to this structural change, a film with a higher N content has lower electrical conductivity, lower hardness, lower damage threshold in a scratch test, weaker adhesion to the silicon substrate, and may have higher toughness or ductility as consequences. By controlling the level of N incorporation, the electrical conductivity of the film could lie in a suitable range to prevent from failure in reading signals or dielectric bread down. The hardness of the film can also be adjusted within the range of 24.3 - 11.7 GPa to suit various requirements for surface protective of devices. Furthermore, CN_x films with higher N content are less brittle, consequently suppress the formation of debris, and prolong the lifetime of the head. The friction of all the CN_x films is as low as that of the hydrogenated diamondlike carbon (DLC) films. Low friction favors the reduction of stiction, which is the resistance against the rotation of the hard disk when it is just powered and in contact with the head.

In addition, the mechanical properties of hydrogenated DLC films prepared by electron cyclotron resonance deposition and direct-ion-beam deposition were measured by the nanoindenter, which are currently used as protective coatings of magnetic devices. Moreover, the hardness of various kinds of films, expected to have great potential as protective coatings, were measured. They include CN_x/TiN multilayers, cubic boron nitride (c-BN), boron-silicon-nitrogen (B-Si-N), boron-carbon-nitrogen (B-C-N) and boron-carbon-nitrogen-oxygen films (B-C-N-O).

Table of Contents

List of Tables

List of Figures

1. Introduction

1.1 Protective overcoat on recording head

Protective overcoats on recording head sliders and hard-disks of computer disk drives are essential for increasing their durability and reliability. This is because the head and disk would slide against each other when the drive starts and stops. Even the air bearing has been set up to lift the head slider during operation, the two parts may collide occasionally. Collisions becomes more frequent as the effective magnetic spacing (ems) is further reduced in order to achieve increasing higher recording storage density in magnetic drives [1,2]. In general, the ems includes flying height of the head slider from the disk ($\approx$ 50 nm) and thickness of the overcoats on the slider and the disk ($\approx$ 20 nm) [3].

Nowadays, diamondlike carbon (DLC) has been widely employed as hard surface coatings on magnetic recording heads and disks. However, new overcoat materials with superior mechanical properties are desired for reducing the wear of the two parts. New overcoats materials should have adjustable hardness for adopting various head slider and disk materials with different mechanical properties, higher wear resistance, lower friction coefficient to reduce the stiction, appropriate electrical insulation to insulate the head and disk, have great chemical inertia to prevent the corrosion of the parts.

1.2 History of carbon nitride

Extensive studies have been carried out in recent years, tempting to synthesize a hypothetical β-phase carbon nitride (β-C_3N_4) which is predicted to have mechanical properties as good as those of diamond [4]. Therefore carbon nitride (CN_x) films are expected to have great potential to replace hydrogenated DLC for surface protection of magnetic recording devices. Though for most of the samples obtained to date, the N content and the hardness observed are below the predicted values for the β-C_3N_4 [5-16], however, CN_x has already emerged as a new material of both fundamental and application interest [17-19].

One problem of particular interest is to know how the structure and the mechanical properties of CN_x films depend on the N content such that their properties can be adjusted to suit various requirements of the disk drives. Nevertheless, in many reports, more than one preparation parameters other than the N content were varied [20-22], so that the net influences coming from the change in the N content are not readily to be separated. Furthermore, as reported by different authors, the hardness of CN_x films could be basically unchanged [23], or be reduced [24] when the N content increases, or could have a maximum value for the N content at around 25 at.% [25], so that no consensus has been reached at this moment.

1.3 Objectives

The purpose of this study is to find out the relationship between the N content, the structure and the mechanical properties of ion beam deposited CN_x films. The N content in films was controlled by adjusting the relative N_2^+ flux in assist beam, with the intention of keeping all other preparation parameters unchanged. X-ray photoelectron spectroscopy (XPS) and Fourier transform infrared absorption (FTIR) were employed to examine the film composition and structure. Nanoindentation and nanoscratch tests were carried out to determine the hardness, elastic modulus, friction coefficient and damage threshold of the films. Micrographs of the scratch tracks obtained using a scanning electron microscope (SEM) were studied to investigate the damage mechanisms in the scratch tests. In addition, thermal stability of the films was observed.

To compare current coating materials on heads, the investigation includes the mechanical properties of hydrogenated DLC films prepared by electron cyclotron resonance deposition (ECR) and direct-ion-beam deposition (DBD), provided by the SAE magnetics (H.K.) Ltd. (the Teaching Company Scheme partner) as functions of preparation parameters including the flow rate of operation gas (CH_4), the substrate bias voltage for ECR, and the ion beam voltage for DBD. Moreover, various hard-coating materials will be considered as protective overcoats on recording heads and some data of the mechanical properties of the materials such as CN_x/TiN multilayers, cubic boron nitride (c-BN), boron-silicon-nitrogen (B-Si-N), boron-carbon-nitrogen (B-C-N) and boron-carbon-nitrogen-oxygen films (B-C-N-O) are also discussed.

2. Sample Preparation

Three different systems were used for sample preparation. A three-ion-gun system at The Hong Kong Polytechnic University (HKPU) was used to prepare diamondlike carbon (DLC), carbon nitrate (CN_x), CN_x/TiN multilayers, cubic boron nitride (c-BN), boron-silicon-nitrogen (B-Si-N), boron-carbon-nitrogen (B-C-N) and boron-carbon-nitrogen-oxygen films (B-C-N-O). An electron cyclotron resonance (ECR) system and a direct-ion-beam deposition (DBD) system at SAE magnetics (H.K) Ltd. (the Teaching Company Scheme partner) were used to synthesize DLC films. DLC films prepared at SAE are being used as protective overcoats on magnetic recording heads in the production of SAE. The features of these systems conditions of the films are described as follow.

2.1 Preparation systems

Three-ion-gun system at the HKPU

The three-ion-gun system at the HKPU is shown in Fig 2.1, which contains two 3cm-filament-type Kaufman guns (Ion Tech. 3-1500-100), denoted as Gun *A* and *B*, and a 3cm-RF-actived Kaufman gun (Ion Tech. 3-1200-100) labeled as Gun *C*. Gun *A* was flange mounted for sputtering the target *I* or *II*. The targets are mounted on the two opposite faces of a motor driven target holder, so they can be sputtering alternatively. Gun *B* and *C*, one internally mounted and one fixed on the top plate of the chamber, were used to assist the deposition with incident angles of 16° and 60° to the substrate normal respectively. Ar gas was admitted into Gun *A*

for generating an Ar^+ ion beam, while mixture of Ar and N_2 gases were admitted into Gun *B* or Gun *C* to produce an Ar^+/N_2^+ ion beam.

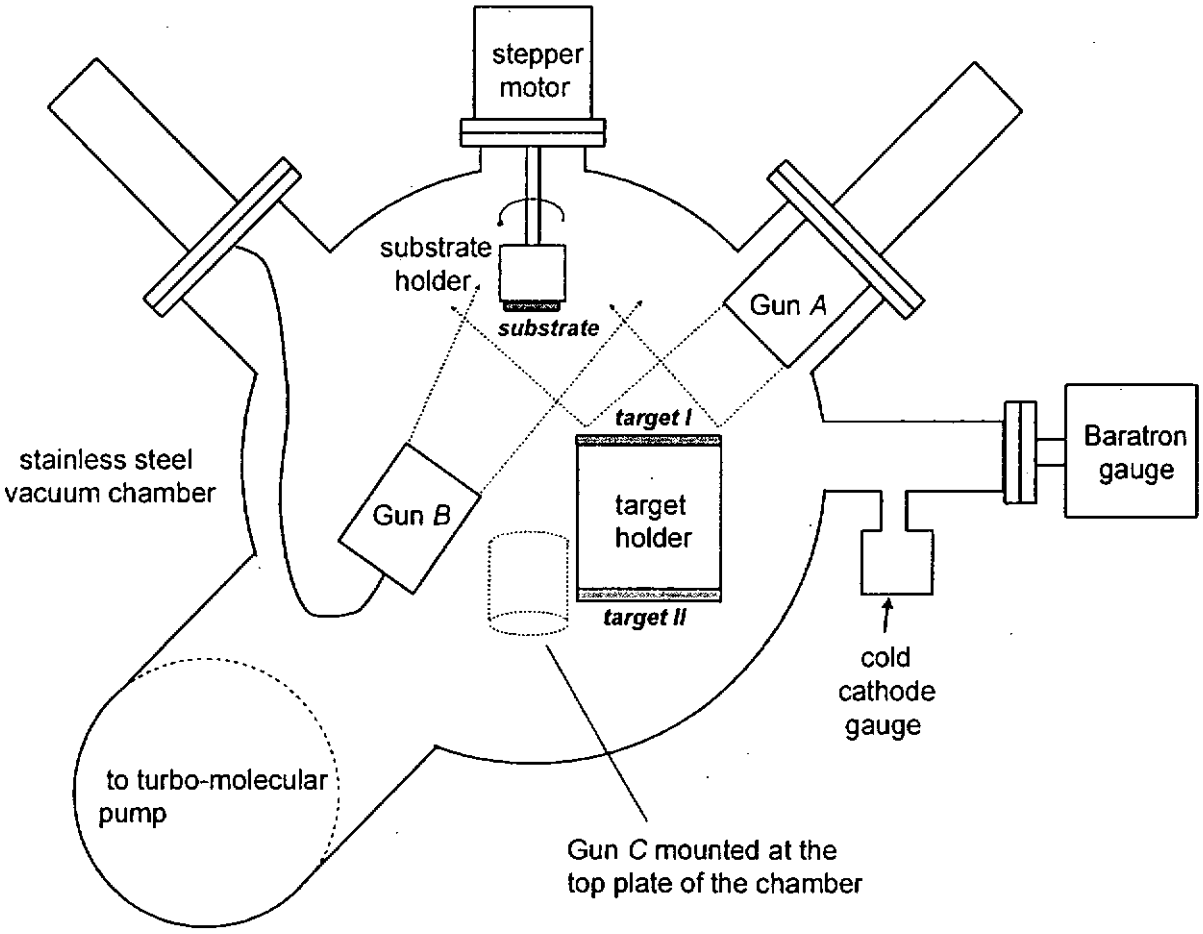

Figure 2.1 Three-dual-ion-gun deposition system at HKPU

The system was first evacuated to a background pressure $\leq 2 \times 10^{-6}$ Torr by a turbo molecular pump (KYKY, FB1500, 1500 l/s) equipped with an oil rotary pump (15 l/s) before pre-cleaning and deposition. The operation gases were fed into the ion guns, with their flow rates being controlled steadily by using the mass flow controllers (MKS Model 1259). The pressure in the stainless steel chamber was

monitored by a capacitance pressure transducer (MKS, 122A) in the range of 20 - 1 $\times 10^{-3}$ Torr and a cold cathode gauge tube (HPS, 941) in the high vacuum range.

Before deposition, Gun *B* or *C*, was first powered to produce an ion beam for pre-cleaning. To start deposition, Gun *A* was energized to produce an Ar^+ ion beam (typically 1200 eV and 50 to 70 mA) to sputter a target (100 mm in diameter) or to sputter two targets alternatively for preparing multilayered structures.

P-type (100) silicon wafers (25 mm × 16 mm) and fused quartz plates (25 mm × 7 mm) were used as substrates, and were mounted on a holder rotated with a rate of 2.7 rpm to ensure uniform film thickness. The substrate holder was heated by a resistive heater which can rise the substrate temperature (T_s) in the range from room temperature to 700°C.

Compared with other deposition methods, dual-ion-beam deposition is flexible in controlling the assist beam and current independently. Since the discharge region is confined within the ion gun body, the substrate would not be exposed to the radiation of the plasma. The assist beam energy can be risen to rather high values without danger of producing uncontrollable discharge. Furthermore, the operation pressure in the chamber is low ($\leq 10^{-4}$ Torr), such that contamination from the ambient residue is reduced. In addition, the assist gun can be used to pre-clean the substrate so as to improve the film adhesion.

ECR system at SAE magnetics (H.K) Ltd.

In electron cyclotron resonance (ECR) system, microwave with frequency of 2.45 GHz was generated and directed through a dielectric quartz window into a discharge chamber. In the discharge chamber, a magnetic field **B** is produced by an external solenoid (Fig 2.2). For preparing DLC films, methane (CH_4) was admitted to the chamber. Electrons oscillated with the frequency of the microwave and collided with the reactant gas molecules, such that the molecules were dissociated and a plasma was generated. The plasma was further confined by the **B** field. By applying a negative DC voltage bias, the ions were extracted from the plasma and accelerated towards the substrate. As a consequence, a DLC coating was then deposited. The typical growth rate of DLC films is about 14 nm min^{-1}. In general, the DLC films contain hydrogen. As the system was designed for mass production, it can accommodate a wafer with diameter of 6 inches.

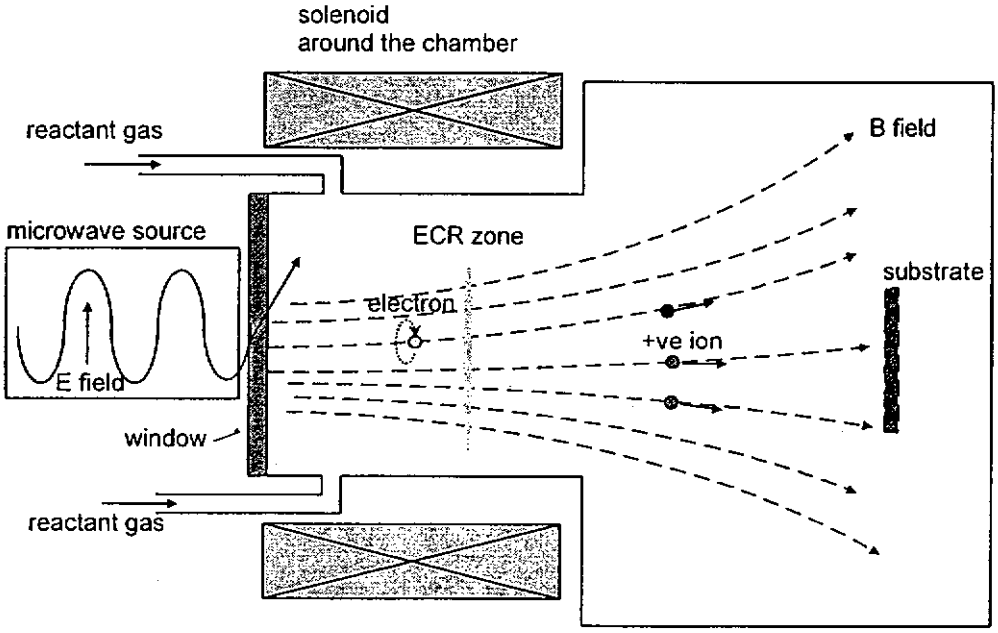

Figure 2.2 Schematic diagram of the electron cyclotron resonance system

DBD system at SAE magnetics (H.K) Ltd.

In the direct-ion-beam deposition (DBD) system, the DLC overcoats were fabricated on Si wafers 6 inches in diameter. After the chamber was pumped down to high vacuum, CH_4 ($\approx$ 60 sccm) was fed into the ion source and used as carbon source. The CH_4 molecules was ionized by a hot filament, the ionized species were extracted and accelerated to have beam energies varying in the range of 200 to 350 eV, and an ion current of about 360 mA. A hot filament neutralizer was mounted at the exit of the gun to neutralize the ion beam. In general, DLC films produced by this method contain certain amount of hydrogen.

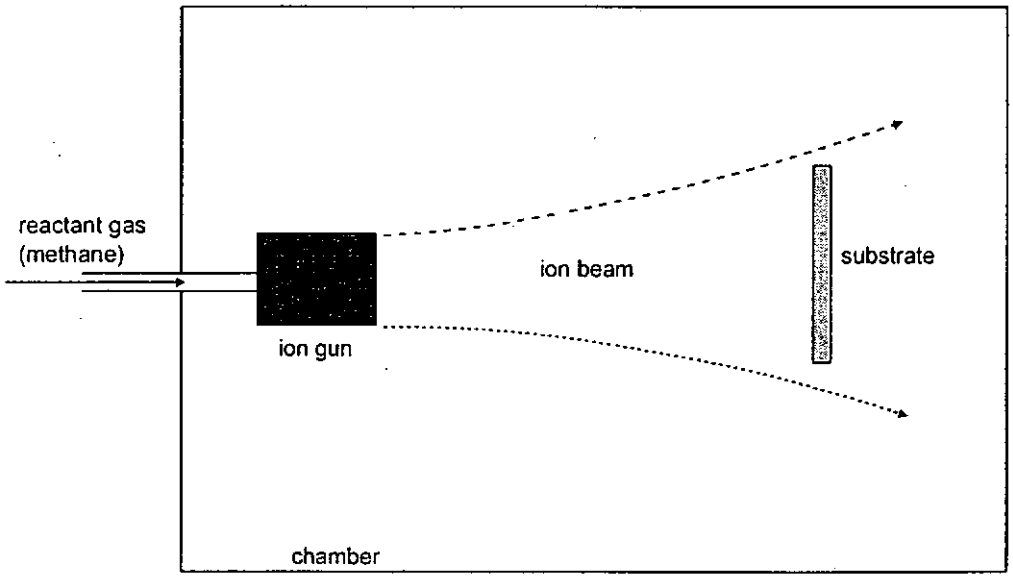

Figure 2.3 Schematic diagram of direct-ion-beam deposition

2.2 Description of the samples

Series of DLC films, CN_x films, CN_x/TiN multilayers, cubic boron nitride (c-BN), boron-silicon-nitrogen (B-Si-N), boron-carbon-nitrogen (B-C-N) and boron-carbon-nitrogen-oxygen films (B-C-N-O) were deposited using the systems. Studies in the DLC and CN_x films are particularly emphasized. The preparation conditions of the films were tabulated in Table 2.1 and 2.2 for the sake of clarity.

DLC and CN_x films

DLC and CN_x films (Table 2.1a) were grown by the three-ion-gun system. The base pressure was $\approx 2 \times 10^{-6}$ Torr. Gun *B* was first powered to pre-clean the substrate with an Ar^+ beam (600 eV and 54 mA) for 5 min. To start deposition, Gun *A* was energized to sputter a graphite target (purity $\geq$ 99.995%) with an Ar^+ ion beam (1200 eV and 70 mA) for the growing 120 min. For preparing DLC films, an Ar^+ beam with 160 eV and 20 mA was generated by Gun *B* to bombard film surface. A DLC film without Ar^+ assist was also prepared as reference. For preparing CN_x films, an Ar^+/N_2^+ assist beam (160 eV and 20 mA) was used instead. To generate the Ar^+/N_2^+ beam, a mixture of Ar and N_2 gases was admitted into Gun *B*. The total flow rate ([Ar]+[N_2]) was fixed at 33.5 sccm, such that the ambient pressure in the chamber was maintained at 8×10^{-5} Torr, while the fractional flow rate N_2, denoted by [N_2]/([Ar]+[N_2]), was adjusted from 0 to 1, such that the relative N_2^+ flux in the assist beam was varied from 0 to 100%. It is noted that the low assist beam energy of 160 eV was used in order to minimize the resputtering of the

deposits, and the low assist beam current of 20 mA was used for low level N injection. Another separated series of CNx were also prepared with the assist beam energy and current being varied as parameters, where a $[N_2]/([Ar]+[N_2])$ gas ratio was kept constant at 0.09 (Table 2.1b).

Sample :	**N_2 flow rate (sccm)**	**Ar flow rate (sccm)**	**$[N_2]/([Ar]+[N_2])$**
CN_x102	0	33.5	0
CN_x109	3	30.5	0.09
CN_x110	6	27.5	0.18
CN_x111	9	24.5	0.27
CN_x105	18	15.5	0.54
CN_x108	27	6.5	0.81
CN_x106	30	3.5	0.90
CN_x103	33.5	0	1.00
CN_x112	No ion assist		

Table 2.1a Preparation conditions of CN_x and pure carbon films deposited at various $[N_2]/([Ar]+[N_2])$ in the assist beam. Assist beam energy and current = 160 eV and 20 mA.

Sample :	**Beam Energy (eV)**	**Beam current (mA)**
CN_x113	300	20
CN_x114	90	20
CN_x115	90	10
CN_x116	160	35

Table 2.1b Preparation conditions of CN_x films deposited at assist beam energy and current. gun. $[N_2]/([Ar]+[N_2]) = 0.09$

Other two series of DLC films were deposited on Si wafers by the ECR system and the direct ion beam system at the SAE Magnetics (H.K.) Ltd., with the preparation conditions summarized in table 2.2 a and b.

Sample code:	CH_4 flow (sccm)	negative bias voltage (eV)
SAE27 *(S16)*	40	150
SAE22 *(batch 9)*	40	300
SAE23 *(S7)*	40	450
SAE28 *(S10)*	40	550
SAE30 *(S12)*	80	150
SAE19 *(batch 8)*	80	300
SAE21 *(batch 9)*	80	450
SAE29 *(S9)*	80	550

Table 2.2a Preparation conditions of DLC films deposited using the ECR system

Sample code:	CH_4 flow (sccm)	Beam voltage (eV)	Beam current (mA)
SAE26 *(V8)*	60	200	360
SAE24 *(V3)*	60	250	300
SAE33 *(V4)*	60	350	300
SAE31 *(V2)*	60	350	360
SAE34 *(V11)*	60	400	300
SAE25 *(V18)*	70	200	360
SAE35 *(V22)*	80	200	360

Table 2.2b Preparation conditions of DLC films deposited using the DBD system

Other films synthesized using the three-ion-gun system (at HKPU)

A series of CN_x/TiN multilayers was prepared using the three-gun-system. A carbon (C) target and a titanium (Ti) target were mounted on two opposite faces of the motor driven target holder. They were sputtered alternatively by the Ar^+ beam from Gun *A*, with surface assist by an Ar^+/N_2^+ ion beam from Gun *C*.

A series of B-Si-N films was deposited at 620 °C. Boron (B) and silicon (Si) atoms were sputtered from a pure B disc (purity ≈ 99.9%) partially covered by a Si segment. The fraction of Si flux was controlled by varying the coverage of Si on the target surface. Each sample has two layers. A buffer layer was deposited first, with the assist beam energy set at a lower value. A top layer was then deposited with the assist beam energy and current set at 450 eV and 25 mA respectively. With low Si content, the top layer deposited contains high volume fraction of cubic boron nitride (c-BN) phase.

A series of B-C-N films was synthesized with the B target partially covered by a C segment. For the films deposited at room temperature, conspicuous amount oxygen was found in the films and thus the films was denoted as the B-C-N-O films. For the films deposited at high temperature, the O content is greatly reduced, and the films with low C content have high volume fraction of c-BN phase.

For each series of films, the preparation parameters of the three-ion-gun system were listed in Table 2.3.

Thin film sample	Deposition time	T_s	Target used	Sputtering beam (gun *A*)	Assist beam (Gun *B* or *C*)			Remark
					Gun used	$[N_2]/([Ar]+[N_2])$, fractional flow rate of N_2	Beam power	
CN_x/TiN multilayers	40 min. except single-layer CN_x = 160 min	room temp. except one of 4-layers at 250 °C	C and Ti targets were sputtered alternatively.	1200 V 50 mA Ar^+	*C*	0.50 or (N_2:Ar =1: 1)	200 eV, 36 mA	No. of layers deposited = 1, 4 and 10. The coating rates of the single-layer $CN_{0.3}$ and TiN = 0.2 and 0.09 nm s^{-1} respectively.
B-Si-N	120 min. (for the top-layer)	620 °C	pure boron disc partially covered by a Si segment with the coverage varying from 0 to 100 %	1200 eV 70 mA Ar^+	*B*	0.42 or N_2:Ar =1: 1.4 (total flow rate =33.5 sccm)	450 eV, 25 mA	A buffer layer was added to improve the adhesion of the top layer. To prepare the buffer layer, the assist beam energy was increased from 200 to 360 eV in three equal steps (10 min. each), with a fixed beam current = 20 mA.
B-C-N	120 min. (for the top-layer)	620 °C	pure boron disc partially covered by a C segment with the coverage varying from 0 to 46.2 %	1200 eV 70 mA Ar^+	*B*	0.42 or N_2:Ar =1: 1.4 (total flow rate =33.5 sccm)	450 eV, 25 mA	A buffer layer was added with the same conditions as those for B-Si-N films.
B-C-N-O	120 min.	room temp.	pure boron disc partially covered by a C segment with the coverage varying from 14 to 86 %	1200 eV 70 mA Ar^+	*B*	0.42 or N_2:Ar =1: 1.4 (total flow rate =33.5 sccm)	450 eV, 25 mA	No buffer layer was added.

Table 2.3 : A list of the films deposited by the three-ion-gun system (at HKPU)

3. Sample Characterization

In this chapter, the methods of characterizing the film structure, electrical, mechanical and tribological properties will be given. To characterize the film structure, the film thickness was measured by an alpha-step surface profiler, the crystallinity was examined by X-ray diffractometer, the composition and chemical structure between the elements determined were investigated using an X-ray photoelectron spectroscopy (XPS), the chemical bonds were examined using Fourier transform infrared absorption spectroscopy (FTIR) and Raman scattering spectroscopy.

To characterize the film properties, the electrical conductivity (σ) of the films was measured. The mechanical and tribological properties of the films, including the hardness (H), elastic modulus (E) , friction coefficient (μ) and damage threshold (DT), were evaluated using a nanoindenter. In addition, for studying the thermal stability of the films, the samples were annealed at different temperatures using rapid thermal annealing (RTA), and the changes of the electrical conductivity, mechanical and tribological properties were observed.

3.1. Structural and compositional Analyses

Thickness measurements by Alpha-step surface profiler

A Tencor 500 alpha-step surface profiler was used to measure the film thickness t. The vertical displacement of a diamond stylus scanning across film edge give a direct readout d. t is determined as (Fig. 3.1)

$$t = d + e$$

where e is the etching depth due to the substrate material being etched away by pre-cleaning process.

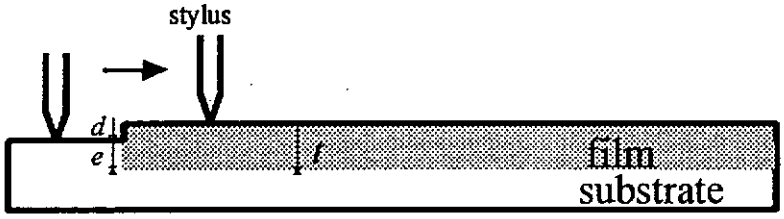

The stylus scan across the edge of the films

Figure 3.1 Thickness measurement process

FTIR Analyses

A Nicolet's, Magna-TR^{TM} system 750 was used to investigate the IR absorption spectra of the films, with wavenumber in the range of 400 to 4000 cm^{-1}. Each spectrum was obtained by averaging the data of 32 identical scans.

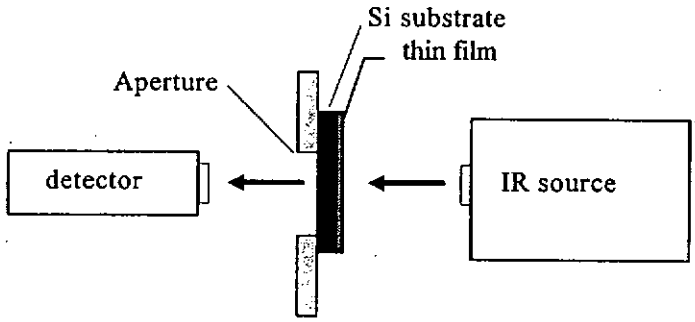

Figure 3.2 Schematic diagram of an IR absorption experiment

An absorption band occurs when the incident photon has an energy to excite a vibrational mode of a chemical bonds [26]. Furthermore, the relative intensities of the absorption bands can reflect the relative concentrations of the bonds [27].

For IR measurements, films on Si wafer were used. The background caused by the Si substrate (Fig.3.3) must therefore be subtracted so as to obtain the net absorption spectrum of the film .

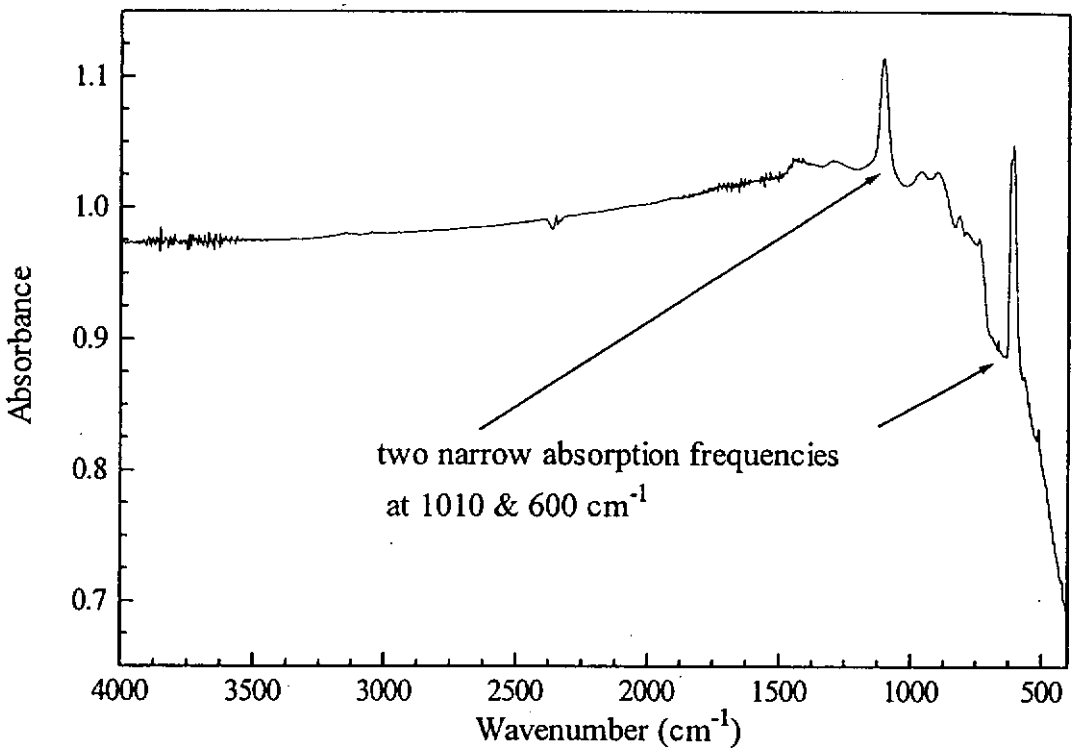

Fig. 3.3 IR absorption spectrum of Si substrate shows it is IR transparency.

XPS Analysis

An XPS (Kratos Analytical) with Mg Kα radiation with photon energy $h\nu$ of 1253.6 eV or Al K_α 1486.7eV was used to determine the relative composition of the elements in films. An incident x-ray photon with energy $h\nu$ knocks out an electron from the inner shell of an atom, e.g. the K shell, whereas the kinetic energy E_K of the emitted photoelectron was measured by an electron energy analyzer. The binding energy of the electron E_B can thus be determined by the relationship $E_B = h\nu - E_K - \phi_{SP}$ where ϕ_{SP} is the work function of the sample stage which has already determined by calibration procedures. Therefore, the elements in the film can be identified by the corresponding characteristic energies E_B.

Spectra of elements before and after surface cleaning by Ar^+ ions (4 keV,20mA) for 2 minutes were recorded. The clean process can reduce the surface contamination after deposition. The areas of the spectra of different elements above the Shirely background were used to determine the elemental composition of the film. As an example, the relative content F_x of an element x is $F_X = \frac{A_X/f_X}{\sum_i A_i/f_i}$, where the subscript i goes through all the elements contained in the film, A_i and f_i are the integration area of the spectrum and the corresponding sensitivity factor of the ith element. The sensitivity factors of the elements involved in this study are tabulated in Table 3.1.

f_C	f_N	f_O	f_B	f_{Si}	f_{Ti}
0.25	0.25	0.66	0.13	0.33	2.00

Table: 3.1 The XPS sensitivity factors of the elements

In addition, by investigating the shift of E_B, the chemical structures of the elements can be studied in more detail.

3.2 Electrical Conductivity (σ) measurements

The electrical conductivity (σ) of a film was determined by measuring the resistance of the film deposited on insulating substrates (glass slide or quartz). Two electrodes (silver paste) were made on top of the film with a separation of 5 mm.

3.3 Mechanical and tribological measurements

Nano-indentation

For measuring H and E, a nanoindenter (Nano Instruments Inc., Model IIs) was used in indentation mode. A 3-sided Berkovich diamond tip is driven into the thin film under the control of a computer, with a theoretical depth resolution of 0.04 nm and a load resolution of 50 nN, such that the displacement and load can be acquired simultaneously to obtain a set of load, and unload curves.

An indentation is made on the film surface such that the hardness H of the film is obtained as $H = P/A$, where P is the maximum load of the indentation, and A is the contact area between the tip and the film at the maximum load. A is function of the contact depth h_c, where h_c is determined from the stiffness S of the unload curve (Fig. 3.4) [29-32], and is equal to $h_c = h_{max} - 0.75\ L_{max}/S$. Next the reduced elastic modulus E_r is determined by the formula: $S = \frac{2}{\sqrt{\pi}} E_r \times \sqrt{A}$. E_r is given by:

$$E_r = \left[\frac{1 - \nu_s^2}{E_s} + \frac{1 - \nu_i^2}{E_i} \right]^{-1}$$ where ν_i and E_i are the Poisson's ratio and elastic modulus of the indenter, ν_s is the Poisson's ratio of the sample and is assumed to be 0.25. E_s, elastic modulus of the sample, can thus be determined accordingly.

In the experiments, an array of indents were made, with two consecutive indents separated 75 μm apart. Usually, ten identical indentations were made on

different positions on the surface of a film, and the data obtained are averaged to give representative values of H and E.

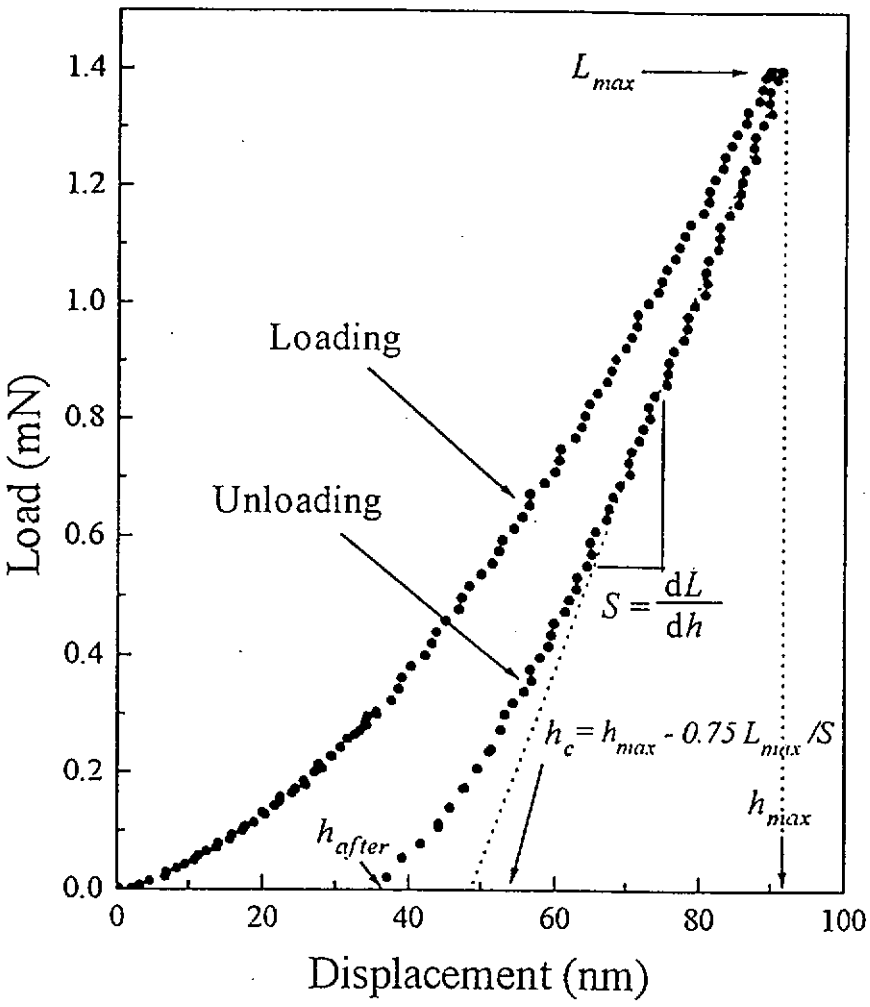

Fig. 3.4 A typical load (L) -displacement (h) curve,
where S is stiffness of the sample, h_{after} is the final depth of residual hardness impression, h_c is the contact depth and h_{max} is the displacement at the maximum load L_{max}.

The accuracy and reliability of the data of H and E rely considerably on the correct calibration of the load frame compliance and the tip area function $A(h_c)$ [29]. Both calibrations was carried out by ourselves. With these calibrations, if the films have thickness ≥ 100 nm, the values of H and E measured at indentation depths

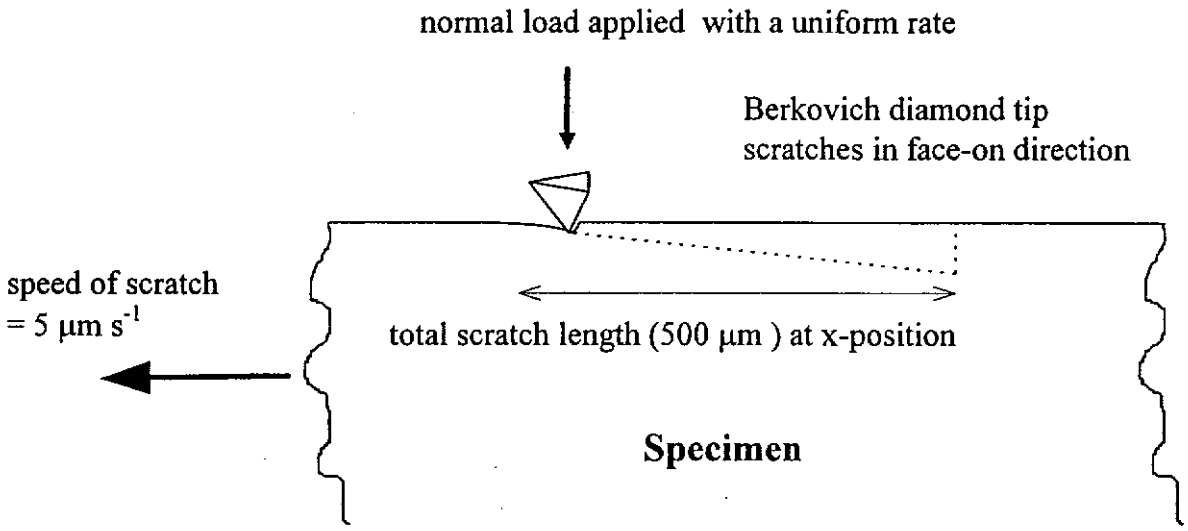

Figure 3.5 Schematic diagram of ramping-load scratch experiment

3.4 Thermal annealing

A rapid thermal annealing furnace was used to anneal the samples. To carry out the annealing process, the film was positioned in a graphite crucible placed inside a quartz tube 22 mm in diameter, which was then illuminated by six 1200 W tungsten lamp, such that the pre-set annealing temperature is reached within 20 seconds. Each annealing process lasted for 1 hour. Nitrogen was admitted into the quartz tube during annealing in order to protect the film from being oxidized.

4. Results and Discussions of CN_x Films

4.1 Thickness and coating rate

The thickness of dual-ion-beam deposited (DIBD) CN_x films on (100) Si wafers and quartz plates was determined to vary from 215 to 335 nm (after corrections of the etching of the substrates by the pre-cleaning process, i.e. 129 nm for quartz and 113 nm for Si), lying within a rather narrow range. The deposition rate of the films on both kinds of substrates was typically around 2 nm min^{-1} (Table 4.1). This value is much low compared with that of DLC films prepared by electron cyclotron resonance (14 nm min^{-1}) and direct-ion beam deposition (10 nm min^{-1}). However the lower deposition rate of DIBD CN_x films allows the films thickness to be controlled more accurately. Accurate control in thickness of the overcoats on magnetic recording devices is important, because their thickness is in the range as low as about 8 nm.

Sample :	fN_2 = $[N_2]/([Ar]+[N_2])$	N content (at.%)	Thickness (nm) on quartz	Thickness (nm) on Si	Coating rate (nm min^{-1}) on quartz	Coating rate (nm min^{-1}) on Si	T_s (°C)
CN_x112	No assist	0	241	249	2.01	2.08	92.9
CN_x102	0	≈0	249	238	2.08	1.98	119
CN_x109	0.09	7.6	218	216	1.82	1.80	121
CN_x110	0.18	12.0	231	215	1.93	1.79	121
CN_x111	0.27	13.3	241	235	2.01	1.96	122
CN_x105	0.54	16.8	265	265	2.21	2.21	121
CN_x108	0.81	20.3	289	325	2.41	2.71	126
CN_x106	0.90	21.4	301	313	2.51	2.61	122
CN_x103	1.00	22.8	286	264	2.38	2.20	122

Table 4.1 fN_2, N content, thickness, coating rate and T_s of the CN_x films. The assist beam energy and current was fixed at 160 eV and 20 mA.

4.2 Composition and structure of CN_x films

Film composition

The results before surface cleaning (Fig. 4.1a) show that when the fractional flow rate of nitrogen, $fN_2 = [N_2]/([Ar]+[N_2])$, admitted into gun *B* increases. The N content in the films rises and the C content drops. Concurrently, the O content rises gradually to about 10 at.%. After surface cleaning by an Ar^+ beam (4 keV, 20 mA) for three minutes, the O content is reduced to below 3 at.% (Fig. 4.1b), so the O atoms are mainly located near the film surface and do not influence the film properties. After removing the error due to the O content, the N content is found to vary from 0 to 22.8 at.% (Fig. 4.1b and Table 4.1).

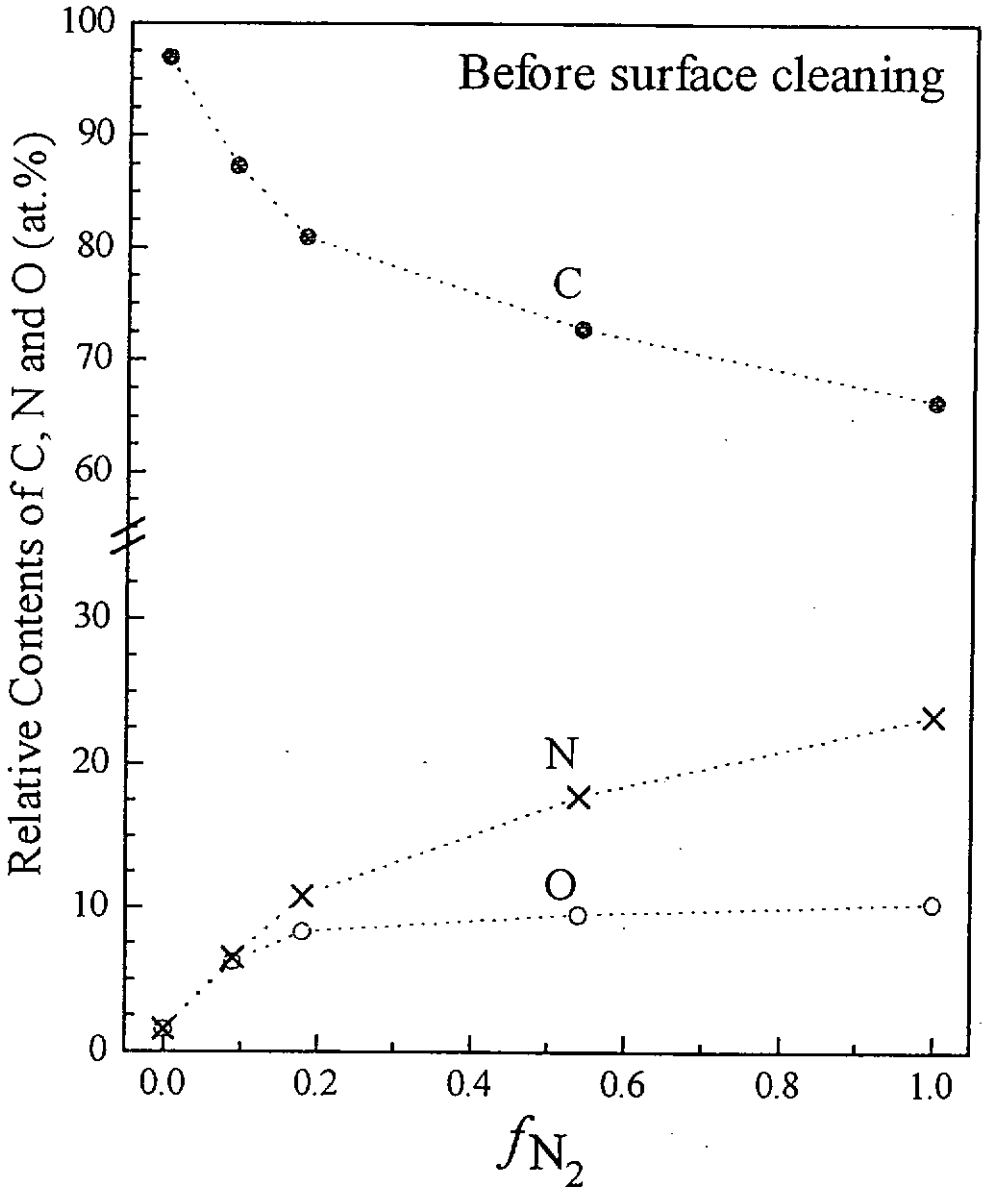

Fig. 4.1a The relative contents C, N and O as a function of f_{N_2} before surface cleaning

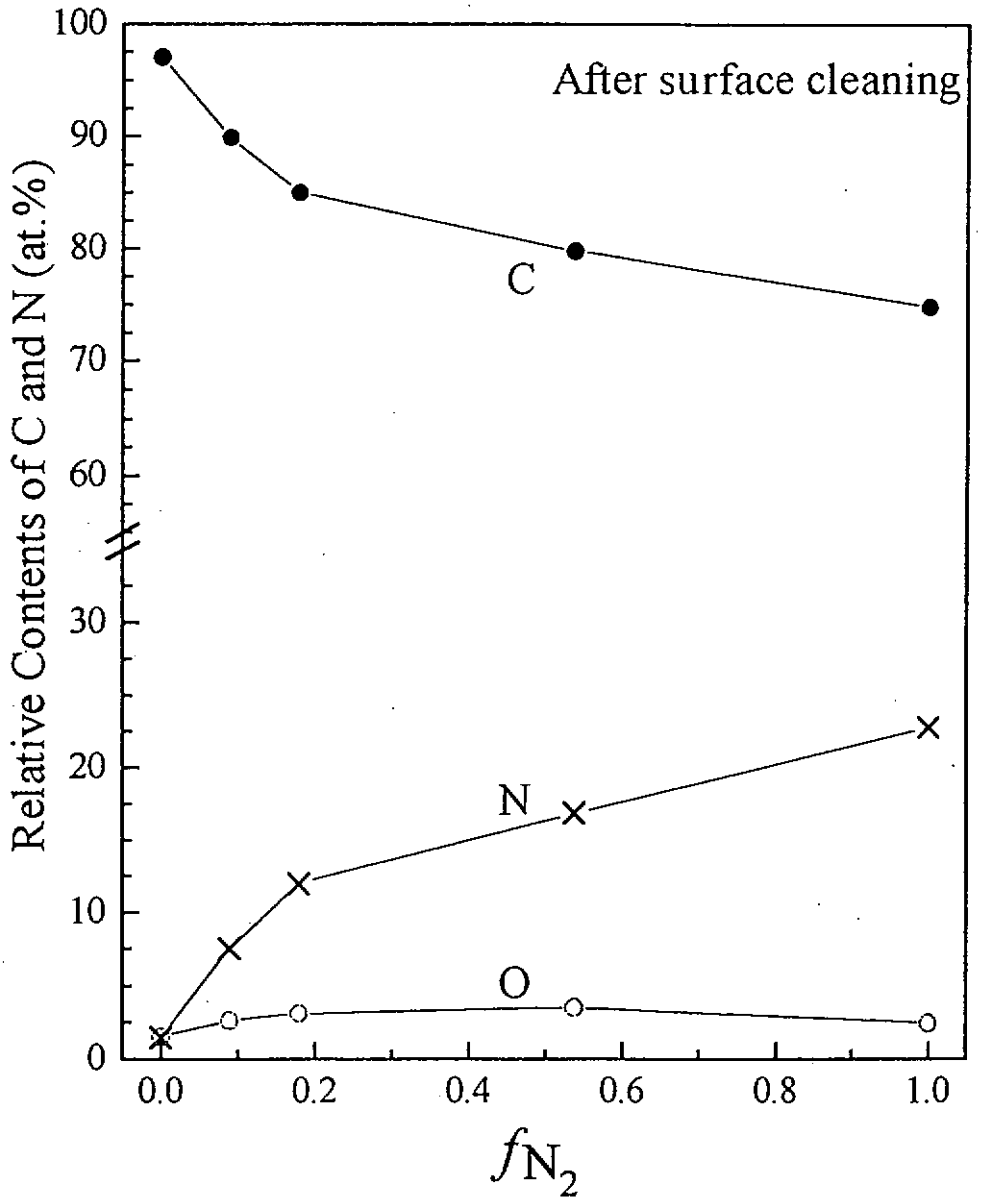

Fig. 4.1b. The relative contents C, N and O as a function of f_{N_2} after surface cleaning

Another series of CN_x films was prepared, with ion beam energy and current as parameters (Table 4.2). For this series, the fractional flow rate of nitrogen, fN_2= $[N_2]/([Ar]+[N_2])$, was maintained at 0.09. Less than 3 at. % of oxygen was detected after surface cleaning process and so does not influence the film properties. The N content of the films determined after surface cleaning process was shown in Table 4.2.

Sample :	Beam energy (eV)	Beam current (mA)	N content (at. %)
CN_x113	300	20	8.2
CN_x114	90	20	7.2
CN_x115	90	10	4.6
CN_x116	160	35	10.3

Table 4.2 The N content of the CN_x series deposited at fN_2 = 0.09, and different beam energies and currents.

Consider samples CN_x113 and CN_x114, both deposited at the same ion beam current of 20 mA. The former is deposited with a higher beam energy of 300 eV, more than 3 times of that of the latter (90 eV), but their N content are about the same, indicating that the beam energy can only have very little influence on the N content. However, for samples CN_x114 and CN_x115 deposited at the same ion beam energy (90 eV), the former was prepared at a beam current of 20 mA, and has a N content two times higher than that of CN_x113, which was prepared at a beam current of 10 mA. This result indicates that the magnitude of the ion beam current is rather significant in determining the N content in the film. This conclusion can be justified

further, by referring to the fact that sample CN_x116 deposited at a highest ion beam current, where a highest N content of 10.3 at.% is also detected.

Chemical structure

The XPS spectra of C 1*s* (Fig. 4.2a) and N 1*s* (Fig. 4.2b) were investigated in more detail to reveal the chemical structures of the elements in the films. The C 1*s* spectra were resolved into two (C^1 and C^2) components, and the N 1*s* spectra were resolved into two (N^2 and N^3) components. Each component is composed of 70 % Lorentzian and 30 % Gaussian constituents. The peak energies, widths and the relative fractions of the components obtained before surface cleaning are tabulated in Table 4.3 a, b and c, while those obtained after cleaning are tabulated in Table 4.4 a, b and c respectively.

Fig.4.2a and 4.2b show the spectrum of the C 1*s* electrons and the N 1*s* electrons for the CN_x films with various N content after surface cleaning process. In the figures, the data point after subtracting the background are represented by the dots. The dot lines represent the resolved components. Finally, the solid lines are the sum of the resolved components. A little correction was made to shift the spectra by smaller values within ± 0.4eV, so as to adjust the peak energy of the C^1 component to be 284.6 eV. The C^1 component is assumed to have peak energy at 284.6 eV, and thus is ascribed to the C 1s electrons from the C atoms in the graphite structure [36]. The C^2 component has higher peak energy at 285.8 eV (Table 4.3 and 4.4), possibly because the related C atoms are associated with some N [7,34-

37]. It is because a N atom is more electronegative than a C atom, so a N atom near a C atom would cause the electron distribution to shift from C atom towards the N atom, resulting in a higher binding energy of the C 1*s* electrons.

The C^2 and N^2 components are assumed to be related to the structure of pyridine (C_5H_5N), in which the C and N atoms are located at sp^2 sites of a six-membered rind. The energies of the C 1s and N 1s electrons in a pyridine molecules are 28.5 and 398.8 eV respectively [38-40], and are close those of the C^2 and N^2 components. In addition, it is believe that the film structure become more polymerlike when more N atoms are incorporated into the films. As a consequence, the C2 component may contain contribution from the C 1s electrons associated with the C≡N bonds, which is found to have a C 1s peak 284.5 eV [41].

A N3 component with peak energies around 399.9 eV was observed, which may be associated with the N 1s electrons from the N=N structure analogous to that in a PhN=PhN molecule was found to have N 1s electrons with a peak energy in the range of 399.6 - 400.1 eV [40,42].

The possible formation of the N-related structures, including the pyridinelike rings, C≡N and N=N bonds as suggested by the XPS results, may give rise to the polymerization of the structure of the CNx films. This structural change explains the results of others some experiments described in the following sections, showing that CNx films with higher N contents are more insulating, transparent and softer.

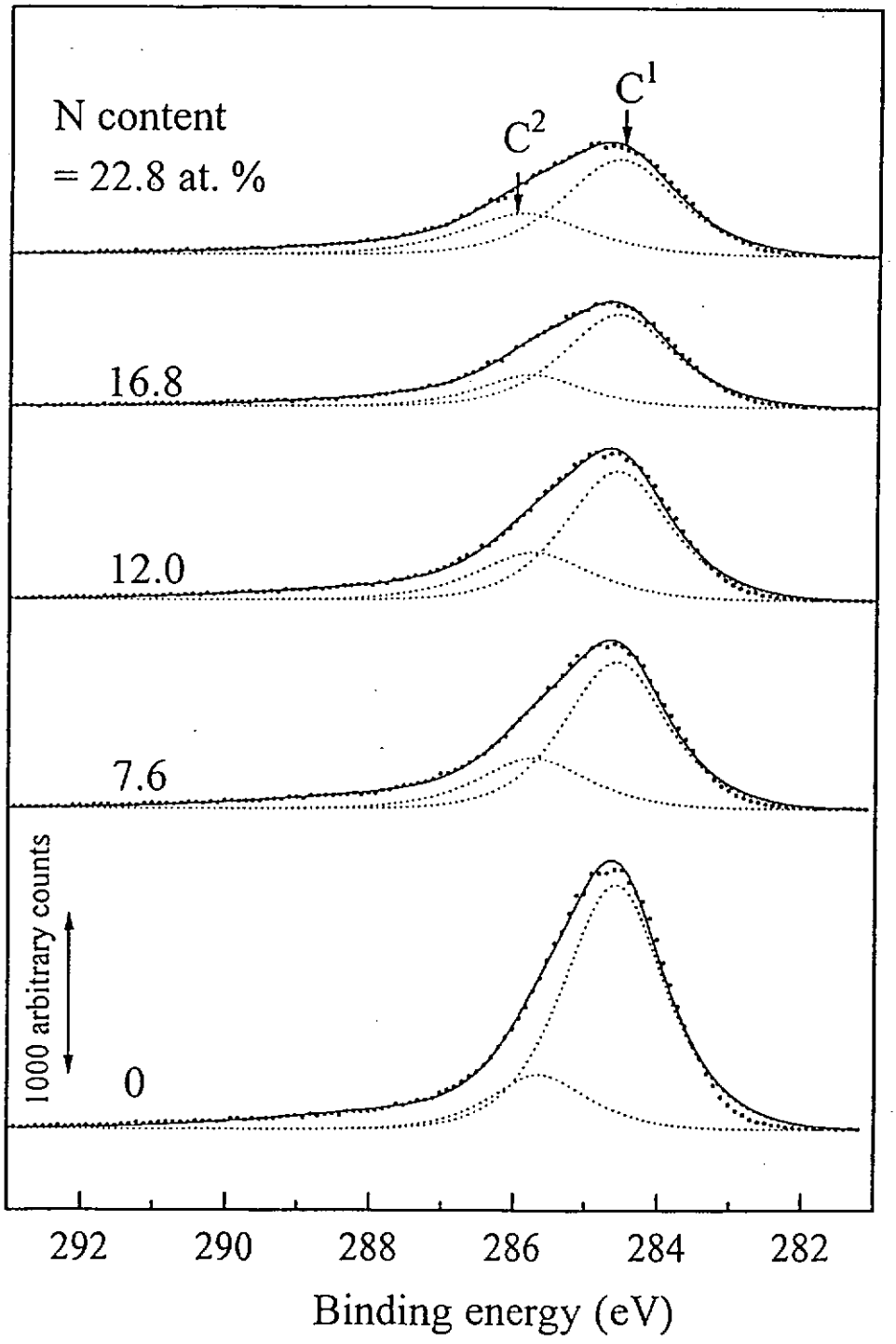

Fig. 4.2a XPS spectra of C 1*s* electrons for the CN_x films with various N content after surface cleaning.

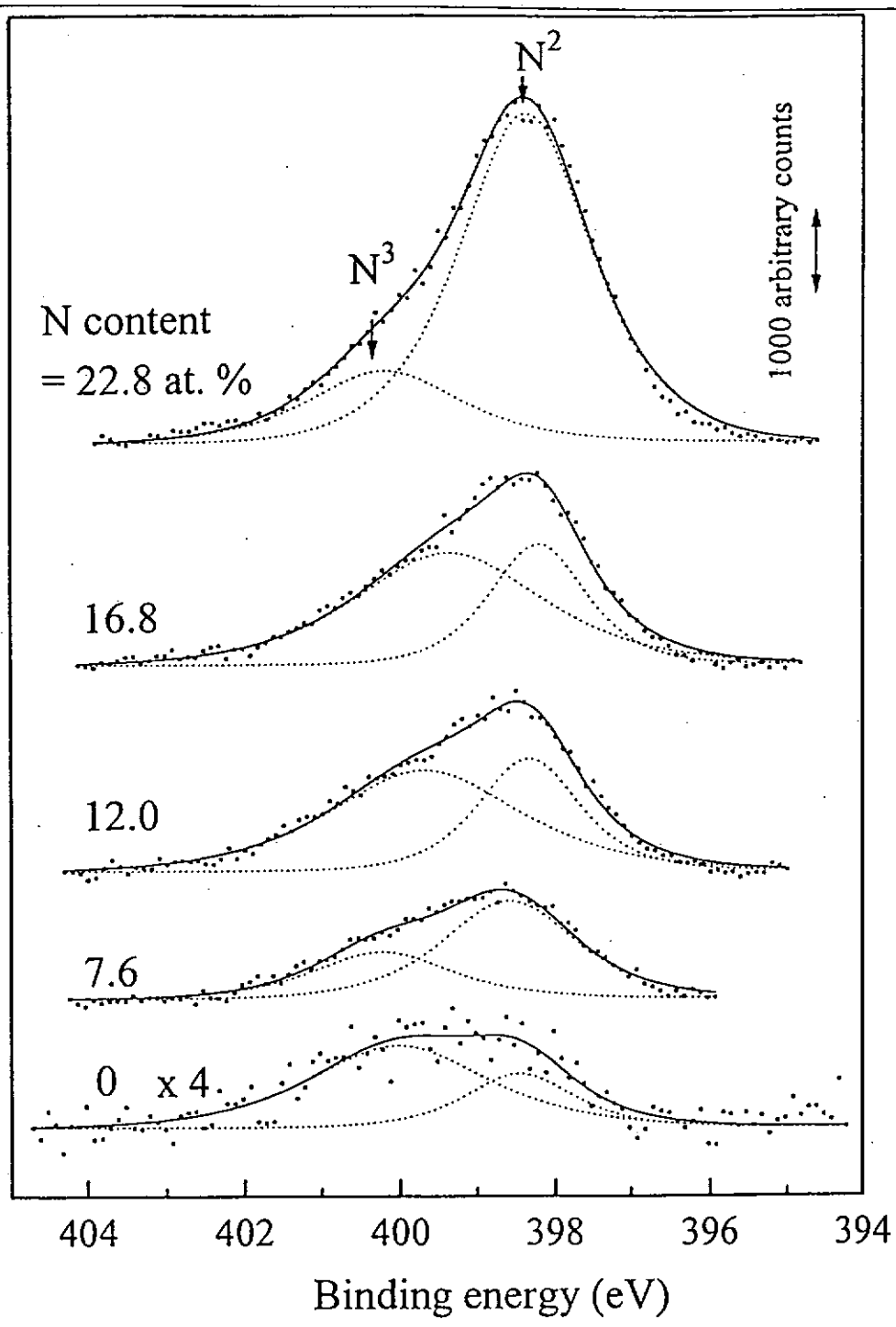

Fig. 4.2b XPS spectra of N 1*s* electrons for the CN_x films with various N content after surface cleaning.

Sample no.	N content (at. %)	C^1 (eV)	C^2 (eV)	N^2 (eV)	N^3 (eV)	O (eV)
CN_x102	0	284.60	285.56	400.63	398.89	532.20
CN_x109	7.6	284.60	285.89	400.44	398.55	531.67
CN_x110	12.0	284.60	286.00	400.43	398.48	531.69
CN_x105	16.8	284.60	285.69	399.95	398.34	531.58
CN_x103	22.8	284.60	285.93	399.28	398.15	531.61

Table 4.3a The peak energies of the components of the C 1*s* and N 1*s* spectra obtained before surface cleaning

Sample no.	N content (at. %)	C^1 (eV)	C^2 (eV)	N^2 (eV)	N^3 (eV)	O (eV)
CN_x102	0	1.57	1.63	2.00	2.47	3.22
CN_x109	7.6	1.68	1.84	2.22	2.01	2.36
CN_x110	12.0	1.70	1.73	2.45	1.97	2.46
CN_x105	16.8	1.65	1.85	3.03	1.71	2.51
CN_x103	22.8	1.73	1.57	2.90	1.34	2.62

Table 4.3b The widths of the components of the C 1*s* and N 1*s* spectra obtained before surface cleaning

Sample no.	N content (at. %)	C^1 (at.%)	C^2 (at.%)	C (at.%)	N^2 (at.%)	N^3 (at.%)	N (at.%)	O (at.%)
CN_x102	0	73.0	24.0	97.0	0.5	1.1	1.5	1.5
CN_x109	7.6	71.9	15.4	87.3	3.6	2.9	6.5	6.2
CN_x110	12.0	66.6	14.4	81.0	4.4	6.4	10.8	8.3
CN_x105	16.8	53.1	19.6	72.7	9.1	8.7	17.8	9.5
CN_x103	22.8	49.6	16.8	66.4	16.9	6.5	23.4	10.3

Table 4.3c The relative fractions of the components of the C 1*s* and N 1*s* spectra obtained before surface cleaning

Sample no.	N content (at. %)	C^1 (eV)	C^2 (eV)	N^2 (eV)	N^3 (eV)	O (eV)
CN_x102	0	284.60	285.62	400.02	398.46	532.15
CN_x109	7.6	284.60	285.74	400.23	398.59	531.80
CN_x110	12.0	284.60	285.75	399.68	398.33	531.88
CN_x105	16.8	284.60	285.80	399.37	398.21	531.75
CN_x103	22.8	284.60	285.91	400.19	398.37	531.58

Table 4.4a The peak energies of the components of the C 1*s* and N 1*s* spectra obtained after surface cleaning

Sample no.	N content (at. %)	C^1 (eV)	C^2 (eV)	N^2 (eV)	N^3 (eV)	O (eV)
CN_x102	0	1.68	1.59	2.71	1.64	3.22
CN_x109	7.6	1.65	1.79	2.07	2.01	3.18
CN_x110	12.0	1.71	1.89	2.87	1.54	3.25
CN_x105	16.8	1.77	1.69	2.82	1.46	3.36
CN_x103	22.8	1.87	2.06	2.28	2.00	3.01

Table 4.4b The widths of the components of the C 1*s* and N 1*s* spectra obtained after surface cleaning

Sample no.	N content (at. %)	C^1 (at.%)	C^2 (at.%)	C (at.%)	N^2 (at.%)	N^3 (at.%)	N (at.%)	O (at.%)
CN_x102	0	79.7	17.4	97.1	1.0	0.4	1.4	1.5
CN_x109	7.6	65.5	24.3	89.8	2.5	5.1	7.6	2.6
CN_x110	12.0	60.1	24.9	85.0	7.5	4.5	12.0	3.0
CN_x105	16.8	59.9	19.8	79.7	10.8	6.0	16.8	3.5
CN_x103	22.8	50.5	24.2	74.7	4.5	18.3	22.8	2.5

Table 4.4c The relative fractions of the components of the C 1*s* and N 1*s* spectra obtained after surface cleaning

	C^1	C^2	N^2	N^3
Peak energies (eV)	284.6	285.8	398.4	399.9
Explanation	graphite structure and C≡N structure [43]	C≡N structure [41] and sp^2 structure [39]	sp^2 structure [42]	N=N structure [40]

Table 4.5 Summary in our results of peak energies of the components of C 1*s* and N 1*s* spectra.

FTIR spectra

For the pure carbon films (deposited with and without Ar^+ assist), three absorption bands I, II and III, with maximum absorption at ≈ 1560, 1300 and 700 cm^{-1} respectively, are observed in Fig. 4.4. Bands I and III are attributed to the vibrational modes of large graphitic domains constructed of sp^2 bonds (1555 - 1575 cm^{-1} and 706 cm^{-1}) [14,15]. Band I also corresponds to the Raman G of amorphous carbon (for graphitelike sp^2) at 1550 cm^{-1} [14,15,44]. Band II can be assigned to the smaller sp^2 domains (1360 cm^{-1}), which position is consistent with that of the Raman D peak of amorphous carbon (for disordered sp^2) at 1360 cm^{-1} [45]. Furthermore, the overall transmittance of the carbon film deposited without surface assist is much higher than that of the carbon film with ion assist. To explain this result, one refer to table 4.1. The temperature detected on the substrate T_s during the deposition of the carbon film deposited without ion assist (CN_x112) is 92.9 °C, but that with ion assist (CN_x102) is higher (119 °C). Since it has been shown that higher temperature environment would enhance the formation of graphitic structure [46] so one effect of using ion assist in preparing carbon film is to rise T_s, and thus the sp^2 fraction is increased. Accordingly, the IR transparency of the film is reduced as a result. Another possible explanation is that the ion bombardment could preferentially sputter removal the sp^3 carbon leaving a graphite rich network.

When the N is incorporated, the following features are observed. First, the intensities of bands I, II and III increase, possibly because the incorporated N atoms

could replace some C atoms from the aromatic rings, such that the ring symmetry is broken and the vibrational modes become IR active [14] . Second, the growth of bands I could be related to the formation of more C=N bonds which are found to have IR absorption band at 1530 cm^{-1} (Table 4.6 [46]). Third, a band IV and a band V grow, with maximum absorption at 2100 and 2000 cm^{-1} respectively. Similar absorption bands were observed by other authors and were assigned to the stretching modes of -N=C=N- groups [22,25,47] and C≡N bonds [14,16,35,48]. If the formation of these N-related bonds is really enhanced by the N incorporation, the film structure would become more polymerlike. A model of the structure of the CN_x films as shown in Fig. 4.3 could be proposed. In the figure, some C rings and N-containing rings, C=N bonds and C≡N bonds are shown. In particular because a N atom has a chemical valence of three, so when it replaces a C atom in a C ring, a terminated site is produced to weaken the linkage between the aromatic clusters [49,50]. In addition, a terminated site can also be found accompanied by the formation of a C≡N bond.

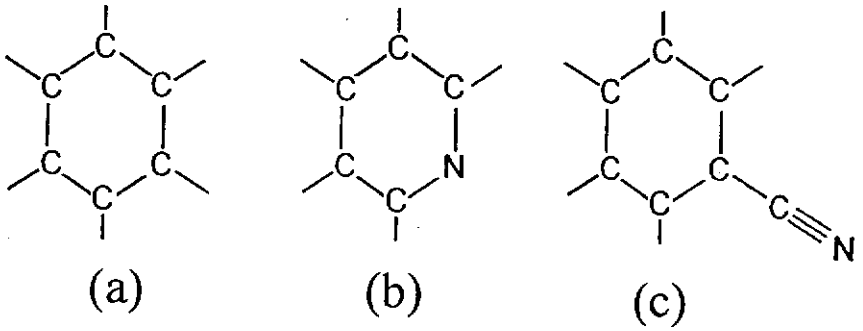

Fig 4.3 a-c Structure diagram of a completed sp^2 cluster, a N-containing six-membered ring and a ring with terminated bond

The polymerization of the film structure explains a lot of the experimental facts observed in this study. Associated with the polymerization of the film structure, first the optical band gap becomes wider. Second, the films are more IR transparency (Fig. 4.4). For example, at 2500 cm^{-1}, the transmittance rises from around 40 to about 100 % when the N content increases from 0 to 22.8 at.%. Third, the weaker linkage between the sp^2 clusters and the polymerlike bonds reduce in the electrical conductivity, hardness, elastic modulus and damage threshold in scratch tests, and possible increase in ductility and toughness of the films.

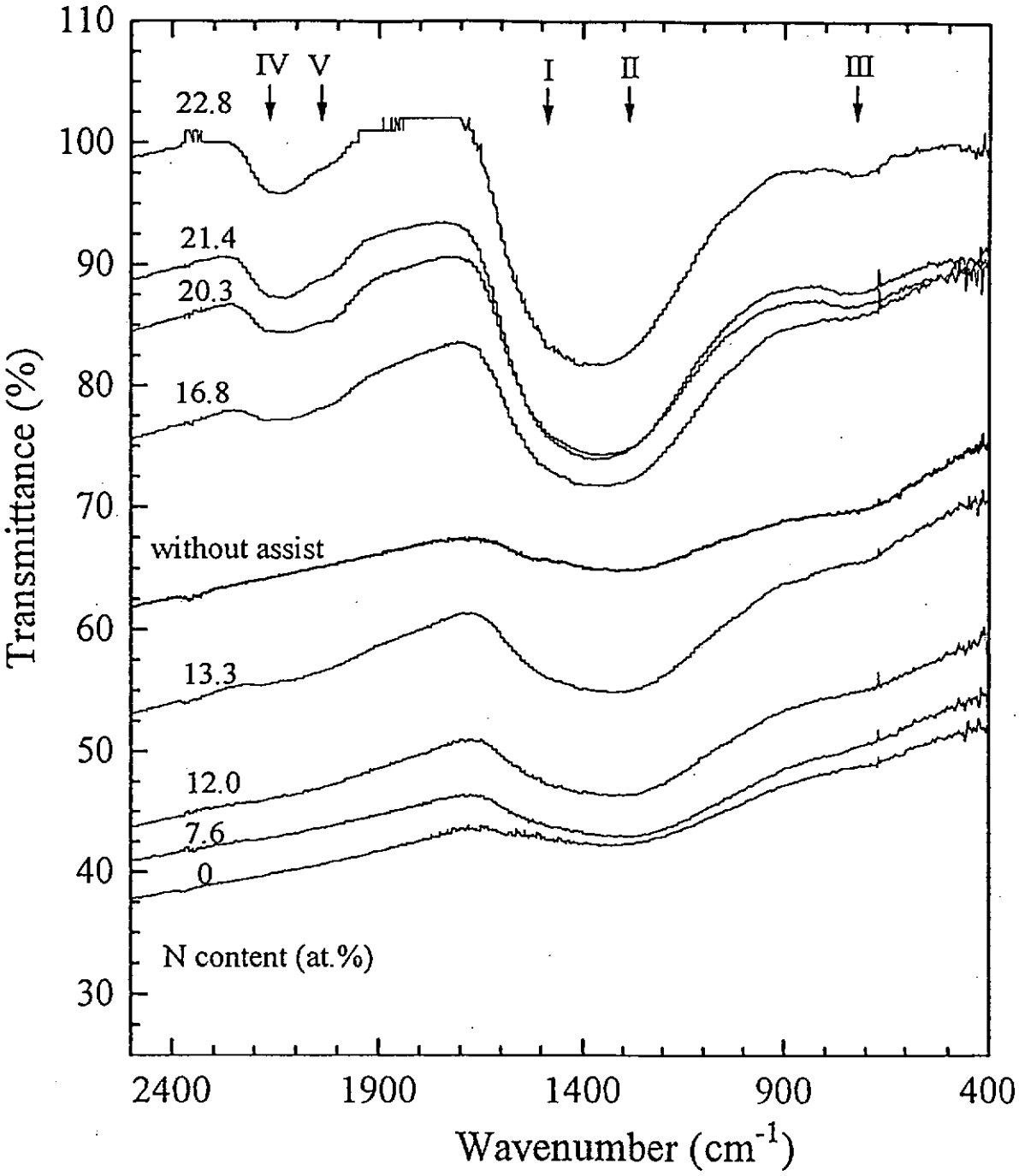

Fig. 4.4 FTIR spectra of the films as a function of the N content.

Band	IR absorption bands (cm^{-1})	IR bands reported in the literature (cm^{-1})	Assignments	Ref.
I	≈ 1560	1530	C=N	46
		1555	graphitelike sp^2 domains	14
		1575	graphitelike sp^2 domains	15
II	1300	1300	C-N	51
		1360	disordered sp^2 domains	14
		1370	disordered sp^2 domains	15
III	700	706	graphitelike sp^2 domains	14
IV	2100	2140	-N=C=N-	25
		2105-2155	-N=C=N-	22
		2155-2130	-N=C=N-	47
V	2000	2170	C≡N	36
		2150	C≡N	14
		2000-2300	C≡N	16
		2190	C≡N	48

Table 4.6 Peak positions of the IR absorption bands of the CN_x films and some relevant published data

4.3 Electrical conductivity

Fig. 4.5 shows the electrical conductivity σ of the films as a function of N content. Comparing the results of the two pure carbon films prepared with and without Ar^+ ion assist, σ of the latter is 4 times lower. This is because the pure carbon film prepared without ion assist contained more sp^3 bonds and is more diamondlike. The application of Ar^+ ion assist induces a larger fraction of graphitic

structure and so the value of σ rises. The graphitization in the film structure is possibly due to risen in T_s caused by the bombardments of the Ar^+ ions (refer to Table 4.1).

With increasing N content, σ drops as a consequence. This is explained by the polymerization of the film structure as indicated by the XPS and IR analyses.

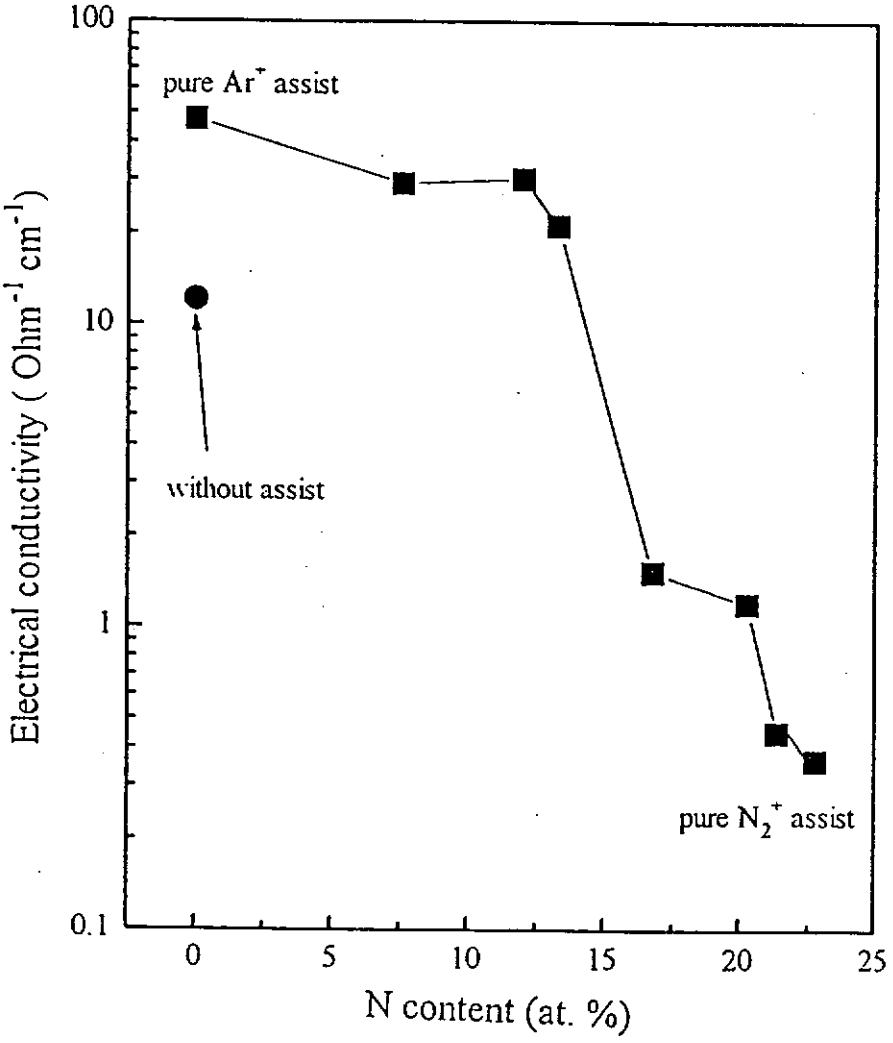

Fig. 4.5 Electrical conductivity of the films as a function of the N content.

4.4 Hardness and elastic modulus

The hardness (H) and the elastic modulus (E) of the films were measured as functions of indentation depth were calculated. The data of the sample CN_x 109 (7.6 at.% N) is an example as follow. Fig.4.6 a and c show the data of H of the film on Si wafer and quartz respectively. It is found that H is insensitive to the indentation depth, when the indentation depth is small. Therefore, the value of H at shallow indentations so are used to represent the true hardness of the film. However, H drops when indentation depth increases further, because the substrate effect becomes stronger. On the other hand, the data of E of the film on Si approach a constant value of about 180 GPa, when the indentation depth reduces (Fig. 4.6 b), but those of the film on quartz increases and lies below 150 GPa. It seems that the results of E obtained from the films of different substrates not consistent. Si has an E of 180 GPa and this value is close to that of the film, so that the substrate effect is not significant, if the indentation depth below 100 nm. Therefore, the measured value of E for the film on Si wafer can be used to reflect that of the film. However, quartz has a much smaller value of E of 72 GPa, and so the substrate effect is much stronger. Consequently, the value of E measured is expected to be lower than of the film.

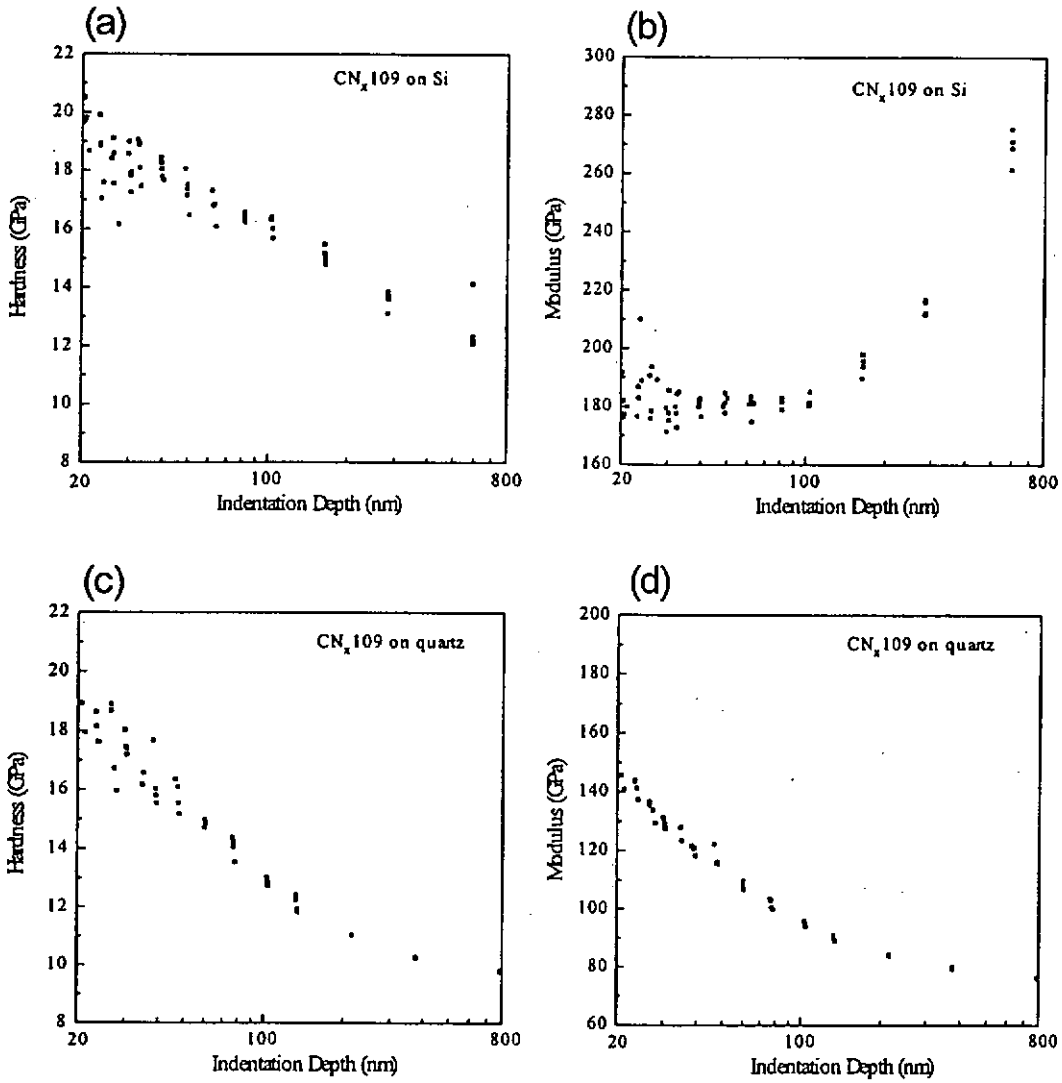

Fig. 4.6 a-d The hardness and modulus of CN_x 109 on Si and quartz vs. indentation depth

The H and E of films on Si and quartz substrates, obtained from averaging the results of ten or more shallow indentations (20- 30 nm), were plotted against the N content in Fig 4.7a and 4.7b. The data for the films on Si and quartz are represented by solid and open circles respectively. In addition, the error bars $\frac{\sigma}{\sqrt{n}}$ reflect the divergence of the data, where σ is standard deviation of data and n (≥ 10)

is number of repetitive measurements. The *H* values of all the films measured on Si (12.2 GPa) and quartz (9.5 GPa) are basically consistent. On the other hand, owing to the difference in the elastic modulus, *E* of films on Si are higher than those on quartz (Fig. 4.8). As explained above, the data of *E* measured for the film on Si are closer to the true elastic modulus of the films.

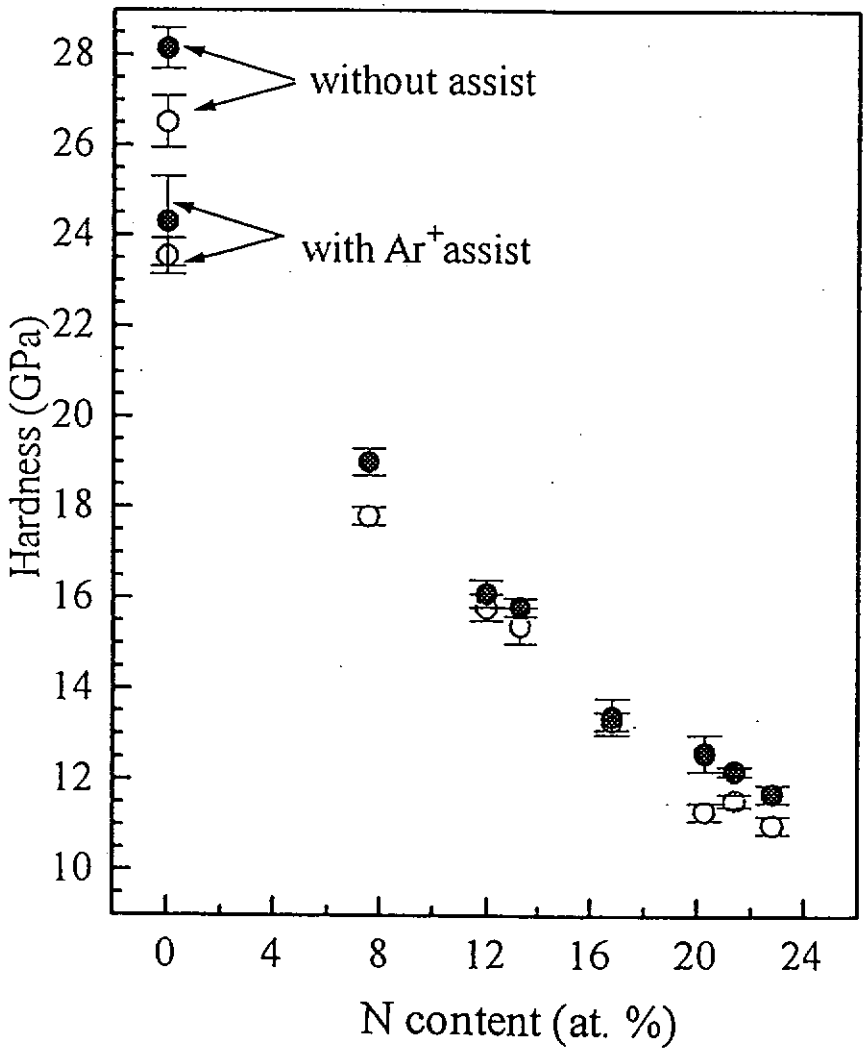

Fig. 4.7a The hardness of the CN_x films as a function of the N content
• : films on Si , o : films on quartz.

Referring to Fig. 4.7 a and b, H and E of the pure carbon film deposited without Ar^+ assist are equal to 28.1 GPa and 285 GPa. These values are so high reflecting that the film should contain certain fraction of diamondlike sp^3 structure. The formation of the diamondlike structure is promoted by the energetic sputtered species from the C target [52].

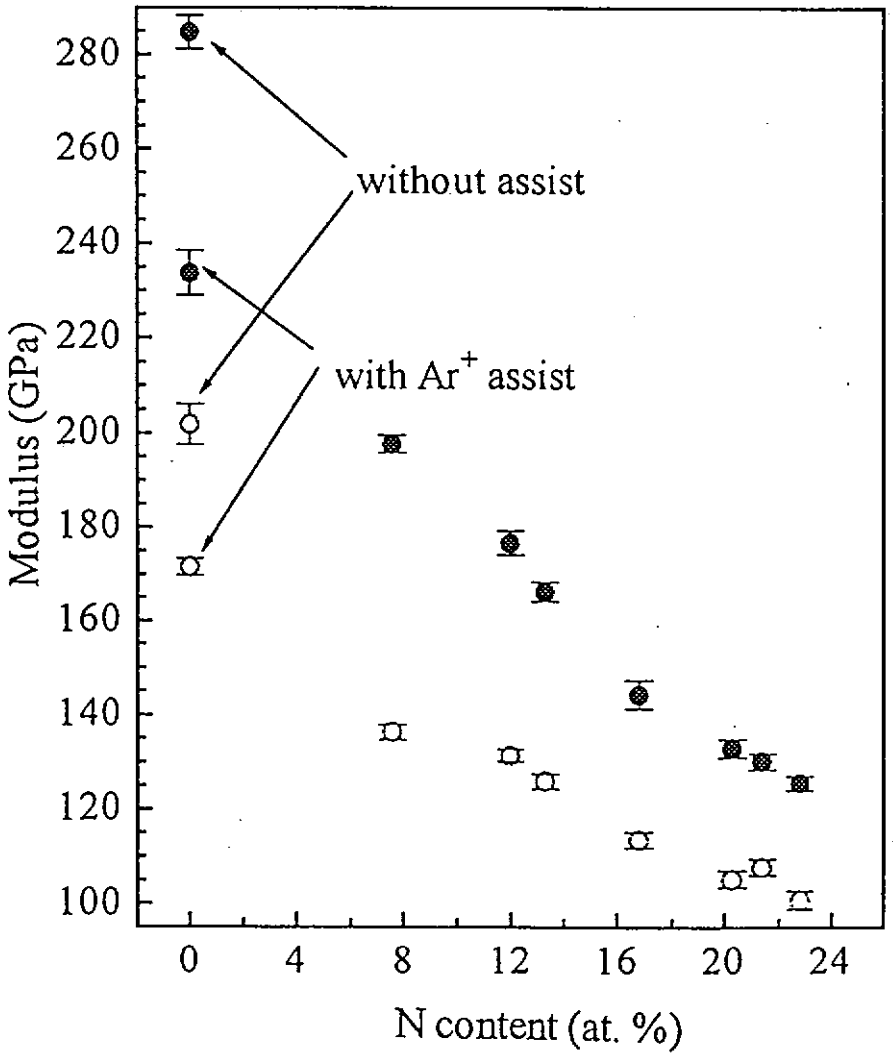

Fig. 4.7b The elastic modulus of the CN_x films as a function of the N content
• : films on Si , o : films on quartz.

H and *E* of the pure carbon film deposited with Ar^+ assist drop slightly (24.3 GPa and 235 GPa respectively) indicating that induction of Ar^+ ion assist reduces the formation of sp^3 bonds, and so the film structure is more diamondlike.

With increasing N content, both *H* and *E* drop monotonically to 11.7 GPa and 165 GPa respectively, when the N content increases from 0 to 22.8 at.%. This is possibly because the addition of N atoms enhance the formation of N-containing six-membered rings having graphitelike characteristics, and suppress the formation of sp^3 bonds. Furthermore, according to the results of structure analyses, C-N, C=C, C=N, -N=C=N- bonds could be formed, leading to a diamondlike-to-polymeric structural transition, such that the films with higher N contents are softer.

Table 4.7 summaries most of the data of *H* published in recent years for the sake of comparison. First, it is noted that most of the values of *H* of the carbon films and CN_x films reported by different authors lie in the range of 1 - 32 GPa [22,25,52-55]. These data are basically consistent with that obtained in the present study, except that the *H* data reported by Dekempeneer et al. [24] are extraordinary high due to the lack of correction calibration of the area function of the diamond tip. In addition, the trend that *H* drops with increasing N content in CN_x films has been observed by many authors [20,24,52,55,56], consistent with the conclusion of our observations.

year and author	film and deposition method	deposition condition	results
1994 D. Li [21]	CN_x film *(by d.c. unbalanced magnetron sputtering of C target in a nitrogen-containing plasma)*	$(Ar+N_2)$ mixture and pure N_2 were used as the sputtering gas.	Maximum *H* (by nano indentation) ≈ 21 GPa
1994 H. Sjöström [56]	CN_x film *(by d.c. unbalanced magnetron sputtering of C target)*	target power = 0.2 to 0.9 kW, N_2 pressure = 5 to 20 mTorr, bias = 7.5 to 200 V, substrate temperature (T_s) 150 to 600°C.	N at.% dropped from 28 to 15% when T_s increased, turbostratic phase CN_x films, *H* from 7 to 9 GPa.
1994 E.H.A. Dekempeneer [24]	C_xN_{1-x}:H *(by r.f plasma assisted chemical vapor deposition)*	(H_2+CH_4) gases mixture was used as reactive gas.	*H* (by depth-sensing hardness test without correction of the indenter tip geometry imperfection) dropped monotonically from about 40 to 15 GPa with increasing the N_2 gas fraction
1995 K.-R. Lee [49]	N incorporated DLC *(by r.f plasma assisted chemical vapor deposition)*	$(NH_3+C_6H_6)$ or $(NH_3+C_6H_6)$ were used as reactive gases.	The knoop hardness monotonically decreased from 2750 to 1700 Kgf mm^{-2} with increasing NH_3 /($NH_3+C_6H_6$), while that in the N_2/($NH_3+C_6H_6$) is unchanged with 2700 ± 300 Kgf mm^{-2}.
1995 T.Y. Tsui [54]	300 nm CH_x , 600 nm CN_x , 210 nm BO_x	CH_x *(by sputtering C in H_2+Ar mixture)*, CN_x *(by DC magnetron sputtering in N_2+Ar atmosphere)*, BO_x *(by ECR).*	CH_x (20 at. % H), CN_x (≈ 23 at. % N) and BO_x with: *H* (by nano indentation) of 13.6, 25.4 and 28.5 GPa respectively , and *E* of 168, 225 and 245 GPa, μ (by load-ramped scratch test) = 0.13, 0.12 and 0.13 critical load of 38, 59 and 50 mN.

Table 4.7: A summary of the work on the mechanical and tribological properties of CN_x films reported in the literature

1995 X. Wang [52]	CN_x and a-C film *(by ion-assisted arc deposition and magnetron sputtering)*	For ion-assisted arc deposition, the ion assist conditions and the background gas were varied. For magnetron sputtering, the background gas was varied.	*H* (by microhardness tests) of CN_x decreased with increasing nitrogen content and was even lower if the nitrogen was incorporated into films by higher energy N^+ ion bombardment. *H* of C, $CN_{0.1}$, $CN_{0.3}$ = 4000, 2570, 1517 kgf mm^{-2} in ion-assisted arc deposition *H* of C, $CN_{0.2}$, $CN_{0.3}$ = 3422, 2453, 2185 kgf mm^{-2} in magnetron sputtering *H* of C film (2187 kgf mm^{-2}) by ion-assisted arc deposition is lower than that deposited without ion assist (*H* = 4000 kgf mm^{-2}),
1995 F.-R. Weber [25]	CN_x film *(by direct plasma beam deposition with r.f. plasma beam source)*	$N_2/(Ar+N_2)$ ratio in the mixture reactant gas was varied	*H* (by microhardness testing) of CN_x films (N ≈ 27 and 41 at.%) ≈ 18 GPa, except a CN_x film (N ≈ 27 at.%) deposited in another condition ≈ 25 GPa.
1995 P. Zou [57]	10nm CN_x and a-C on hard disk *(by rf reactive sputtering deposition)*	C target was sputtered and $N_2/(Ar+N_2)$ ratio (at fixed pressure 1.3 Pa) varied. Finally the coating rates were 0.065 nm s^{-1} for using pure Ar, 0.085 nm s^{-1} for pure N_2.	When N partial pressure increased, μ (by 3 mm dia. sapphire pin with normal load 10 g) and Roughness (by AFM) both dropped (0.5 to 0.3 and 2.1 to 0.2 nm respectively). Take-off velocity increased because of development of wear, and that appeared after less number of revolutions when N partial pressure increased.
1996 A. Khurshudov [43],[58]	1.5-30 nm CN_x *(by dual ion beam deposition)* and commercial C coatings on magnetic disks	Ar^+ ion beam sputtering of C target with N ions assist.	μ (scratch by Si_3N_4 pin with normal load =0.02 N) of CN_x (N ≈ 10 at.%) was 0.12-0.14 and lower than that of the C film (0.28-0.3), and μ (by AFM) of the CN_x was also lower than that of the C film in micro-scale. CN_x provided 3-10 times longer life than C coating against Si_3N_4 pin.

Table 4.7: A summary of the work on the mechanical and tribological properties of CN_x films reported in the literature

1996 N. Axen [59]	CN_x and a-C film *(by a planar magnetron sputter system using both d.c. and r.f. magnetron power sources)*	The sample temp. (50 to 1000 °C) was varied the amount of N_2 in the sputter gas (pressure was varied between 0.3 and 4 Pa)	*H* (by depth-sensing microhardness testing) ≈ 1000 HV for most of the a-CN_x (N = 0 to 58 at.% by RBS), but traditional indentation technique caused high apparent *H* value (some H ≈ 8000 HV).
1996 E. C. Cutiongco [53]	a-CN_x (5 and 30 nm) on magnetic thin-film rigid disks surfaces *(by single-cathode and dual-cathode magnetron sputtering systems)*	The dc substrate bias varied form -50 to -450 V and pulsed bias in single-cathode system with target power of 1 kW and $N_2/(Ar+N_2)$ pressure ratio in mTorr = 0.2/4. $N_2/(Ar+N_2)$ pressure ratio was varied with target power of 1 kW and total pressure at 4 mTorr	a-CN_x with no significant pinholes at thickness down to 5 nm, have *H* (by nano indentation) = 22-28 GPa (compared to 7-12 GPa for a-C), and r.m.s. roughness as low as 0.25 nm and better contact-start-stop performance (stiction performance superior to that for a-C)
1996 G. Wang [18]	CN_x and a-C film on Al_2O_3-TiC head slider *(by facing target sputtering)*	C films were deposited by using pure Ar gas as sputtering, and CN_x films by using pure 60%Ar+40%N_2 gas as sputtering gas	CN_x (N = 22 at.%) and C films both can protect the head from wear failure in continuos drag tests (CDT) and CNx is better. The head may fail before the disk fails and the area of Al_2O_3 is the most possible place where wear begins.
1996 P. Hammer [22]	CN_x *(by ion beam assisted sputtering)*	A graphite target was sputtered by Ar^+ or N ions and the growing film was simultaneously bombarded by a focused N ion beam (100-800 eV) at 100 and 400 degree C.	Maximum *H* (by nano indentation) was to 18 GPa at atom-to-ion arrival ratio = 0.7 (roughness N content = 25 at.%), minimum was 15 GPa.
1996 P. Hammer [20]	CN_x *(by dual ion beam deposition at low temp.)*	Conditions of the sputter beam were 100-1500 V, 18-35 mA, N ion for sputtering C target and that of assist beam 80-500 V, 1.5-8.5mA, N ion. T_{sub} was varied from 80 to 673k	When Ts increased (80 to 673k), *H* (by nano indentation) increased (1 to 20 GPa), σ increased (1×10^{-14} to 1 $\Omega^{-1}cm^{-1}$), but optical band gap dropped (2.2 to 0.2 eV) *H* (N =44 at.%) = 1 GPa *H* (N =32 at.%) = 8 GPa, *H* (N =24 at.%) = 20 GPa,
1996 R.L. White [55]	a-CN_x (by RF sputtering)	using RF sputtering deposition	From 2 to 40 at% N, *H* (by nano indentation) was found to linearly decrease from 32 to 13 GPa with increasing nitrogen content.

Table 4.7: A summary of the work on the mechanical and tribological properties of CN_x films reported in the literature

Table 4.8 summaries the *H* and *E* of the CN_x films on Si substrates deposited at various ion beam energies and currents (at fixed f_{N_2} = 0.09). In particular, the results of the *H* are plotted against the N content in Fig. 4.8. One can see that both *H* and *E* drop with increasing N content, consistent with the same trends shown in Fig. 4.7 a and b. The variation of the N content is mainly due to the change in the ion beam current. For example, the ion beam current used for preparing sample CN_x114 is two times of that for preparing sample CN_x113 (both with the same ion beam energy), and as a consequence sample CN_x114 contains as much higher N content. On the other hand, the beam energy used for fabricating sample CN_x113 (300 eV) is 3.3 times higher than that used for prepared sample CN_x114 (90eV), but the difference between their hardnesses is below 11 %.

Sample :	Beam energy (eV)	Beam current (mA)	N content (at. %)	*H* (GPa)	*E* (GPa)
CN_x113	300	20	8.2	18.3	193.0
CN_x109	160	20	7.6	19.0	197.6
CN_x114	90	20	7.2	16.3	207.2
CN_x115	90	10	4.6	19.0	215.7
CN_x116	160	35	10.3	15.3	199.3

Table 4.8 *H* and *E* of the CN_x films on Si deposited at various ion beam energies and currents.

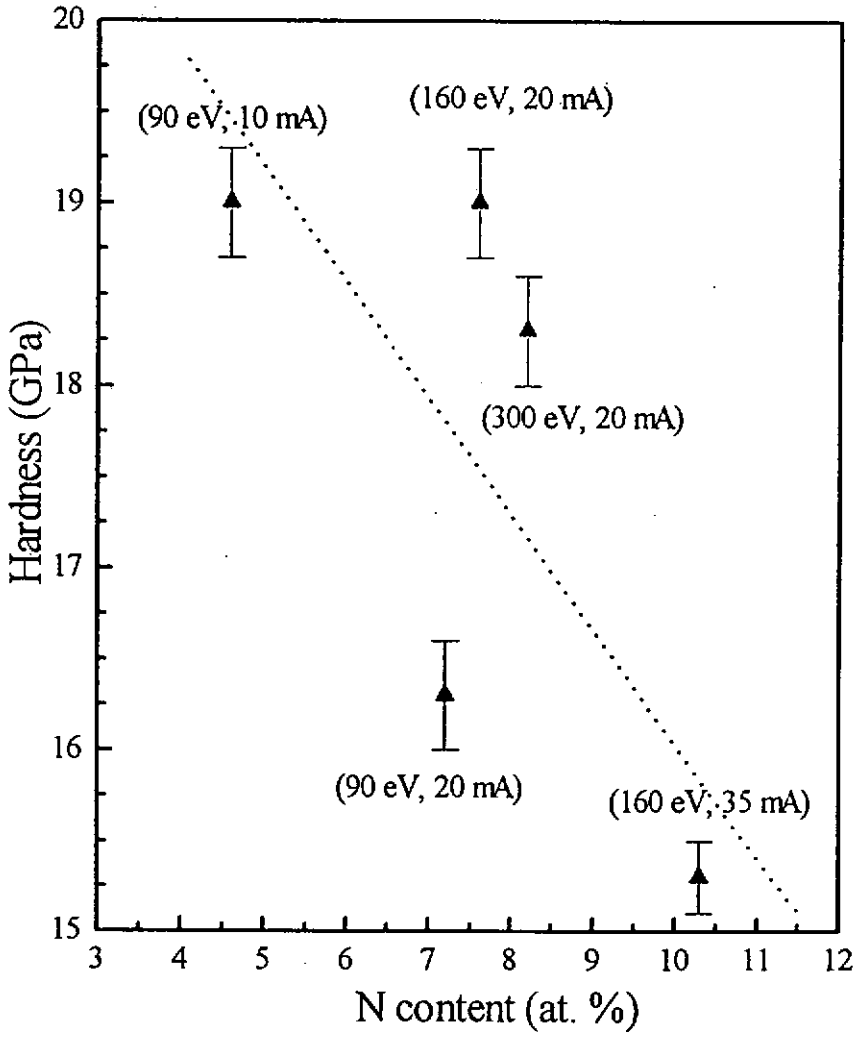

Fig.4.8 *H* of the films on Si deposited at various ion beam energies and currents against the N content

4.5 Nanoscratch tests

This section will present and discuss the results of the nanoscratch tests. They include: (1) the friction coefficient μ, (2) the damage threshold and the damage mechanisms, and (3) the irreversible plastic wear of the films as functions of the N contents.

Friction coefficient

Fig. 4.9 a to 4.9 i show the data of μ obtained from constant load scratches (with normal fixed load = 0.2, 0.4, 0.7 and 2.5 mN) and ramping load scratches (with rates = 6 and 150 $\mu N\ s^{-1}$), for the films with 0 to 22.8 at.% N. In each figure, the open circles represent the values of μ obtained by the constant load scratches. The corresponding total vertical displacements of the diamond tip (total depth) were also labeled. The two curves corresponding to the lower and higher load ramping scratches are shown. In general, the values of μ obtained from three schemes are consistent. First, μ is not a constant, but increases faster when the diamond tip ploughs into the film at shallow depths, and then becomes flatter as the penetration depth rises.

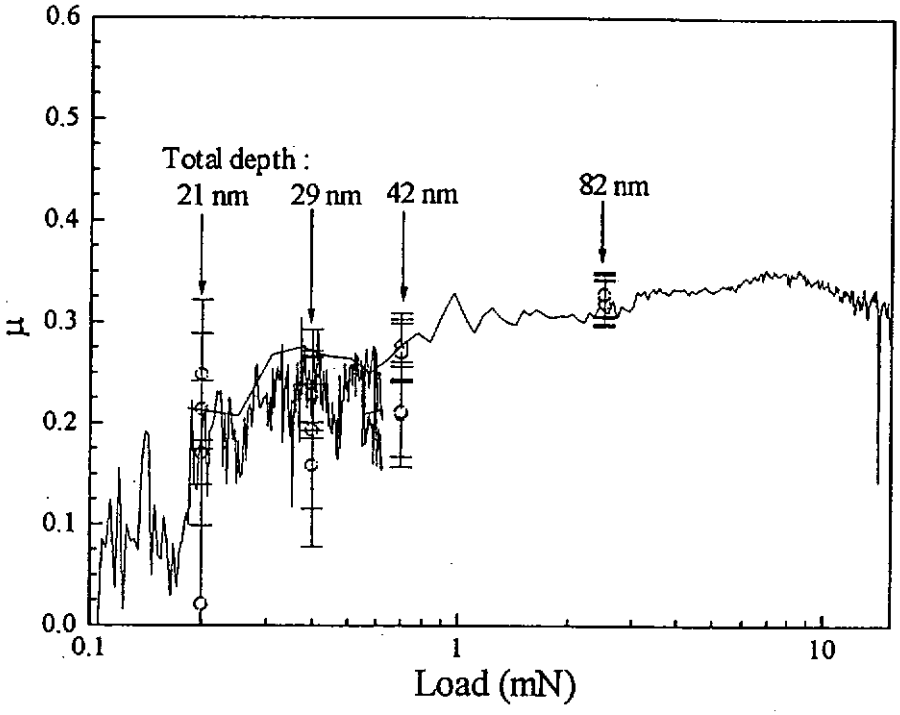

Fig. 4.9a μ as a function of normal load of CN_x112: pure carbon film deposited without ion assist.

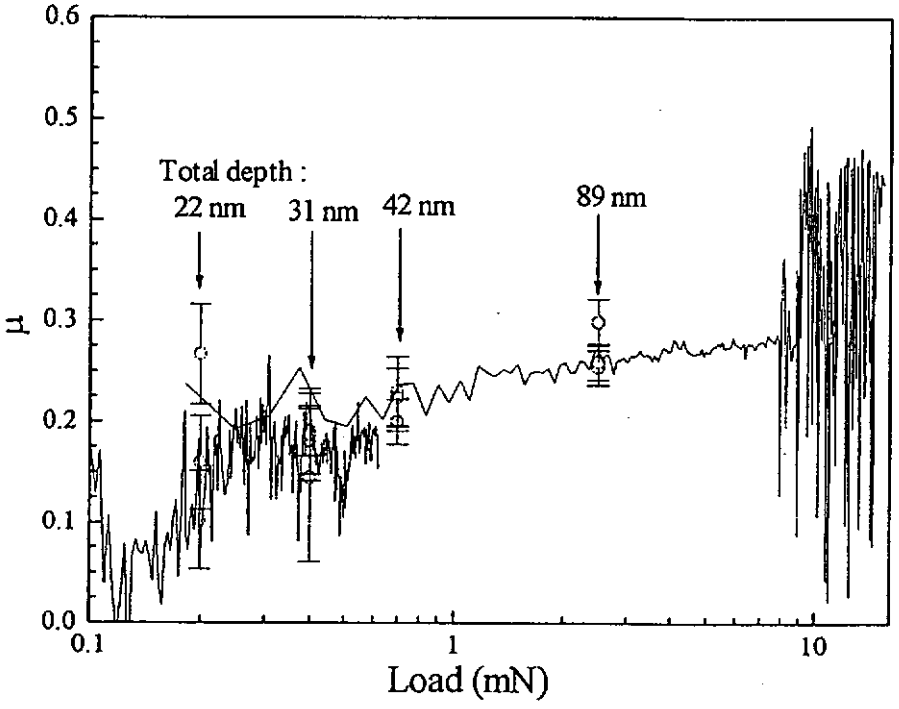

Fig. 4.9b μ as a function of normal load of CN_x102: pure film deposited with Ar^+ assist.

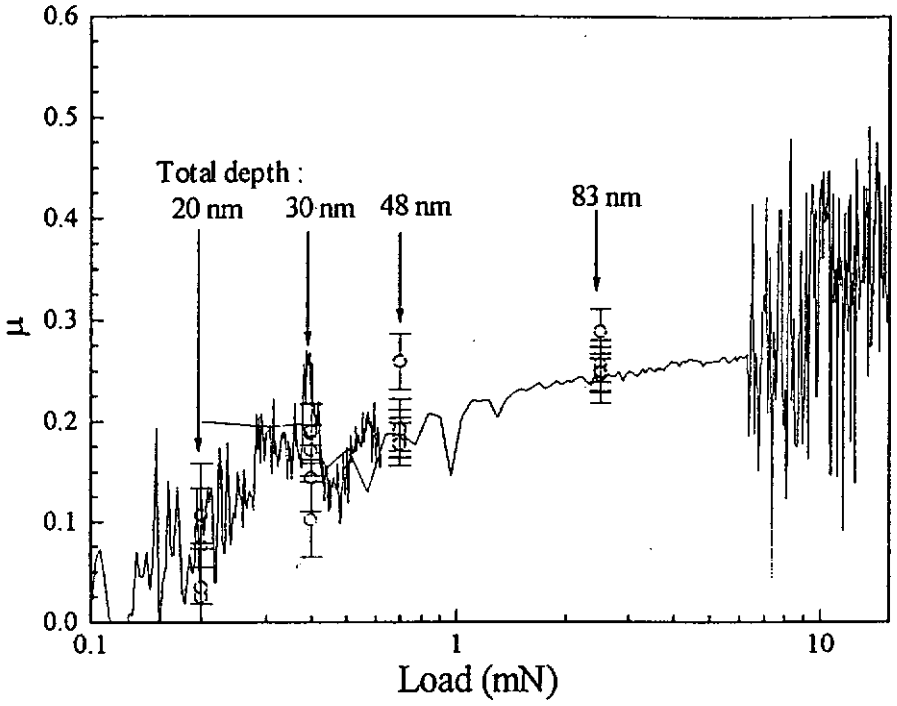

Fig. 4.9c μ as a function of normal load of CN_x109: carbon nitride film with 7.6 at.% N content

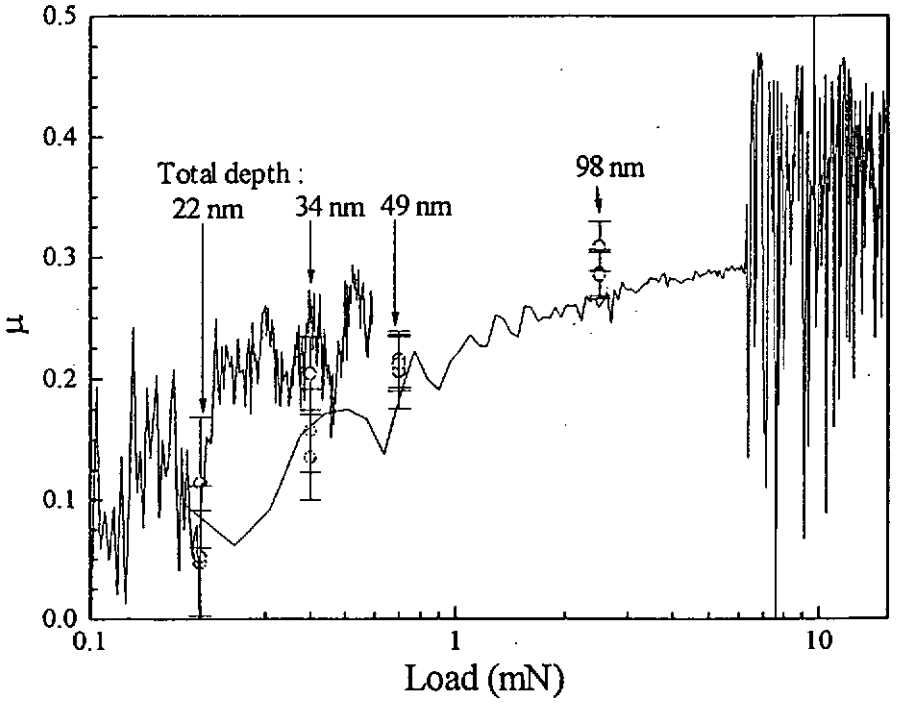

Fig. 4.9d μ as a function of normal load of CN_x110: carbon nitride film with 12.0 at.% N content

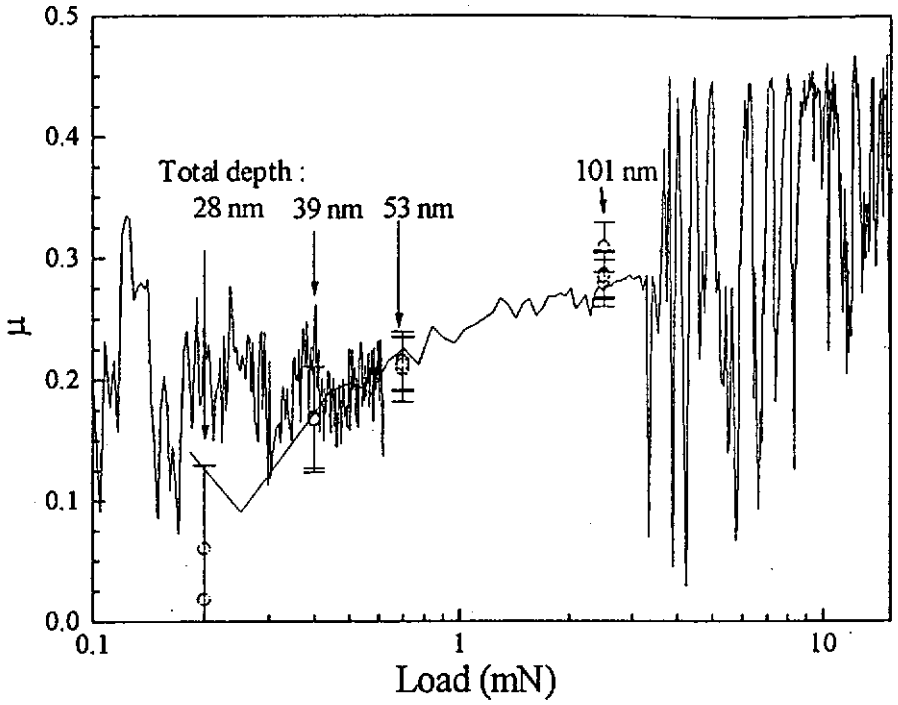

Fig. 4.9e μ as a function of normal load of CN_x111: carbon nitride film with 13.3 at.% N content

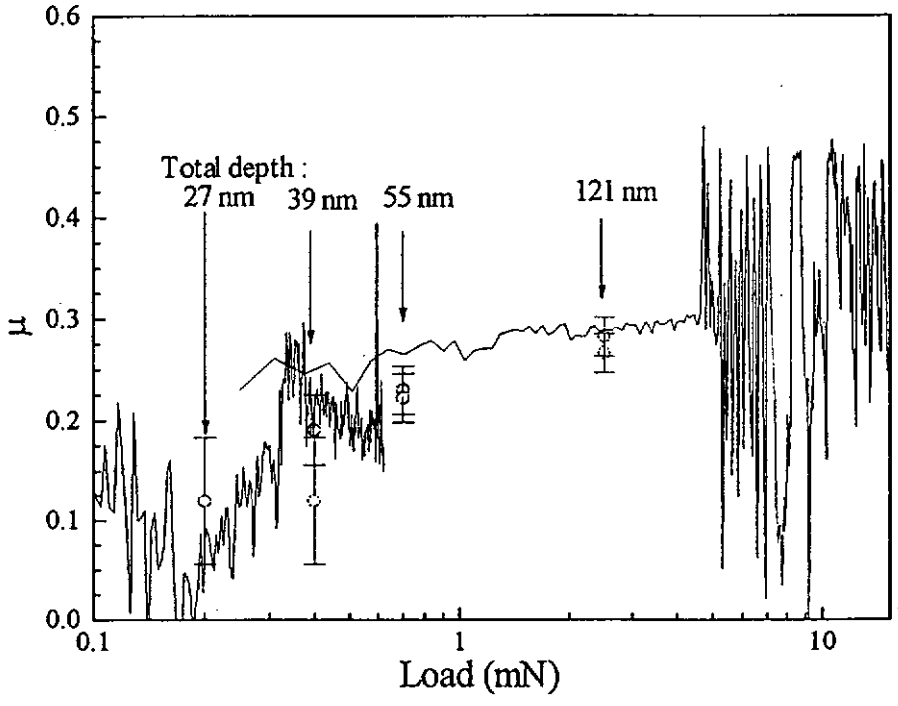

Fig. 4.9f μ as a function of normal load of CN_x105: carbon nitride film with 16.8 at.% N content

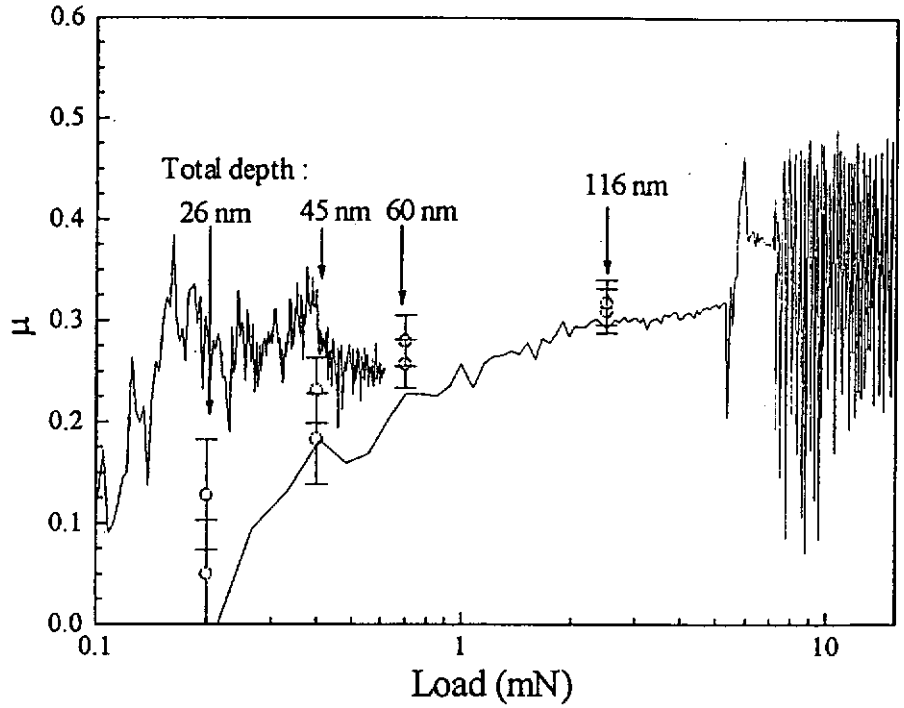

Fig. 4.9g μ as a function of normal load of CN_x108: carbon nitride film with 20.3 at.% N content

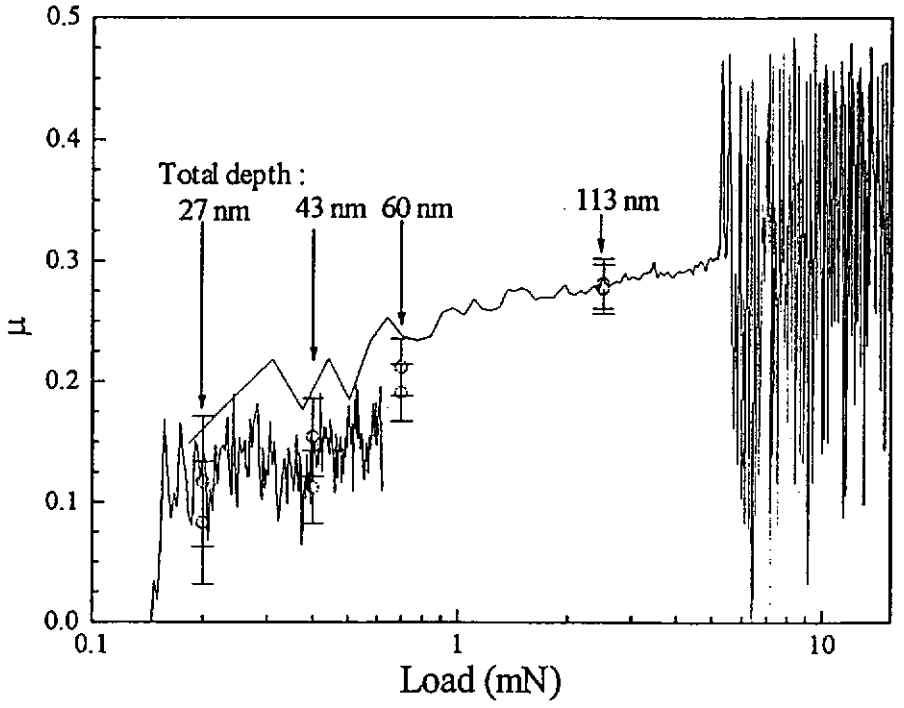

Fig. 4.9 h μ as a function of normal load of CN_x106: carbon nitride film with 21.4 at.% N content

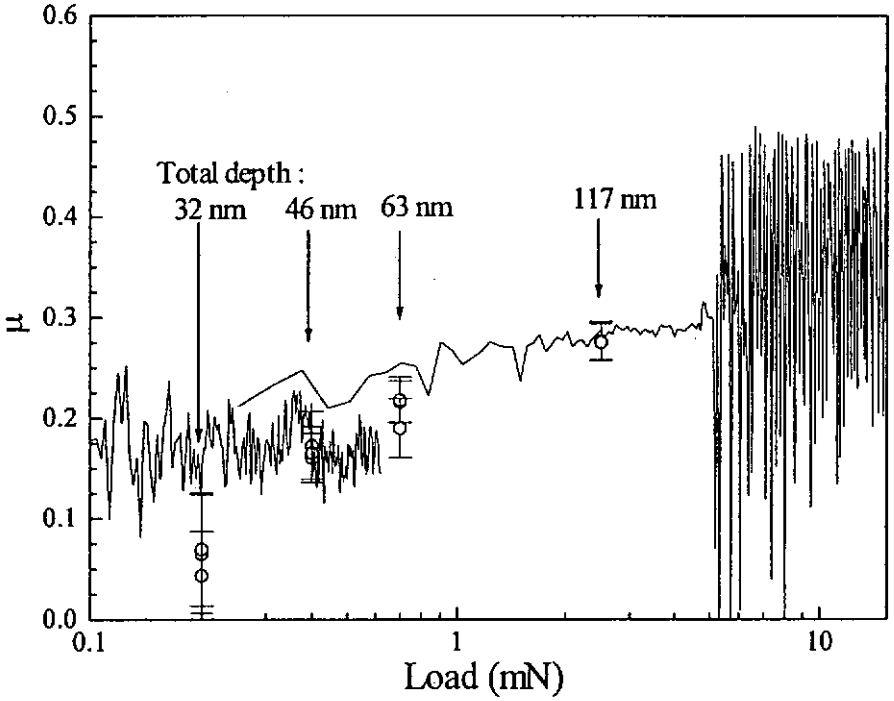

Fig. 4.9i μ as a function of normal load of CN_x103: carbon nitride film with 22.8 at.% N content

This could be explained if the frictional force is composed of two components. One is the chemical/physical sorption between the film surface and the diamond tip materials as they are in touch and slide with respect to each other relatively, while the next one is due to the resistant force applied by the materials to the tip, when the tip is driven to plough deep into the specimen.

Referring to the fact that μ is not a constant in a scratch test, the values of μ of different films at a certain normal load can still be compared, e.g. 0.4 mN is selected in Fig. 10. Results show that within the range of the error bars, μ is basically independent of the N content in the films, and has a value of around 0.17, where the corresponding penetration depth of the tip is in the range of 30 - 47 nm.

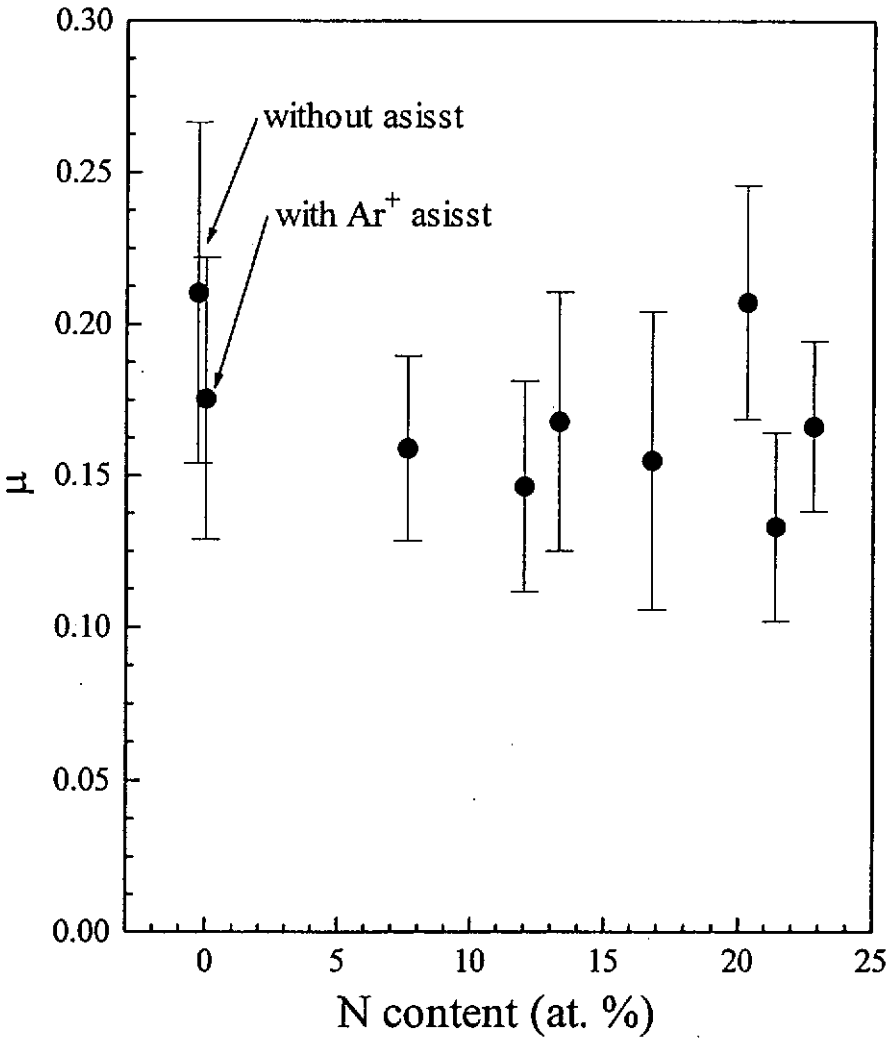

Fig. 4.10 μ measured at constant load = 0.4 mN vs. N content, where the corresponding penetration depth of the tip is around 30 -47 nm.

Damage mechanism

Fig. 4.11a shows the profile of the scratch track of the pure C film deposited without Ar^+ assist (CN_x112). The dotted line represents the original film surface before the scratch. The profile during the scratch lies below that of the post scan, because the former is produced under normal load and so includes the total deformation of the film as well and the substrate. Furthermore, on the left of *A*, the profile of the post scan is almost completely recovered to overlap with the original surface after the normal load is removed. This indicates that the deformation of the film/substrate during the scratch (on the left of *A*) is basically elastic. Starting from point *A*, the profiles of the scratch track and μ remain smooth, but that of the post scan is rather zigzag. This may implies that the film started to be damaged at point *A*. As a consequence, the scratched surface becomes rough. One may then define the normal load applied at point *A* to be the damage threshold (*DT*) of the film. It has been reported that *DT* of a thin film is thickness dependent, but since the thickness of the films in this study lies in a rather narrow range, so that the thickness effect is negligible, and the data of *DT* obtained from different films can be directly compared. The micrograph in Fig. 4.11a shows the features of the crack at the point of damage (point *A*) on the sample CN_x112. At this point, the fragments are still attacked to the substrate rather firmly, indicating that the film adhesion to the substrate is strong. This can be understood as the sputtered carbon species from the target have rather high kinetic energies in the range between 10 - 100 eV, favoring the formation of diamondlike sp^3 bonds, and so very strong film adhesion is

resulted. Furthermore, from the features of the propagation of the cracks, one infers that the film is rather brittle.

For the pure carbon film CN_x102 deposited with Ar^+ ion assist (Fig. 4.11b), a point at which the film starts to crack is also observed in Fig. 4.11b. The *DT* of CN_x102 is lower than that of CN_x112, possibly because the assist beam used in preparing CN_x102 heats up the film surface and hence less sp^3 bonds are formed such that the film is less diamondlike (refer to section 4.1). This result is consistent with the smaller hardness of the CN_x102 observed. However, the film is damaged with some underlying substrate material, and so the film adhesion is still rather strong. Some debris was found, around the crack, showing that the film is still rather brittle.

For N content $\geq$ 12.0 at.% (Fig. 4.11 d-i), the films start to delaminate at point *A*. The diamond tip slides smoothly on the substrate surface with a friction coefficient $\mu \approx 0.3$ until a point *B* is reached. Beyond *B*, μ fluctuates rapidly, indicating that the substrate has been damaged. Considering that delamination of a surface coating is not allowed in applications, the load at point *A* is regarded as the *DT* of the specimen. In addition, the load recorded at *B* is the defined as the substrate damage threshold (*SDT*). The complete detachment of the film illustrates that the film adhesion is relatively weak as N is incorporated. Furthermore, very little debris is found, showing that the films are less brittle compared with the pure carbon films, but could be tougher and more ductile. If one assumes that the incorporation of N would hinder the generation of sp^3 bonds so as to reduce the

diamondlike nature, and more linear bonds (e.g. C-N, C=C, C≡N, -N=C=N-) are formed such that the film structure is more polymerlike, then the above results on the CN_x films, including the appearance of lower *DT*, complete delamination of the film from substrates accompanied by a weaker film/substrate bonding, less brittleness and possibly higher toughness and ductility are readily explained.

Fig. 4.11a Scratch profiles and micrograph of CN_x112: pure carbon film deposited without Ar^+ assist

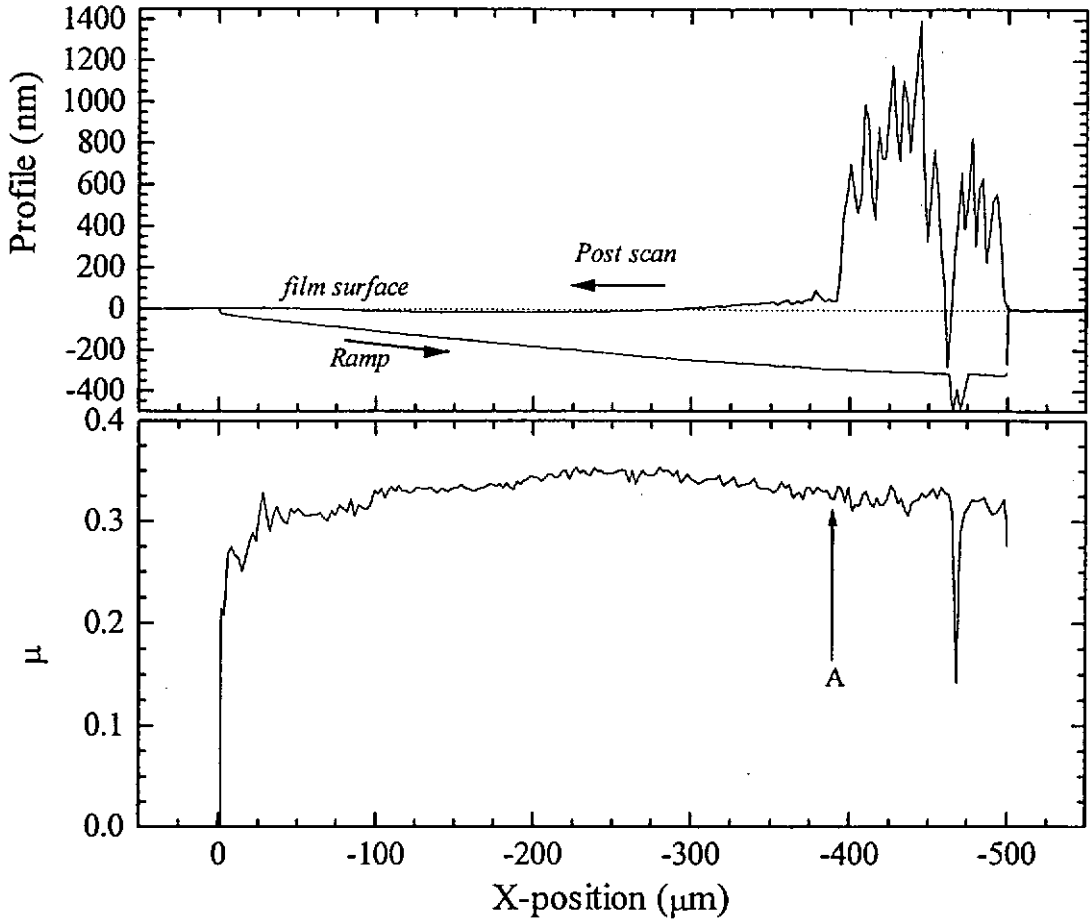

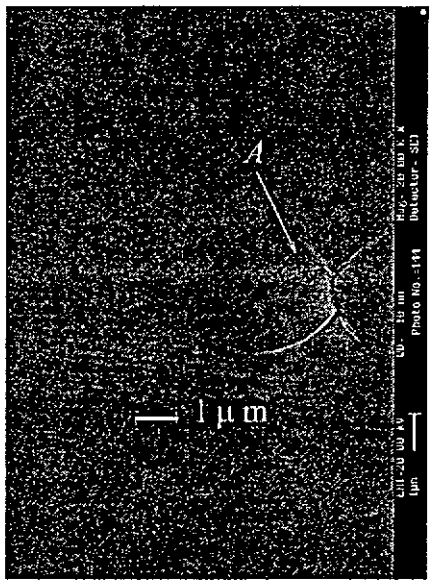

Fig. 4.11b Scratch profiles and micrograph of CN_x102: pure carbon film deposited with Ar^+ assist

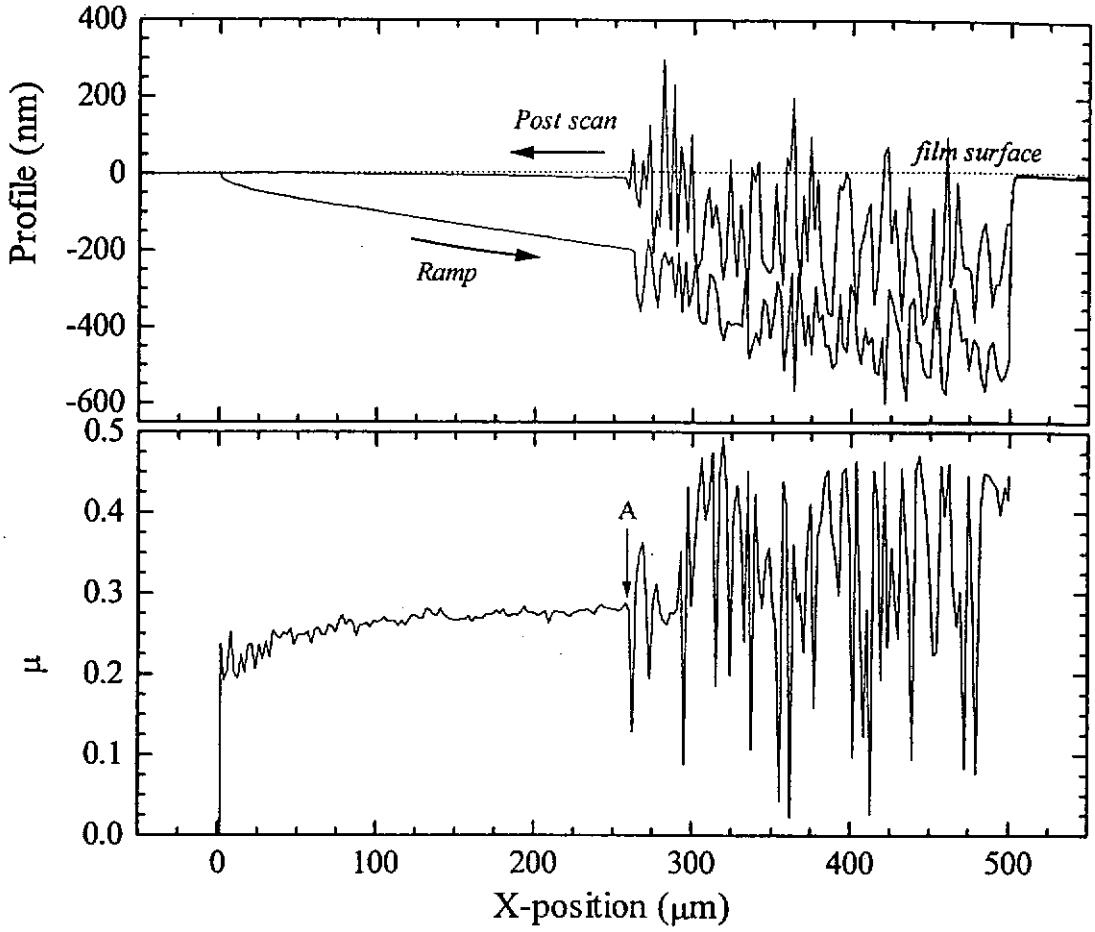

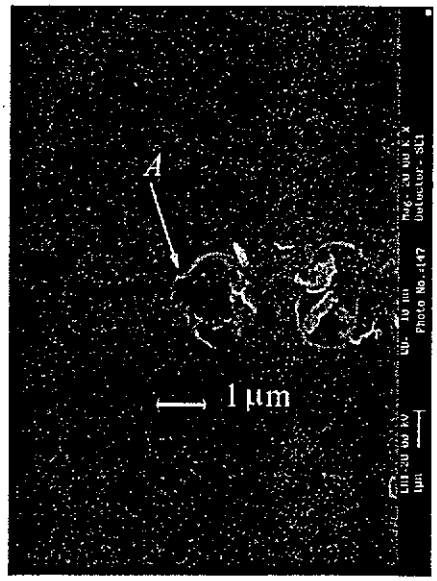

Fig. 4.11c Scratch profiles and micrograph of CN_x109: Carbon nitride film with 7.6 at.% N content

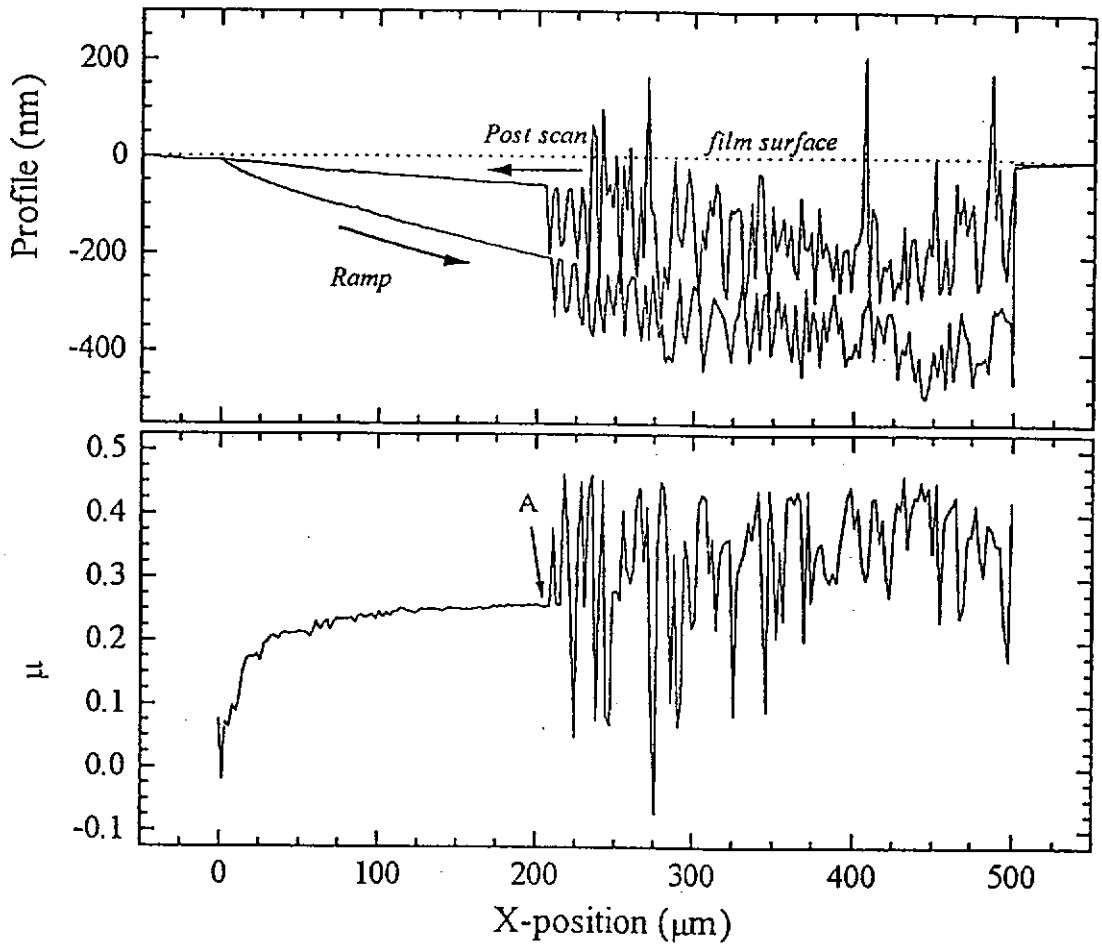

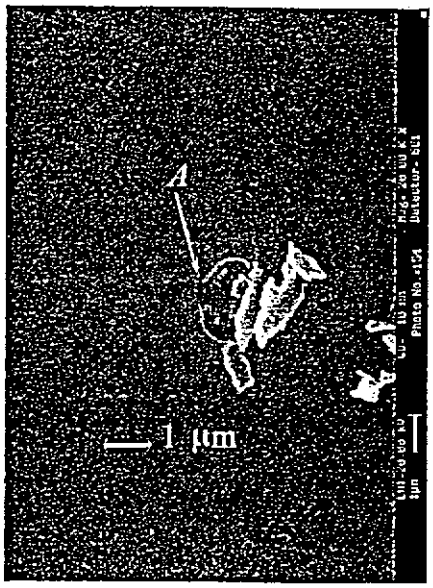

Fig. 4.11d Scratch profiles of CN_x110: carbon nitride film with 12.0 at.% N content

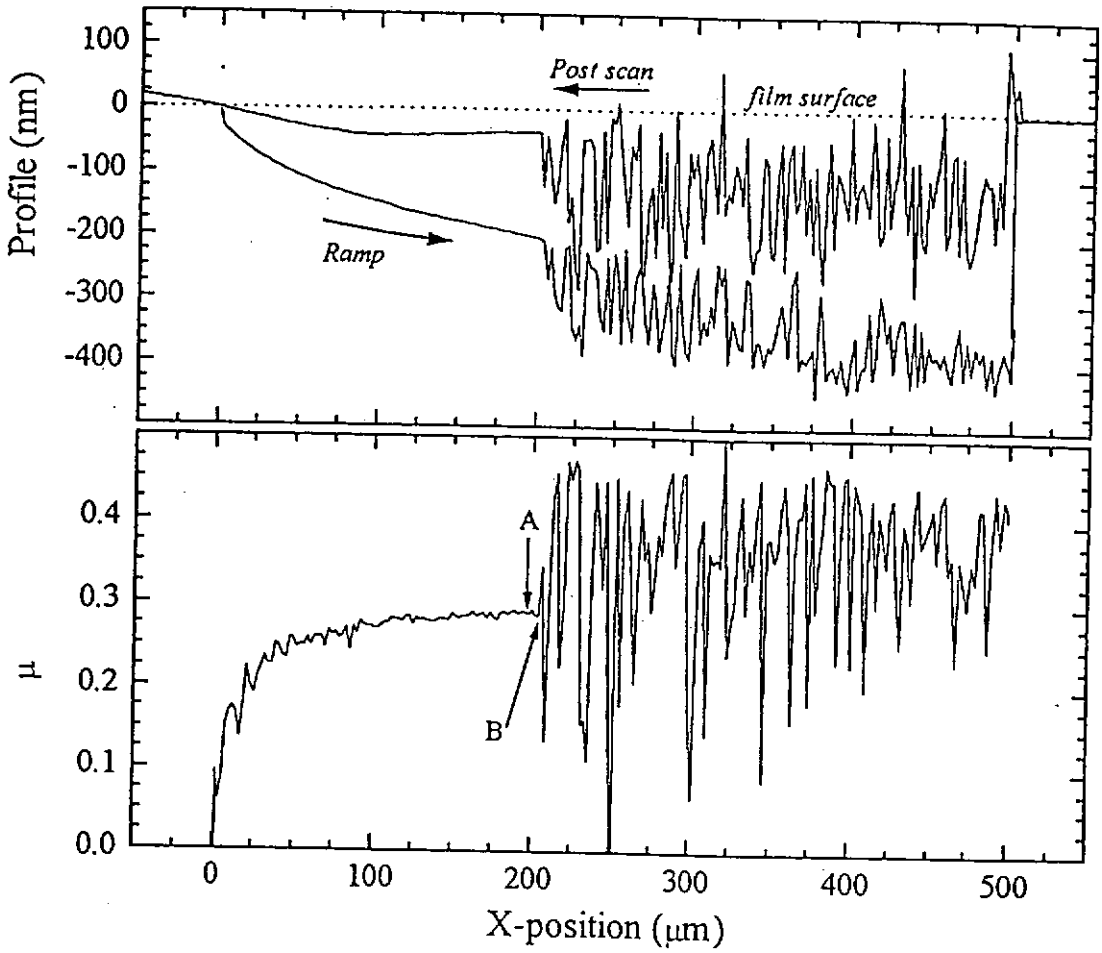

Fig. 4.11e Scratch profiles of CN_x111: carbon nitride film with 13.3 at.% N content

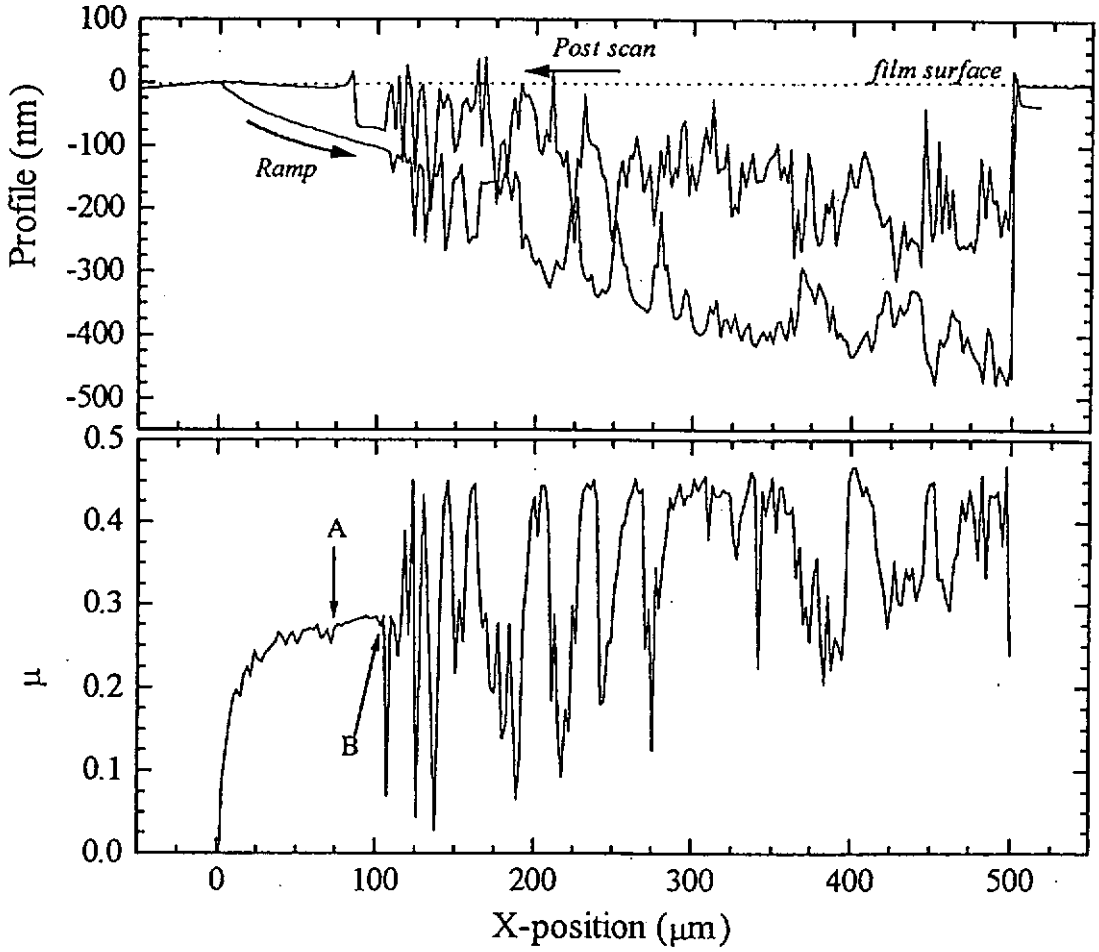

Fig.4.11f Scratch profiles and micrograph of CN_x105: Carbon nitride film with 16.8 at.% N content

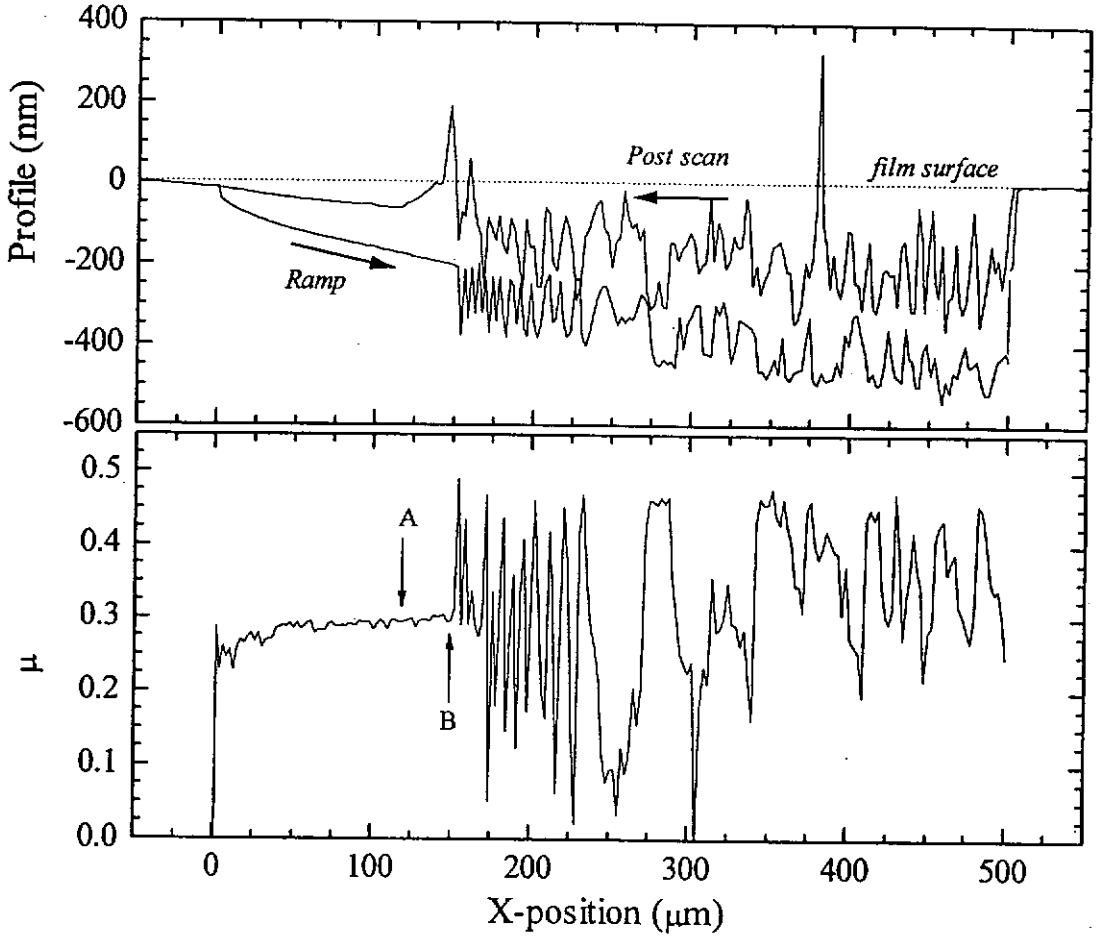

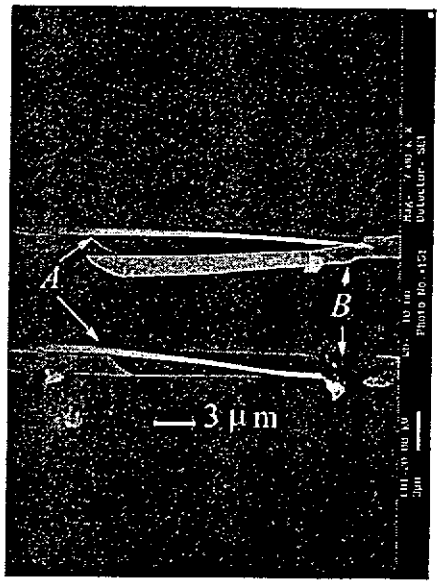

Fig. 4.11g Scratch profiles of CN_x108: carbon nitride film with 20.3 at.% N content

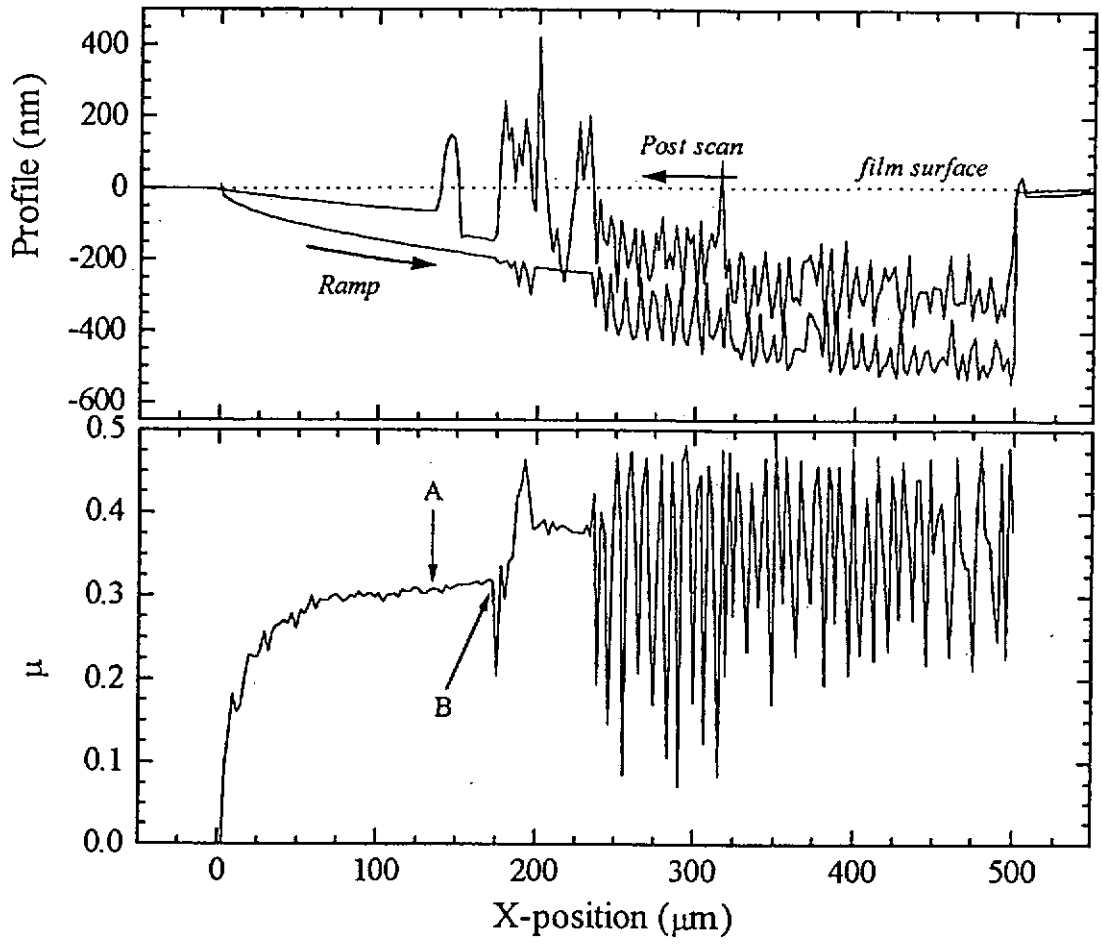

Fig. 4.11h Scratch profiles of CN_x106: carbon nitride film with 21.4 at.% N content

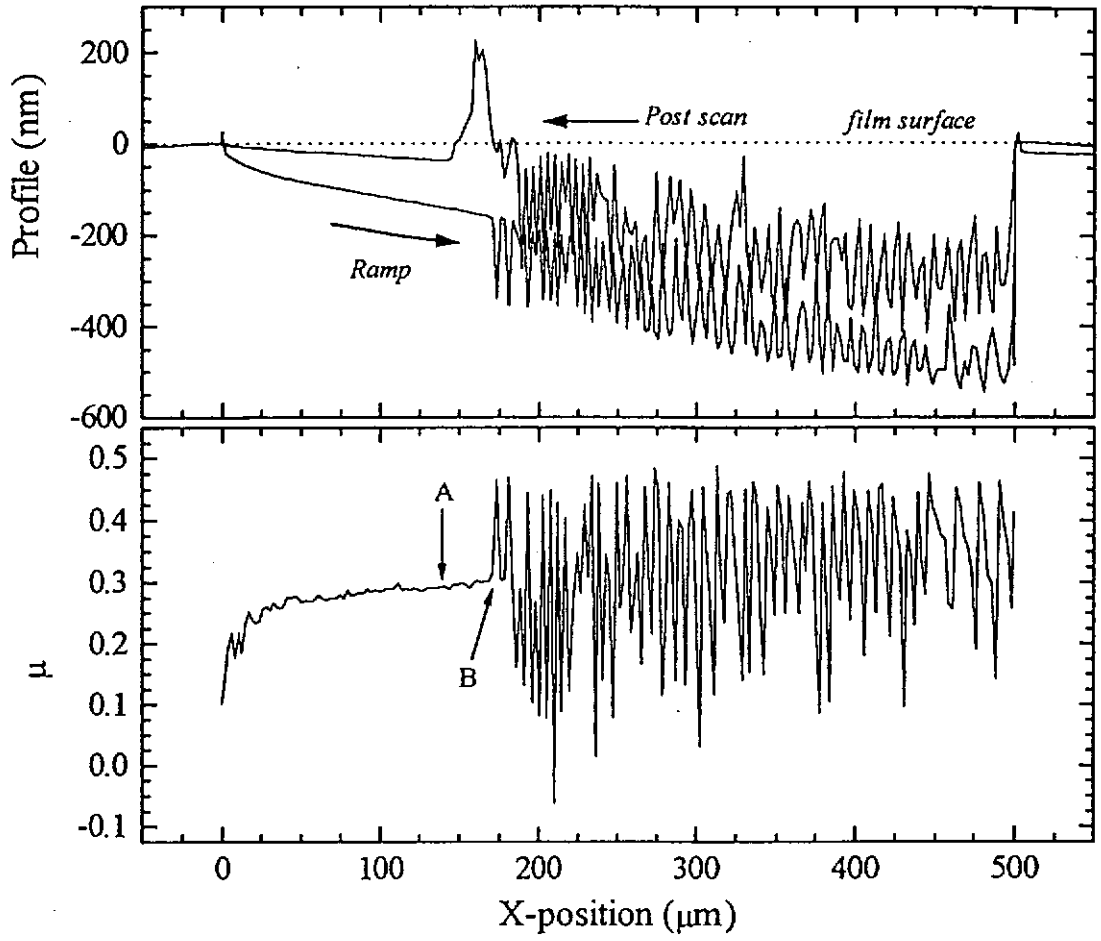

Fig. 4.11i Scratch profiles and micrograph of CN_x103: Carbon nitride film with 22.8 at.% N content

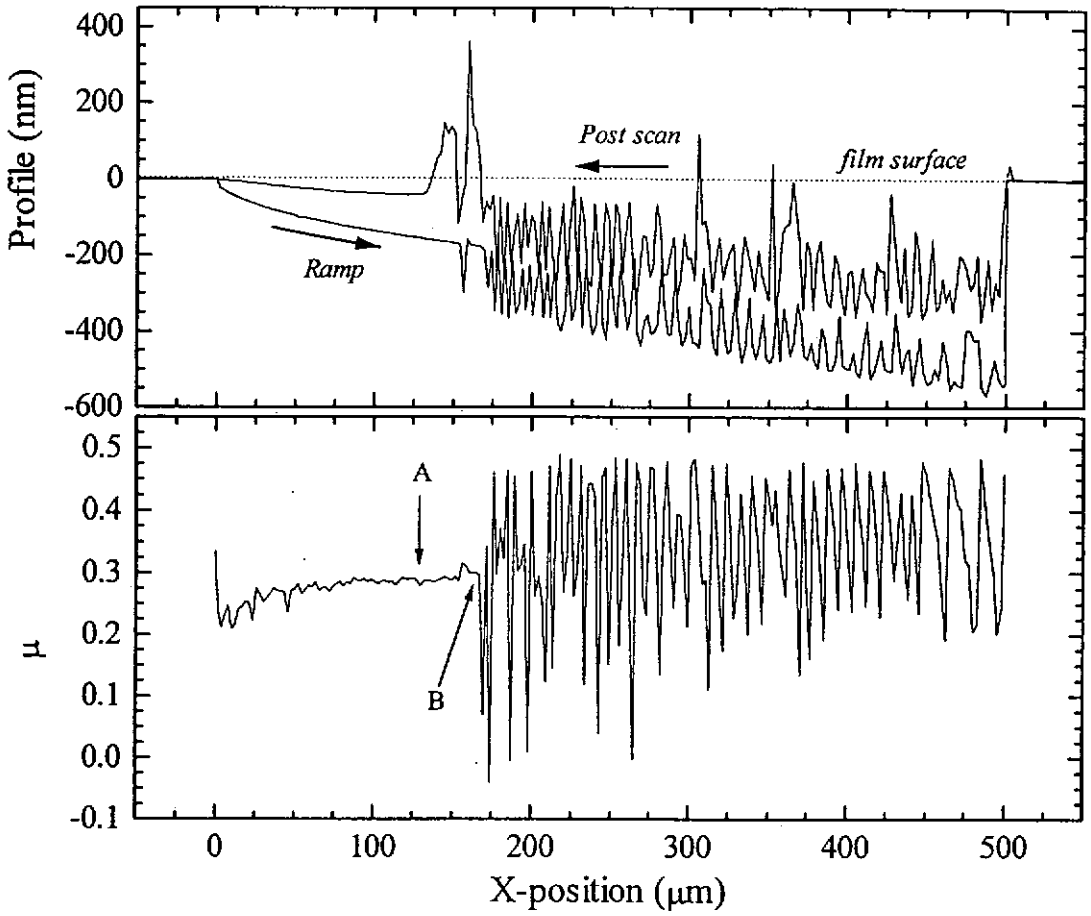

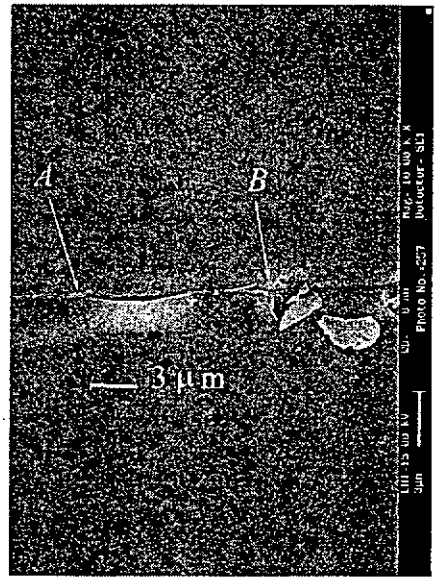

Fig 4.12 summarizes the trends of *DT* of the films against the N content. When the N content varies from 0 to 22.8 at.%, *DT* drops from 7.8 to ≈ 4 mN and that of pure carbon without ion assist is 11.5mN, which is the highest among all of the samples.

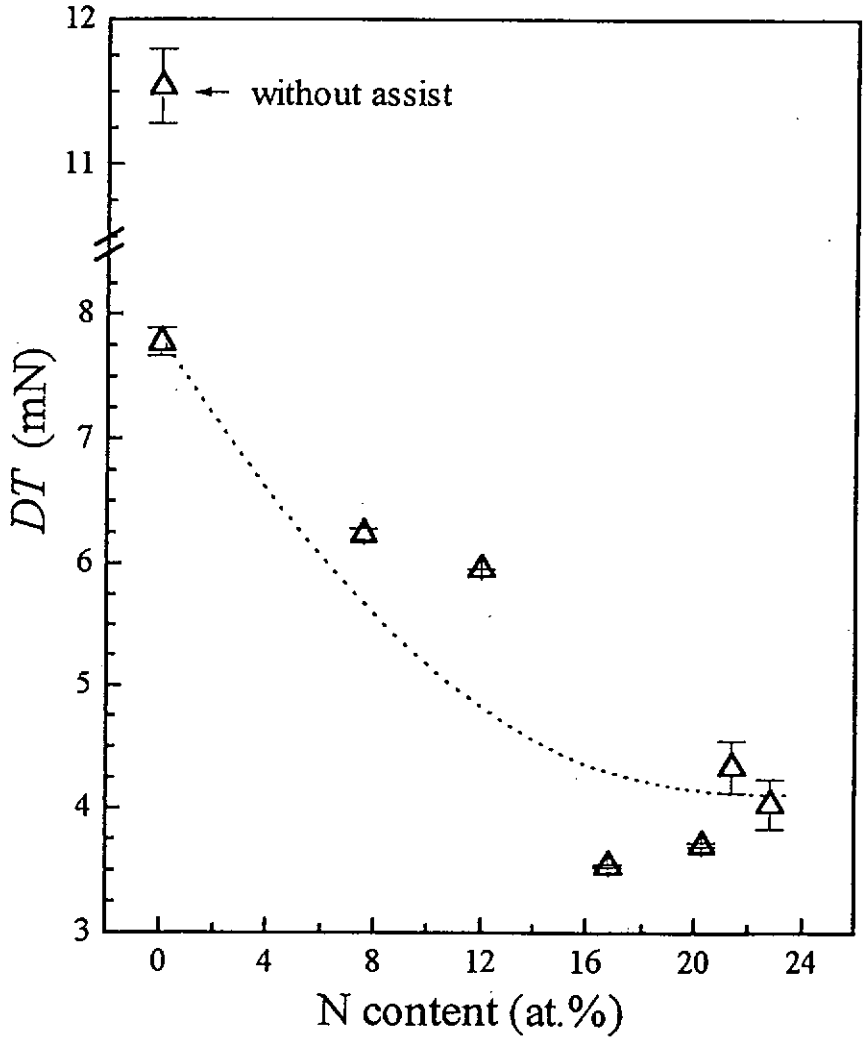

Fig. 4.12 *DT* as a function of the N content

With the drop in *DT*, *DT* falls farther behind *SDT* since *SDT* is more closely related to the Si substrate. The drops in *DT* enlarges the difference *SDT* - *DT* (in Fig. 4.13) from 0 to about 1.5 mN as the N content increases. Finally it is concluded that: 1) both the pure carbon films, especially the one without assist, is more diamondlike and brittle, 2) the incorporation of N causes the films to gradually become polymeric progressively, tougher and more ductile.

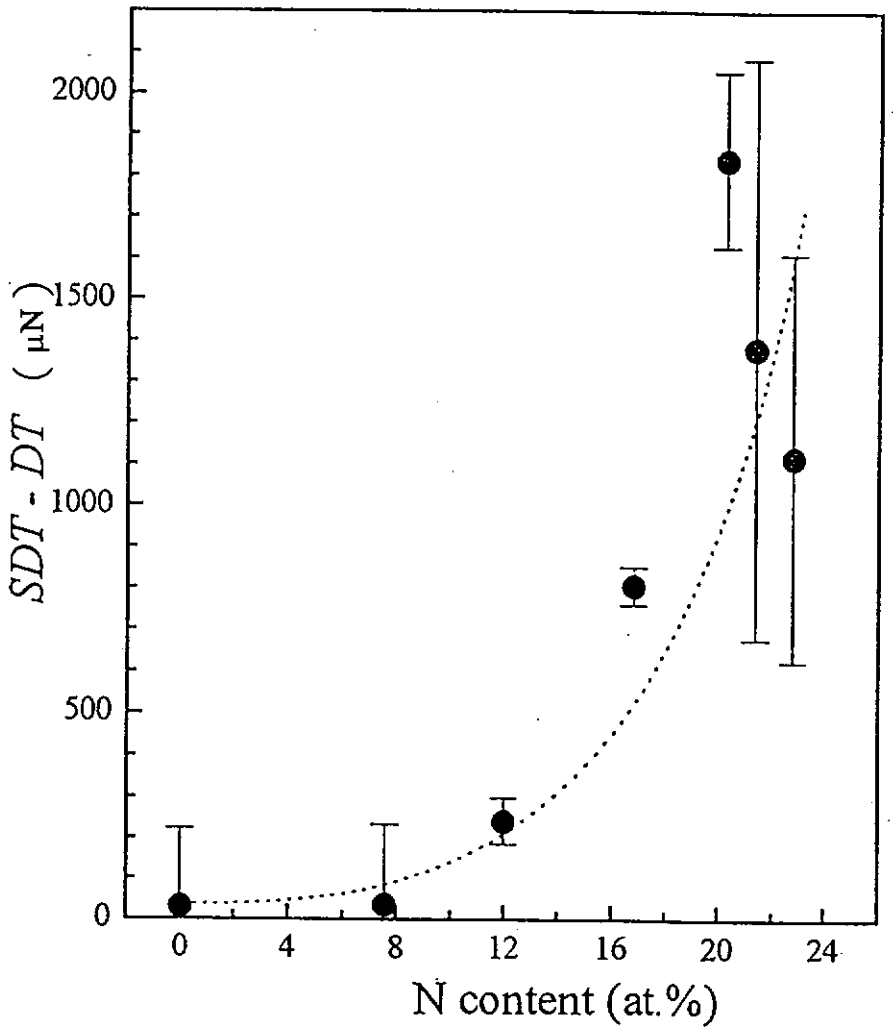

Fig 4.13 *SDT-DT* as a function of the N content

Wear and recoverage

On the left of *A*, namely the region before delimitation of the film occurs, the profile of the post scan could lie below the original surface (Fig. 4.14). The deviation is more pronounced with increasing N content, indicating that plastic wear occurs since the beginning of a scratch, and is more seriously as more N is added. For the carbon films, the profiles of the surface scan and post scan almost overlap with each other, showing that the wear are negligible for these films, because they contain rather high sp^3 fraction. The wear per unit normal load is defined as the vertical displacement *h* of the film surface being scratched from the original film surface, divided by the normal load *L* at a certain point (Fig. 4.14). The open diamonds and the open circles in Fig. 4.15 represent the wear per unit normal load *h/L* at point corresponding to a normal load of 3.01 mN (x-position = 100 μm), and a normal load of 2.26 mN (x-position = 75 μm) respectively. The *h/L* ratio basically rises with increasing N content and has a maximum of 18 nm μN^{-1}, showing that the wear resistance of the CN_x films with higher N contents are lower, consistent with the polymerization transition in the film structure.

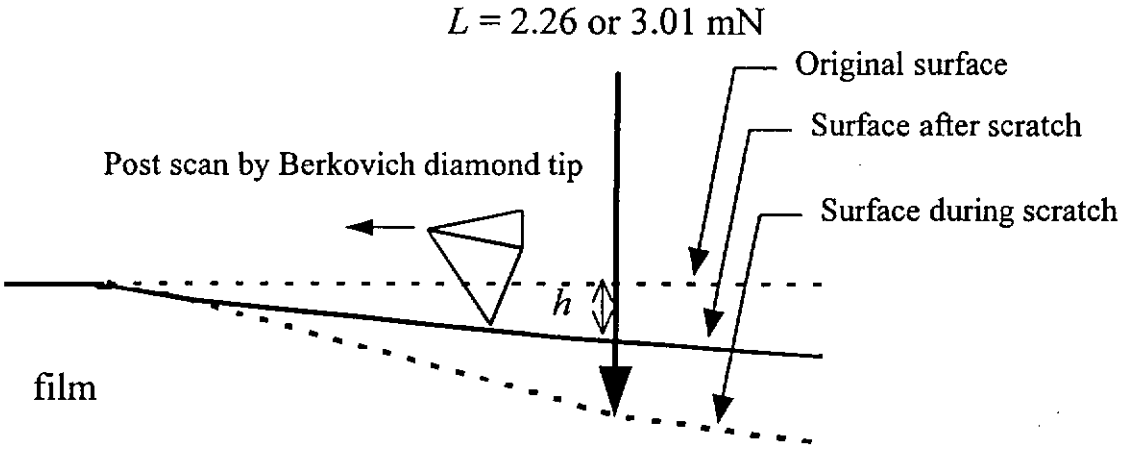

Fig. 4.14 Diagram showing the plastic wear of the film in a nanoscratch test.

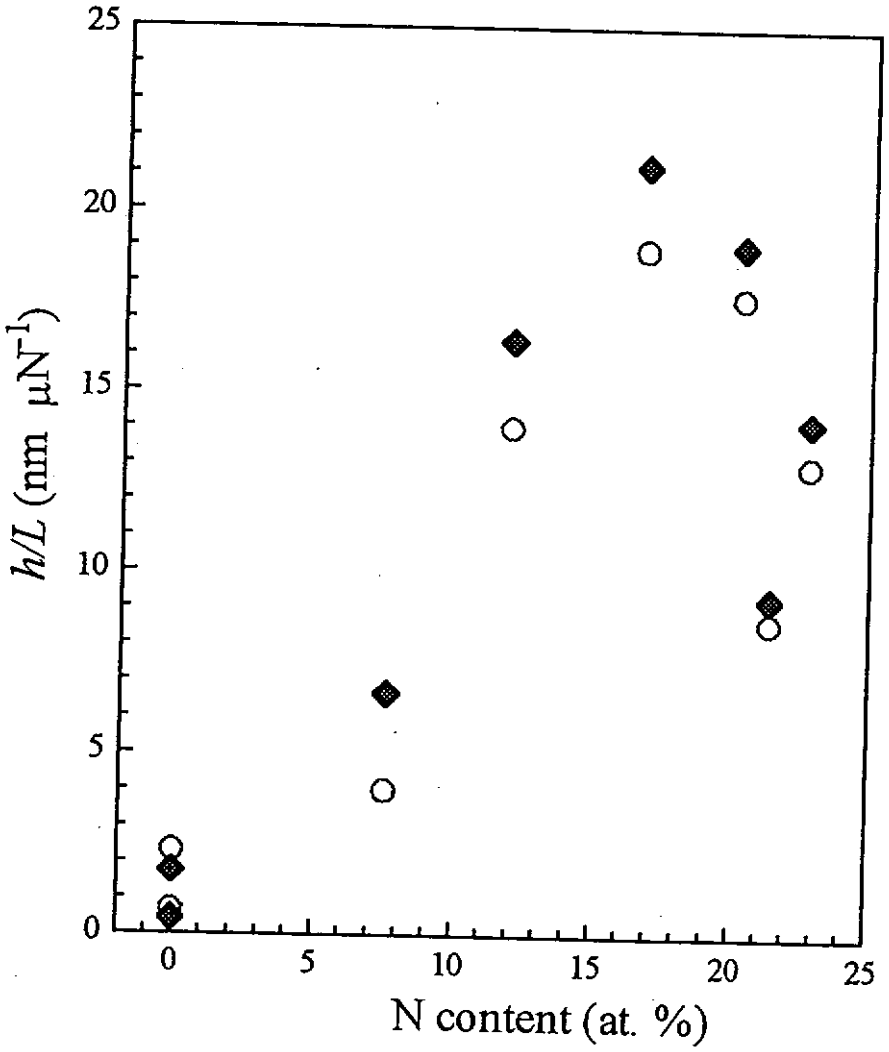

Fig. 4.15 *h/L* ratio as a function of the N content

○ at Load = 2.26 mN (x-position = 70 μm)

◆ at Load = 3.01 mN (x-position = 100 μm)

4.5 Thermal stability

As the flying height of the magnetic heads in the disk continuously reduces (≈ 50 nm) [3], collision between heads and disks could happen more frequent. Collision may generate some locally heated regions: The thermal stability of the pulse laser deposited (PLD) DLC were found to be not quit satisfactory, and would be graphitized when they experienced temperature ≥ 110 °C [46]. This experiment was carried out to investigate whether the CN_x films would have thermal stability better than that of the DLC films, and so the advantage of using CN_x film for replacing DLC films in magnetic head protective coating could be justified.

After rapid thermal annealing process, the samples were heated up at various temperatures between the room temperature (T_{rm}) and 400 °C. Each annealing lasts for one hour. Their properties were then characterized in order to evaluate their thermal stability. Table 4.9 shows that their electrical conductivity (σ) does not change with the annealing temperature.

Sample	f_{N_2}	σ T_{rm} (Ω^{-1} cm^{-1})	σ 70°C (Ω^{-1} cm^{-1})	σ 120°C (Ω^{-1} cm^{-1})	σ 200°C (Ω^{-1} cm^{-1})	σ 250 °C (Ω^{-1} cm^{-1})	σ 300 °C (Ω^{-1} cm^{-1})	σ 350 °C (Ω^{-1} cm^{-1})	σ 400°C (Ω^{-1} cm^{-1})
CN_x112	No	12.10	10.73	10.44	10.99	8.95	12.74	17.91	13.76
CN_x102	0	47.27	34.1	62.75	65.37	77.82	65.91	61.28	40.57
CN_x109	0.09	29.09	40.77	29.12	33.98	40.77	34.36	14.25	2.15
CN_x110	0.18	30.06	33.43	38.74	32.14	45.00	40.63	26.14	12.81
CN_x111	0.27	21.17	-	30.76	26.64	24.42	26.64	13.41	3.21
CN_x105	0.54	1.52	-	1.76	1.49	1.56	1.41	1.37	0.86
CN_x108	0.81	1.19	1.18	1.02	0.70	0.96	0.83	0.76	0.22
CN_x106	0.90	0.45	-	0.37	0.45	0.43	0.50	0.43	0.30
CN_x103	1.00	0.36	0.3	0.30	0.31	0.28	0.26	0.22	0.27

Table 4.9 The Electrical conductivity of the CN_x films after annealing at various temperatures

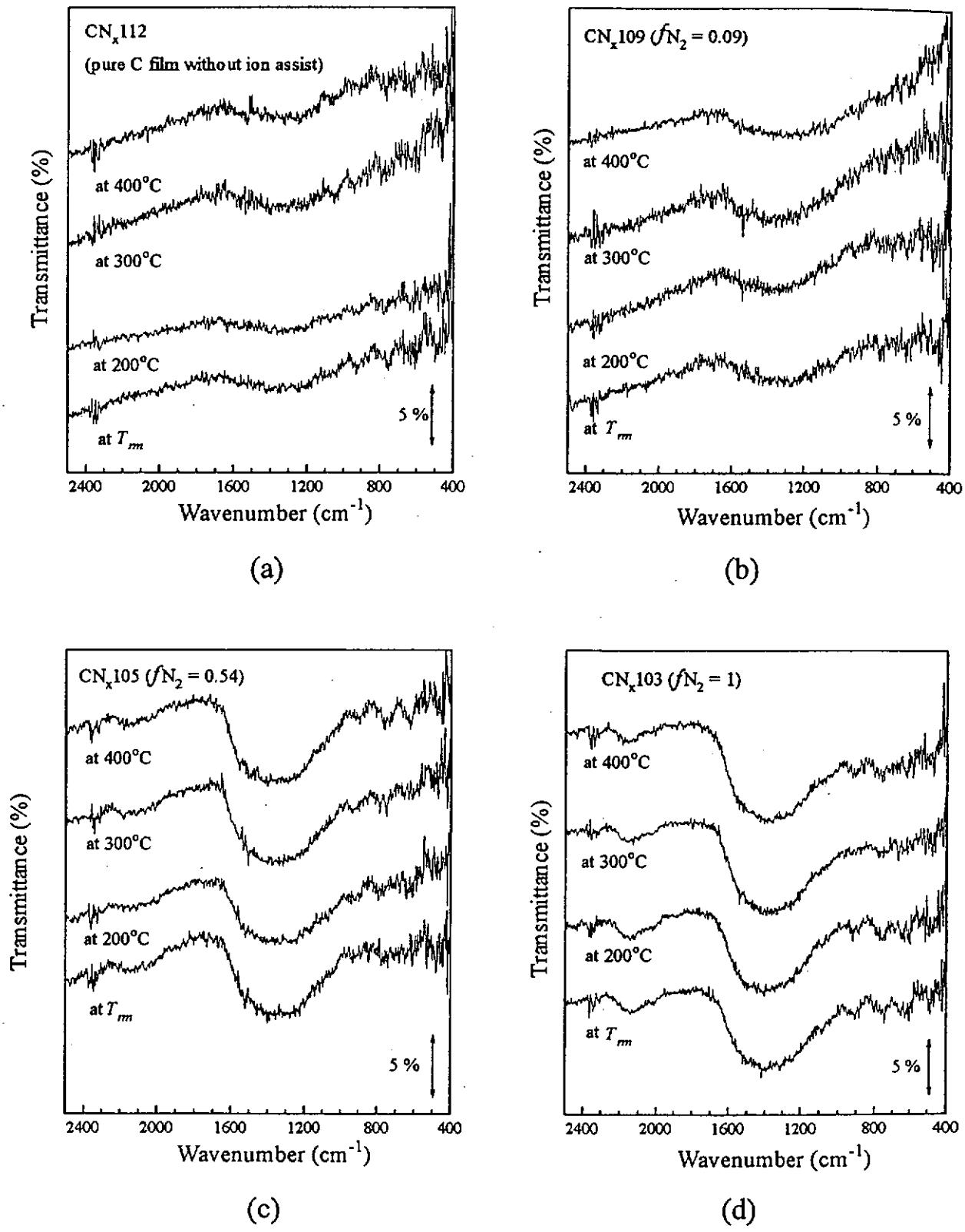

Fig 4.16 a-d . FTIR spectra of samples CN_x112 (pure C film without ion assist), CN_x109 (fN_2 = 0.09), CN_x105, (fN_2 = 0.54) and CN_x103 (fN_2 = 1) after annealing at various temperatures

Fig. 4.16 a-d show that the FTIR spectra of the films are basically not changed by annealing temperatures in range of room temperature to 400 °C. In particular, the results indicate the sample CN_x105 and CN_x103 still contain some N after annealing, because the absorption bands at 2100 cm^{-1} and 2000 cm^{-1} (associated with the -N=C=N- and C≡N bonds respectively) are still observed.

When the N content increases, although both *H* and *E* show higher thermal stability of at higher annealing temperature (Fig. 4.17 a and b), however, the magnitudes of *H* and *E* becomes smaller at the same time.

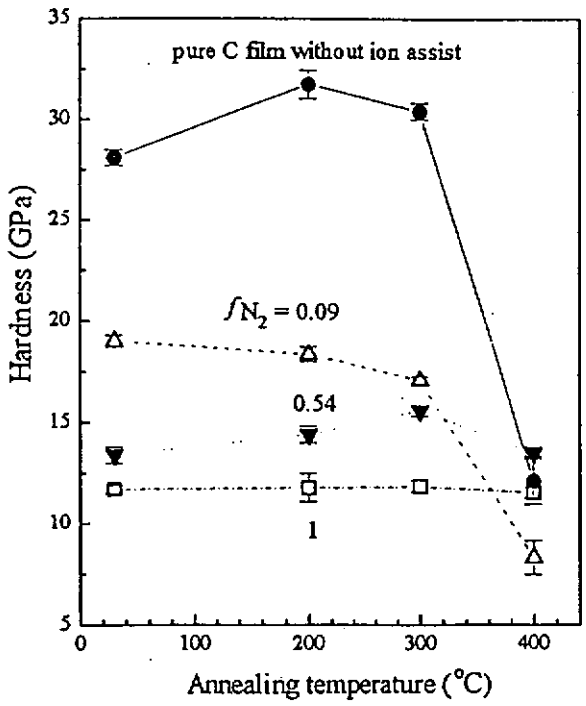

Fig. 4.17 a Hardness of the pure carbon film and the CN_x films as functions of annealing temperature.

●: CN_x112 (pure C film without ion assist), Δ : CN_x109 ($fN_2 = 0.09$),
▼: CN_x105 ($fN_2 = 0.54$), □: CN_x103 ($fN_2 = 1$).

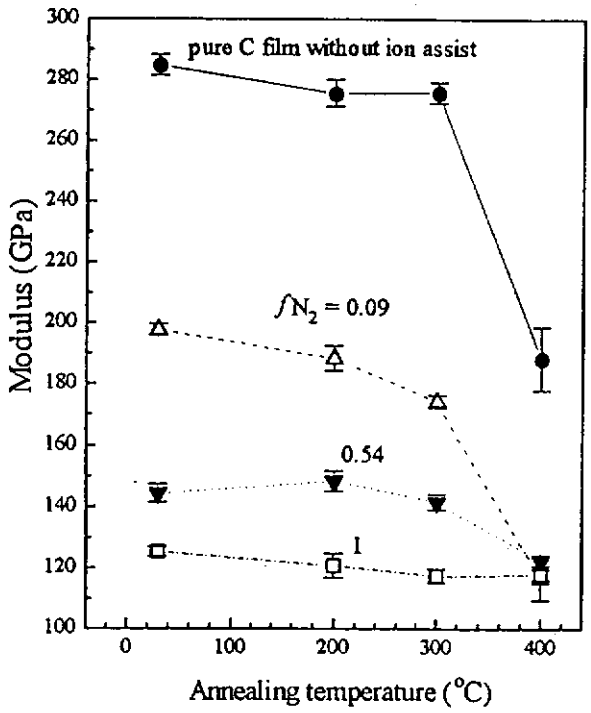

Fig. 4.17 b Elastic Modulus of the pure carbon film and the CN_x films as functions of annealing temperature.

●: CN_x112 (pure C film without ion assist), Δ : CN_x109 (fN_2 = 0.09),
▼: CN_x105 (fN_2 = 0.54), □: CN_x103 (fN_2 = 1).

Associated with the results in H and E, the friction coefficient μ of the films were measured as a function of annealing temperature. As shown in Fig.4.18, μ of the pure carbon film (deposited without ion assist) lies between 0.14 and 0.21 for annealing temperature ≤ 300 °C, but rises considerably to 0.26 after annealing at 400 °C. This change seem to occur in consistent with drop of H and E, and is attributed to the graphitization of the film structure. With increasing N content, one sees that the rise in μ after annealing at 400 °C is less obvious, possibly because the film structure is less affected by annealing due to the higher thermal stability induced by the incorporation of more N atoms.

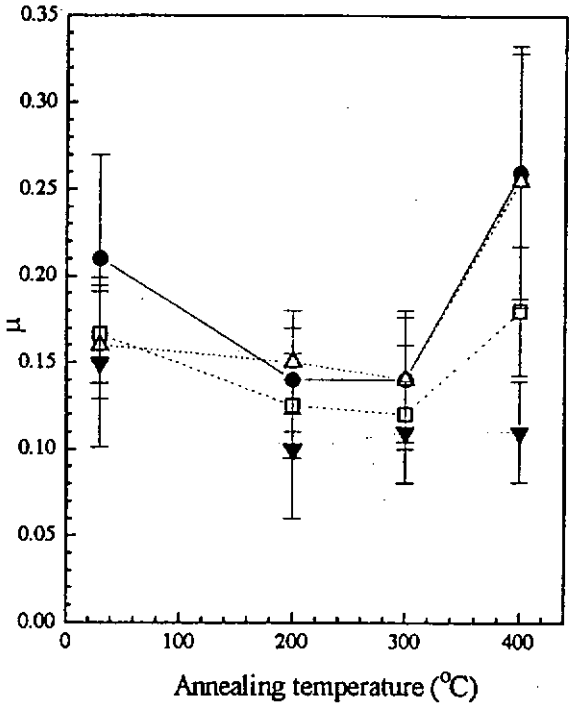

Fig 4.18 μ of the pure carbon film and CN_x films (at a normal load of 0.4 mN) as functions of annealing temperature

●: CN_x112 (pure C film without ion assist), Δ : CN_x109 (fN_2 = 0.09),
▼: CN_x105 (fN_2 = 0.54), □: CN_x103 (fN_2 = 1).

5. Hydrogenated DLC films Prepared by Electron Cyclotron Resonance and Direct-ion-beam Deposition

Mechanical properties of hydrogenated DLC films synthesized using an electron cyclotron resonance (ECR) system and a direct-ion-beam deposition (DID) system at SAE magnetics (H.K) Ltd. will be reported in this chapter. DLC films prepared by these two techniques are being used as be protective overcoats on magnetic recording heads in SAE.

5.1 DLC films deposited by electron cyclotron resonance

The hardness (H) and elastic modulus (E) of the hydrogenated DLC films deposited by ECR were listed in Table 5.1. For the convenience of discussion, H was plotted as a function of negative bias voltage (V_{dc}) in Fig. 5.1. For gas flow rates of CH_4 = 40 and 80 sccm, H and E are quit stable when $-150 < V_{dc} < -450$eV. Beyond - 450 eV, both H and E decrease with increasing the V_{dc}. One possible reason is that the high negative bias voltage accelerates positively charged particles to have high kinetic energies, which bombard and heat up the a deposit, enhancing the sp^2 fraction to grow. As a consequence, the values of H and E drop.

The enhancement of the formation of the graphitic sp^2 structure has been observed for our dual-ion-beam deposited carbon films (in section 4.3) if an Ar^+ assist beam is introduced, causing the substrate temperature to be risen from 90 to

110 °C. It is observed that the structure laser deposited DLC experiences a diamondlike-to-graphitic transition when the substrate temperature is increased to above 110 °C [46].

Sample code:	CH_4 flow (sccm)	V_{dc} (eV)	Hardness (GPa)	Modulus (GPa)
SAE27 *(S16)*	40	-150	26.2	213.6
SAE22 *(batch 9)*	40	-300	26.6	220.2
SAE23 *(S7)*	40	-450	25.3	201.6
SAE28 *(S10)*	40	-550	18.3	151.0
SAE30 *(S12)*	80	-150	25.4	279.3
SAE19 *(batch 8)*	80	-300	27.6	226.4
SAE21 *(batch 9)*	80	-450	25.6	204.7
SAE29 *(S9)*	80	-550	23.1	188.2

Table 5.1 Deposition conditions, hardness and elastic modulus of DLC films deposited by ECR

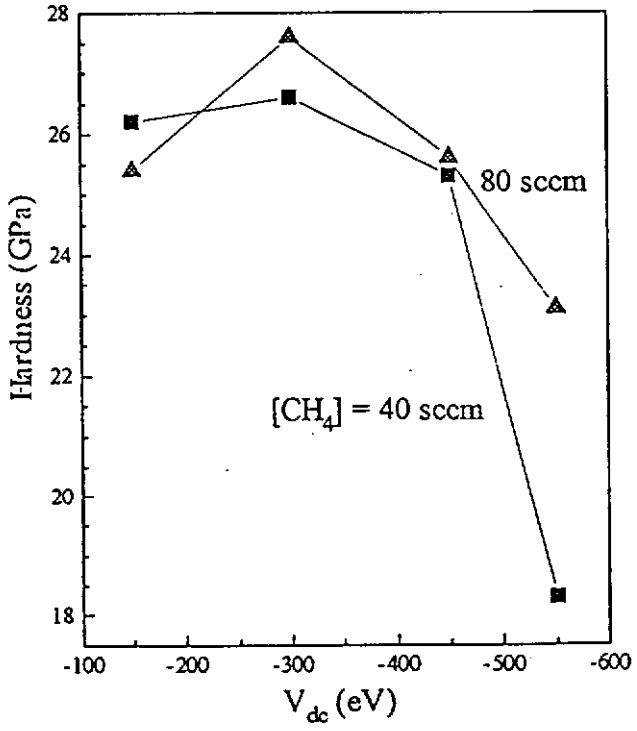

Fig 5.1 Hardness of ECR deposited DLC films against the bias voltage
■: CH_4 = 40 sccm and ▲ :80 sccm

Fig. 5.2 shows a typical profile of μ of the DLC films deposited by ECR along the scratch. The features of the profile are similar to these of the ion-beam-deposited CN_x films (refer to Fig. 4.9). In general, μ obtained from the constant load scratches (with normal load = 0.2, 0.4, 0.7 and 2.5 mN) and lamping-load scratches (with rates = 6 and 150 μN s^{-1}) are consistent. First, μ is not a constant during scratch, from around 0.1 to 0.3 when the normal load is applied from 0.1 to the value just before μ becomes fluctuating.

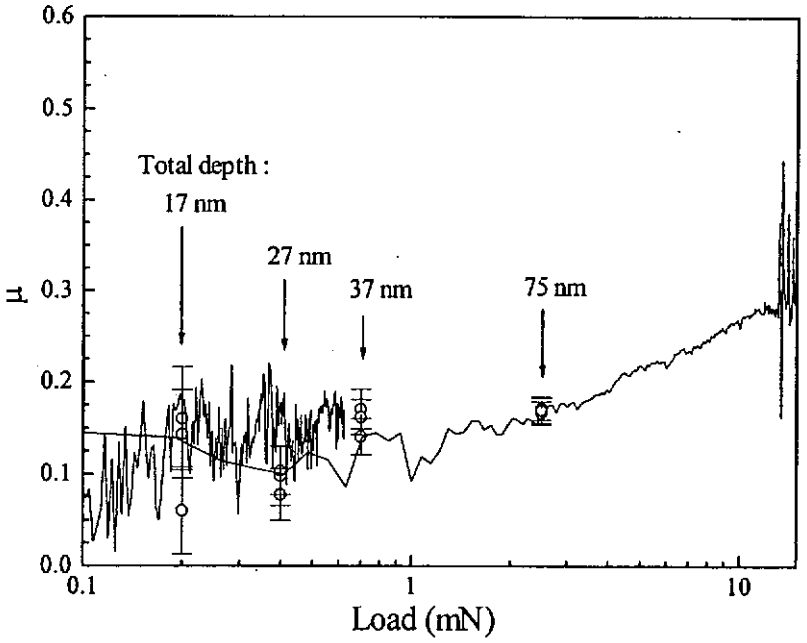

Fig. 5.2 μ as a function of normal load of DLC film SAE 19 deposited by ECR

Fig. 5.3 shows that the damage threshold (*DT*) of the DLC films drops with increasing V_{dc}. Since *H* also drops with increasing V_{dc}, it shows that a film with lower hardness also has a lower *DT*. One may compare the results with that of dual-ion-beam deposited (DIBD) carbons films and CN_x films. *DT* of the DIBD carbon film deposited without ion assist is 11.5 mN, rather close to those of the ECR films. However, both the DIBD carbon films deposited with Ar^+ assist and the CNx films have *DT* in the range of 7.8 to about 4.5 mN, which are lower than those of the ECR DLC films.

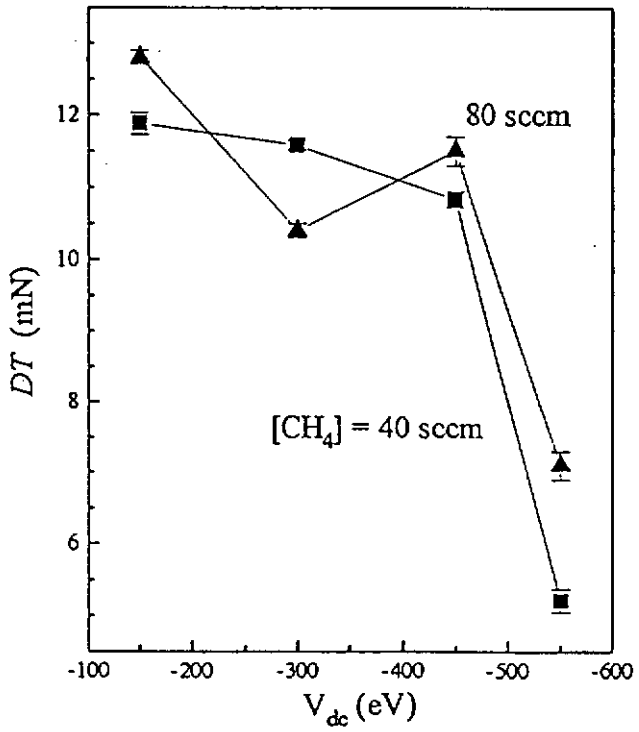

Fig 5.3 *DT* of ECR deposited DLC films against the bias voltage
■: CH_4 = 40 and ▲ 80 sccm

5.2 DLC films deposited by direct-ion-beam deposition

The deposition conditions, *H* and *E* of the hydrogenated DLC films deposited by direct-ion-beam deposition (DBD) are shown in Table 5.2. *H* of the films deposited at the ion beam current = 300, 360 mA and flow rate = 60, 70, 80 sccm are plotted in Fig 5.4 as a function of the ion beam energy. The results show that *H* drops from 21.4 to 16.1 GPa when the beam energy increases from 200 to 400 eV. This shows that the films deposited at higher beam energy is softer. The reason is similar. It is possibly because the bombarding species with high energies generate thermal spikes with higher temperature, enhancing the growth of high graphite sp^2 fraction. Fig. 5.5 shows a typical profile of μ, from which the damage threshold of the film is determined. Fig. 5.6 shows *DT* as a function of beam energy. Though the data seem to be scattered, one can still observed that DT tends to drops with increasing beam energy, accompanied by a drop in *H*.

Sample code:	Beam voltage (eV)	Beam Current (mA)	CH_4 flow (sccm)	Hardness (GPa)	Modulus (GPa)
SAE26 *(V8)*	200	360	60	20.4	157.6
SAE24 *(V3)*	250	300	60	19.0	155.4
SAE33 *(V4)*	350	300	60	17.1	132.3
SAE31 *(V2)*	350	360	60	17.3	129.6
SAE34 *(V11)*	400	300	60	16.1	124.8
SAE25 *(V18)*	200	360	70	19.2	158.5
SAE35 *(V22)*	200	360	80	21.4	169.1

Table 5.2 Deposition conditions, hardness and elastic modulus of DLC films deposited by DBD

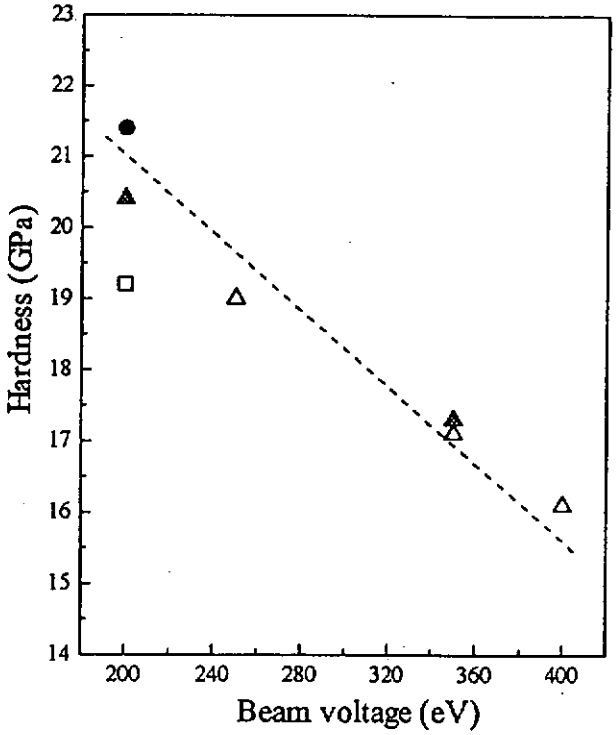

Fig. 5.4 Hardness of DLC films deposited by DBD against beam voltage, with the beam current and flow rate of CH_4 =
●: 360 mA, 80 sccm, □: 360 mA,70 sccm,
▲: 360 mA, 60 sccm, Δ: 300 mA, 60 sccm.

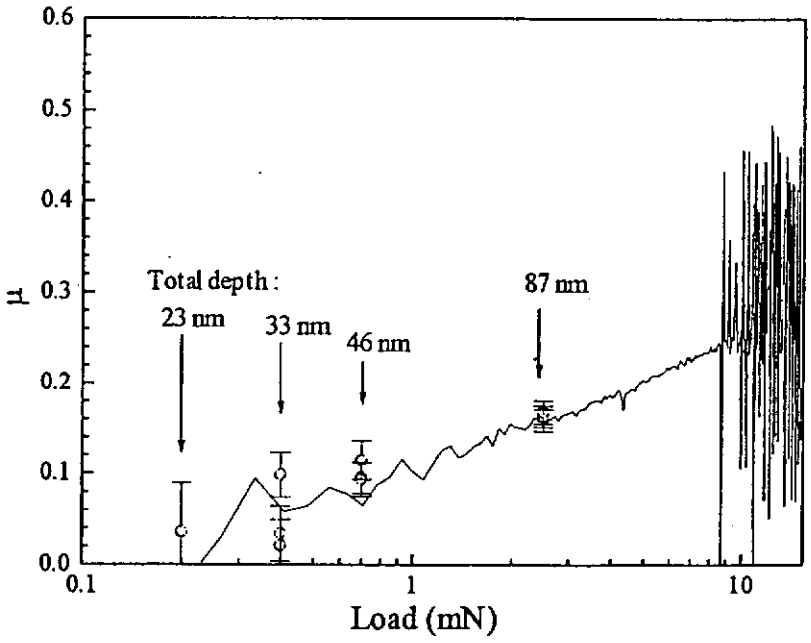

Fig. 5.5. μ as a function of normal load of SAE 26 deposited by DBD

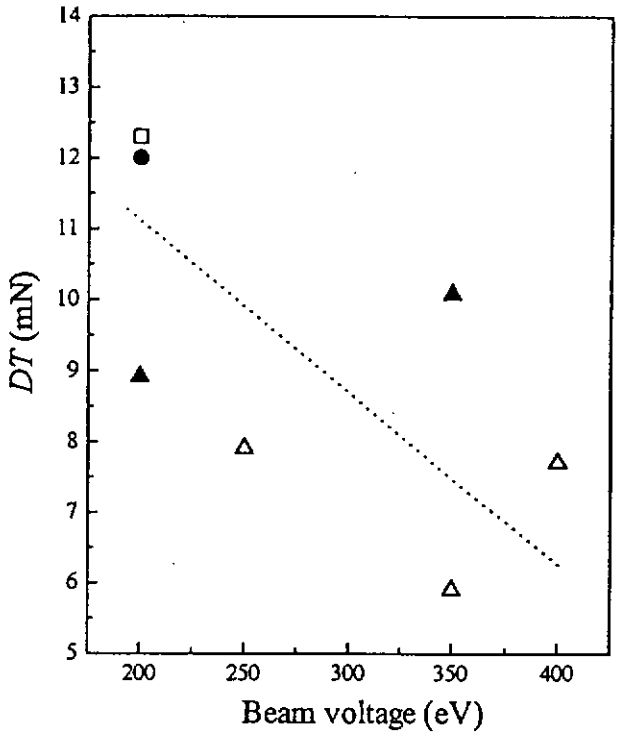

Fig. 5.6 *DT* of DLC films deposited by DBD against beam voltage, with the beam current and flow rate of CH_4 =
●: 360 mA, 80 sccm, □: 360 mA,70 sccm,
▲: 360 mA, 60 sccm, Δ: 300 mA, 60 sccm.

6. Results and Discussions of Other Films in Hard Coating Studies

Besides DLC film and CN_x film, various kinds of hard coatings are of current interest, and could have great application potential in surface protective overcoats on recording heads. They include 1) CN_x/TiN multilayers where Ti-N phase is introduced with the intention of forcing more N to incorporated into the C-N phase, 2) cubic boron nitride (c-BN), which is the second hardest substance just after diamond; 3) boron-silicon-nitrogen (B-Si-N) and boron-carbon-nitrogen (B-C-N) deposited at 620 °C, where Si and C are incorporated respectively to release the internal stress, 4) boron-carbon-nitrogen-oxygen films (B-C-N-O) deposited at room temperature. In this chapter, their mechanical properties obtained using nanoindentation techniques will be discussed.

6.1 CN_x/TiN multilayers

The CN_x/TiN films have layered structure consistent with the sequence of alternative deposition of CN_x and TiN layers. TiN layer was always the first layer to be deposited on the Si substrate since it is expect to have good adhesion to Si. Sample S1 and S6 are single layered CN_x and TiN films, which are used for references in this study. Sample S2 and S5 consisted of four layers (two CN_x/TiN periods). Both sample S3 and S4 had ten layers (five CN_x/TiN periods). All the CN_X layers adjacent to TiN layer(s) contained a noticeable amount of titanium (Ti), possibly coming from diffusion of titanium atoms crossing the

CN_x/TiN interfaces. As a result, the CN_x layers are practically composites of a C-N phase, a Ti-N phase and a Ti-C phase.

Sample	No. of layers	No. of CN_x/TiN periods	*Ts* (°C)	Deposition time (min)	total film thickness (nm)	d_{TiN}/d_{CN_x}	H (GPa)	E (GPa)
S1	1 (CN_x)	single layer	40	160	180	___	11.2	167.8
S2	4	2	40	40	150	2.7	13.7	172.5
S3	10	5	40	40	148	2.7	15.2	194.5
S4	10	5	40	40	170	7.5	19.0	211.5
S5	4	2	250	40	150	2.7	18.0	203.4
S6	1 (TiN)	single layer	40	40	210	___	21.0	224.5

Table 6.1 Hardness and Elastic Modulus of CN_x/TiN multilayers

Sample S1, the single-layer CN_x film, had the lowest hardness (11.4 GPa) among all of the samples. Its nitrogen content was as low as about 18 at.%, much lower than that of the predicted β-C_3N_4 phase. The value of *H* is close to that of the dual-ion-beam deposited CN_x film (CN_x103) with 22.8 at. % N determined to be *H* = 11.7 GPa (refer to Fig. 4.7). On the other hand, sample S6, the single-layer TiN had the highest hardness (22 GPa) which falls within the range of that reported for TiN films (22-69 GPa) [60].

Fig. 6.1 a and b show that both *H* and *E* increase with the volume fraction of TiN in the films. In particular, sample S2 with two TiN layers has higher *H* than that of sample S1, a single layer CN_X. The ten layers sample S4 has a higher ratio of TiN thickness to CN_x thickness (d_{TiN}/d_{CN_x} = 7.5) so that it

is harder than sample S3, which has a lower value of $d_{TiN}/d_{CN_x} = 2.7$. The data of E basically reproduced all of the features as shown in the plot of H. Furthermore, sample S3 is harder than sample S2, possibly due to a larger number of CN_x/TiN interfaces.

It is found that both H and E of sample S5 deposited at $T_s = 250^{\circ}C$ are higher than those of sample S2, deposited at room temperature. This is possibly because the diffusion of Ti atoms from the TiN layers to the CN_x layers is more enhanced at elevated substrate temperatures.

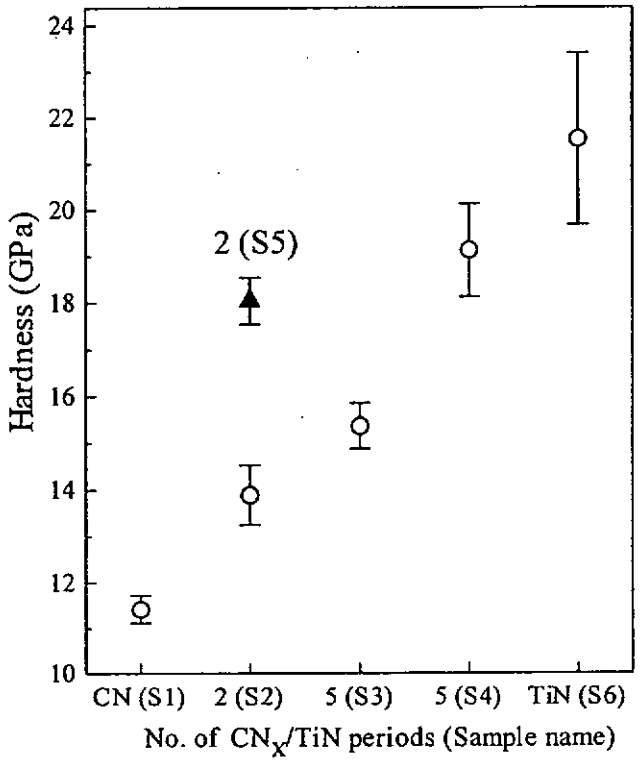

Fig. 6.1a Hardness of CN_x/TiN multilayers

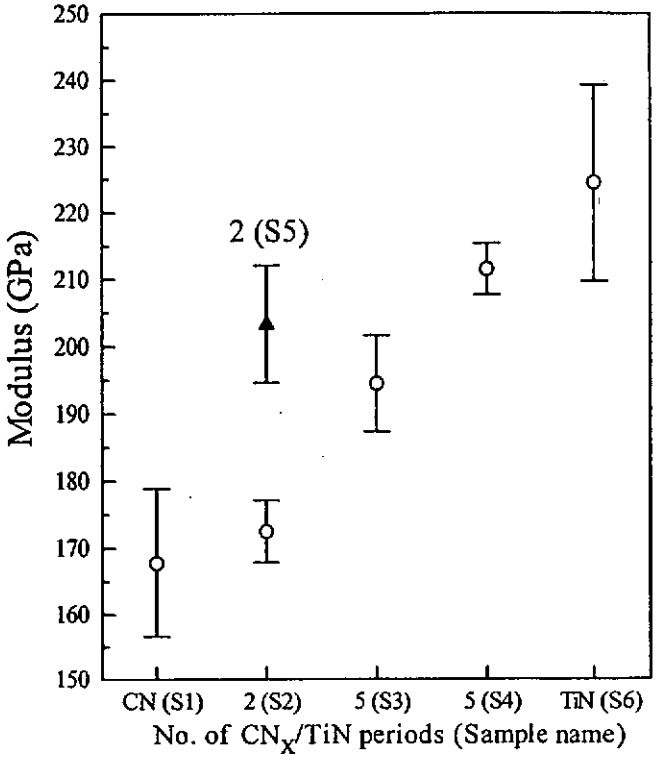

Fig. 6.1b Elastic Modulus of CN_x/TiN multilayers

6.2 Cubic boron nitride (c-BN)

BN films were deposited by ion beam sputtering of a B target 100mm in diameter at 620 °C. The films were found to contain a large fraction of cubic phase (c-BN) as revealed by a strong infrared (IR) absorption band at 1090 cm^{-1}, along with a hexagonal phase (h-BN) associated with an absorption band at 1400 cm^{-1}. The volume fraction of c-BN phase (ϕ_{cBN}) was estimated to be 70 vol % according to the expression proposed by Lu *et al* [61]: $\phi_{cBN} = \frac{I_C}{I_C + I_h} \times 100\%$, where I_c and I_h are the peak heights of the two corresponding bands at 1090 and 400cm^{-1} respectively.

Probably due to the high internal stress, the film peeled off completely about one or two days after deposition if no buffer layers was added. Even after adding buffer layer, c-BN film still completely peeled off from Si substrate, or partially peeled off from quartz substrate two weeks after deposition. Therefore the hardness measurements were carried out before the films peeled off.

The H value of a film dropped with the indentation depth, showing the influence from the deformation of the substrate. Therefore, the film hardness was obtained from the data of shallow indentations with depths of about 40 nm (≤1/5 of the top layer thickness), which was found to be 38 GPa, This is

comparable with the results reported by other authors [62]. The high H comes from the high volume fraction of the c-BN phase included in the films.

6.3 Boron-silicon- nitrogen (B-Si-N)

The next target is to improve the adhesion of c-BN films, to substrate. One idea is to add Si into the c-BN films. This is based on intuitive conjecture that Si atoms may combine with some N atoms to form a Si-N phase so as to release the internal stress. The high internal stress is the main cause for the c-BN to peel off. B-Si-N films are denoted as $(B_{0.5-x}Si_x)N_{0.5}$ films, thereafter, corresponding to the results of composition analyses that N content is fixed at about 0.5 while B and Si changed in the opposite manner. A B-Si-N film is composed of a BN buffer layer was deposited with ion assist at 200 - 360 eV (60 - 400 nm thick), and a top BN layer deposited with ion assist at 450 eV (200-720 nm thick) (refer to table 2.3). The buffer layer was in hexagonal (h-) structure so it has lower $H \approx$ 15 GPa and $E \approx 120$ GPa.

$x = 0$ refers to the c-BN films where the results have been discussion in the previous section. For small amount of Si ($x \leq 0.013$), the films exhibited good adhesion, implying that the incorporated Si has released part of the stress in the films. The most important point is that such a low level of Si incorporation is already sufficient to prevent the film from peeling off, while in addition the cubic structure of the c-BN phase is basically not affected, such

that the high hardness (≈ 38 GPa) and elastic modulus (≈ 227 GPa) are retained. (Fig 6.2 a and b).

For $0.013<x<0.067$, the c-BN phase was replaced by a h-BN phase, as verified by the growth of IR absorption bands at $1400cm^{-1}$. This is because the internal stress is further released to reach an extent that the cubic structure cannot be sustained [63]. This structural change was accompanied by the rapid reductions of H and E to 12 GPa and 123 GPa respectively.

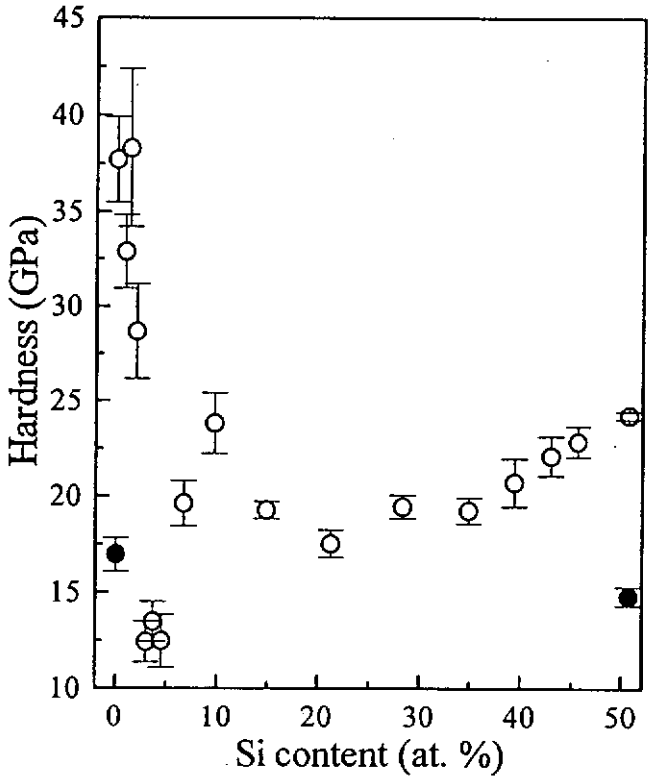

Fig. 6.2 a Hardness of the $(B_{0.5-x}Si_x)N_{0.5}$ films (○) and the buffer layers (●) vs. Si content.

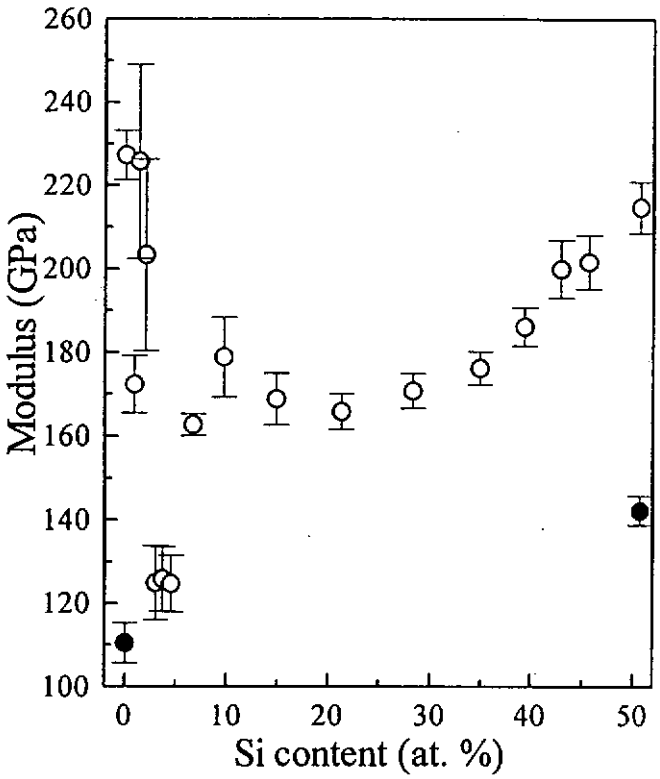

Fig. 6.2 b Elastic Modulus of the $(B_{0.5-x}Si_x)N_{0.5}$ films (○) and the buffer layers (●) vs. Si content.

When Si content was further increased, both H and E increased progressively from the minimum values associated with the h-BN structure towards the values of 24 GPa and 215 GPa respectively. It is noted that the value of H approaches that of silicon nitride films (29.4 GPa in Vickers scale) prepared by plasma-enhanced CVD as reported by Endler et al [64]. This can be attributed to the increase in the fraction of a Si-N phase in the films. Si-N is a strong bond, and so Si_3N_4 is well known as a practically useful hard material.

6.4 Boron-carbon-nitrogen (B-C-N)

In the study of $(B_{0.5-x}Si_x)N_{0.5}$ films, it is attempted to reduce the high stresses in c-BN films to improve their adhesion via addition of Si. Considering an alternative carbon (C), which is similar to B, N and Si and may be able to form sp^3 hybridization, so that it is possible to replace B or N in the zinc-blende structure of the c-BN phase. Since a C atom (0.914 Å) is smaller than a B atom (0.98 Å), so if C atoms can really replace some B atoms in the c-BN structure, the compressive stresses in the B-C-N films could be reduced more effectively, eventually facilitating the improvement of the film adhesion.

To prepare a sample, a B-C-N buffer layer was deposited first with ion assist at 200 - 360 eV (Table 2.3). Then a top layer was deposited with the conditions of T_s = 500 °C and ion assist at 450 eV (refer to Table 2.3). The thickness of the top layers and the buffer layers were found to vary in the ranges of 186 - 229 nm and 70 - 127 respectively. The C content in the B-C-N films was controlled to vary from 3 to 11.8 at. %. For most of the films, the ratio of B to N was about 1.

For C content ≤ 6.2 at. %, the film structure was dominated by a c-BN phase along with high H and E in the range of 36 - 37 GPa and 280 - 320 GPa respectively. When the C content was increased to exceed a threshold value of around 6.2 at. %, both the values of H and E dropped (Fig. 6.3 a and b). It is thereby suggested that when the C content is higher than 6.2 at. %, the internal stress in the films was reduced to an extent that the c-BN phase could not be sustained, eventually leading

to the disruption of the c-BN structure and the formation of the h-BN structure. Under existence of high internal stresses the low C-containing films peeled off quickly from substrates after exposure to air. After the release of the stress by addition of C, the film adhesion is greatly improved as a result.

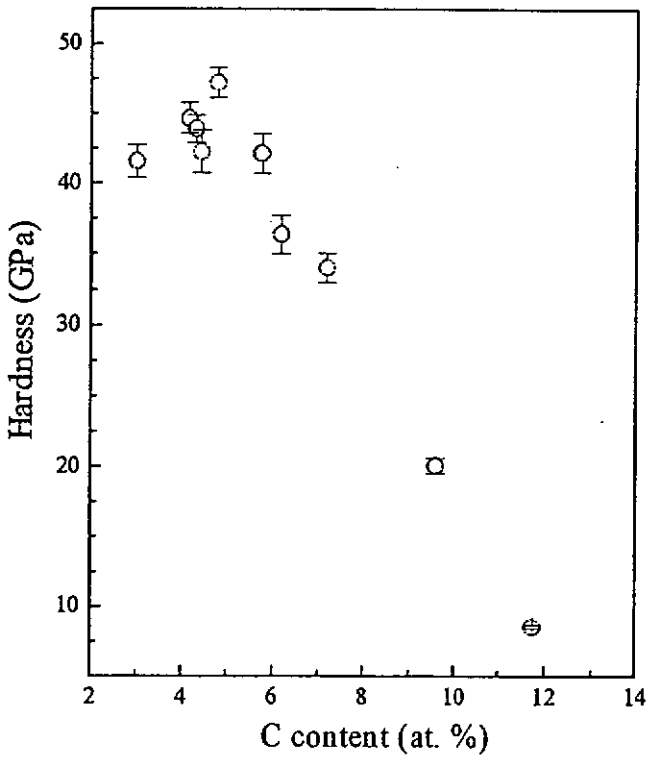

Fig. 6.3a Hardness of B-C-N films as a function of Si content.

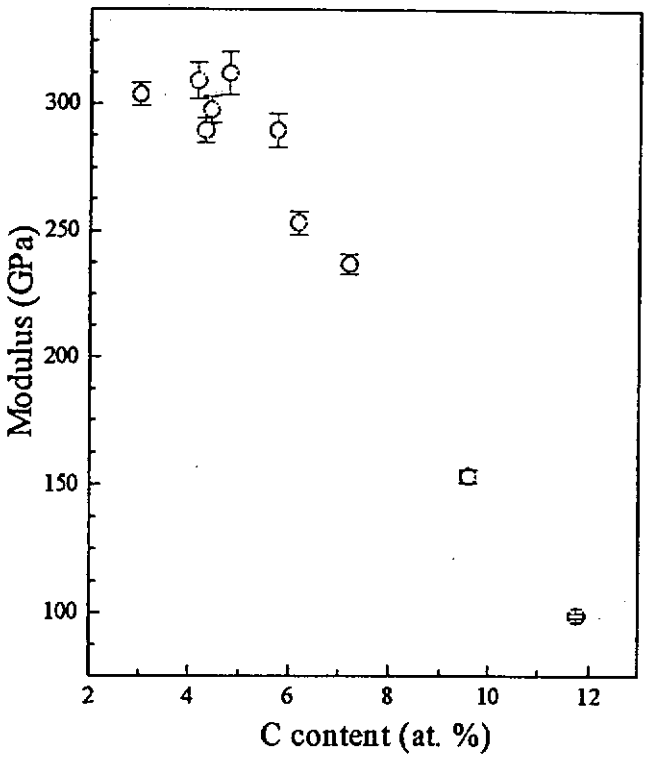

Fig. 6.3b Elastic modulus of B-C-N films as a function of Si content.

6.5 Boron-carbon-nitrogen-oxygen films (B-C-N-O)

In this work, ternary B-C-N films were prepared at room temperature. The B-C-N system is particularly interested because it is proposed to contain some superhard phases.

The film thickness was determined to range from 38 to 390 nm. The B content in the films was controlled by varying the area fraction of B on the sputtering target (B_{area}) from 0.14 to 0.86. Fig. 6.4 shows the relative contents of the four elements as functions of B_{area}. First of all, the C content dropped monotonically

from 82.3 to 4.1 at. % as B_{area} increased in the range shown. Second, the B and N contents increased with increasing B_{area}, and reached peak values of 37.5 and 2.5 at. % respectively, while the oxygen content remained low. For further increase in B_{area}, the change of B content became mild. Meantime, the content dropped, but the oxygen content rose promptly instead. Eventually, the O content saturated at a value as high as 60 at. %, although it was not added during deposition. In view of such a high O content, it was thereby more appropriate to denote the films as B-C-N-O films. In several reports [65-67], some oxygen content ranging from 5 - 32 at. % was found in the synthesized B-C-N materials although oxygen was not added on purpose. For this case, it is suggested that it should come from the oxygen residue in the chamber.

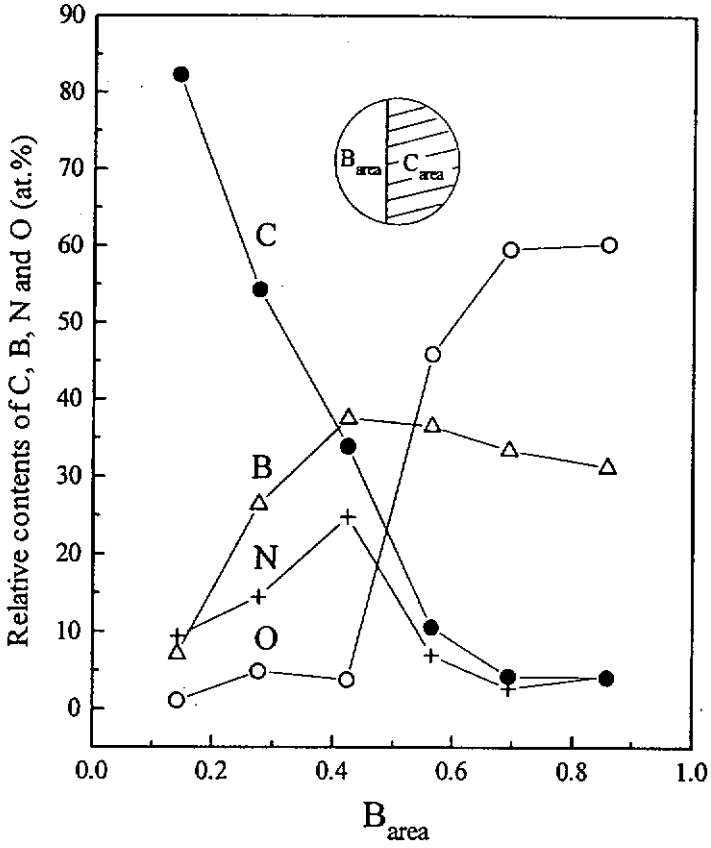

Fig. 6.4 Relative contents of the B-C-N-O films vs. B_{area}

C (●), B (Δ), N (+) and O (○).

The XPS spectra of the elements were investigated to reveal the chemical structure in the films as a function of composition. As shown in Fig 6.5 a, the C 1*s* spectrum of a film with 82.3 at. % C was fitted by a C^1 and a C^2 components. The C^1 component at 284.5 eV was ascribed to the C-C bonds in the graphitic structure. The C^2 component at 285 eV was smaller and can be assigned to come form those C atoms involved in the C-N bonds. For lower C content, the relative fraction of the C^2 component became larger, showing that a larger fraction of C atoms were involved in the C-N bonds.

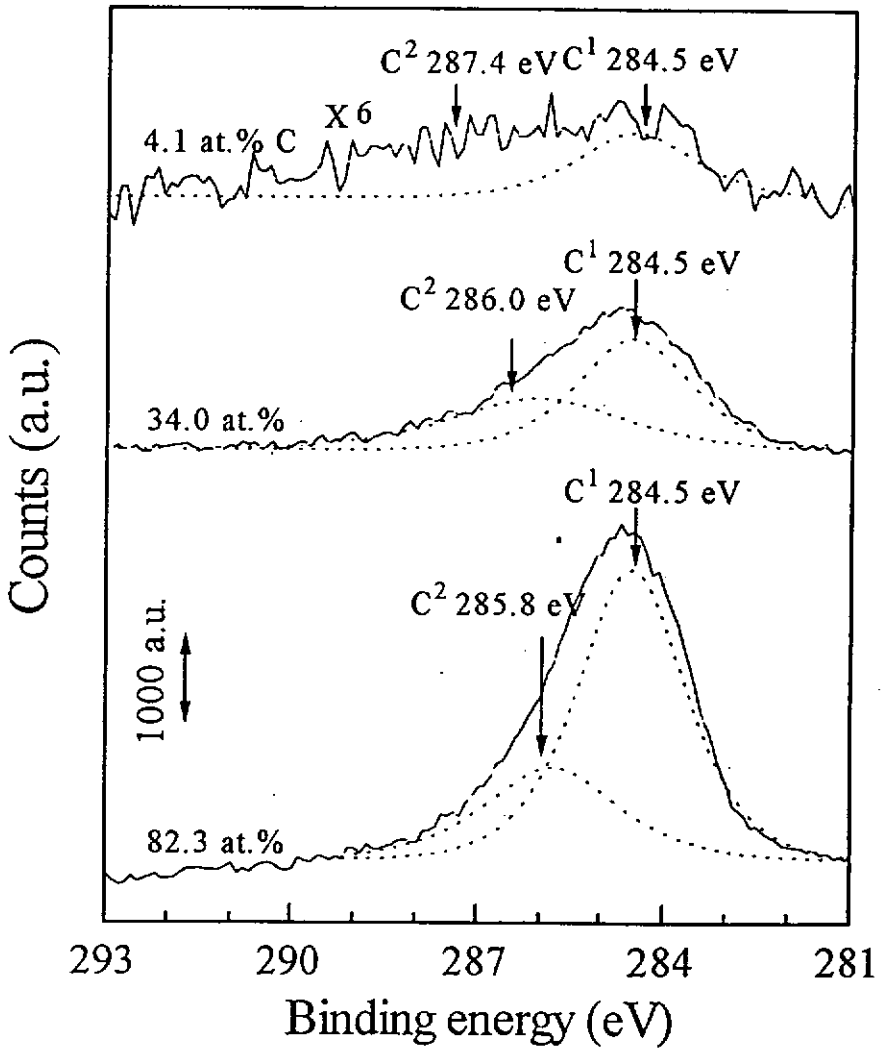

Fig. 6.5 a C 1*s* spectra of the B-C-N-O films with various C contents

Next, the XPS spectra of the B 1*s* electrons was shown in Fig. 6.5 b. For the film with 82.3 at. % C, the spectrum had a peak energy of 190 eV, accompanied by the appearance of a N 1s peak at 398.8 eV. They are close to those of the h-BN structure at 189.8 and 398 eV respectively [67], suggesting that the B and N atoms in the film combine mainly to give a h-BN phase. When the C content is further

reduced, the peak of the spectra shifts to higher binding energies, approaching that of the B_2O_3 structure at 193 eV [68]. Meantime, the O content rose noticeably with concomitant reduction in the N content, leading one to infer that a B-O phase grew progressively and eventually dominates the films structure, whereas the h-BN phase diminishes at the same time.

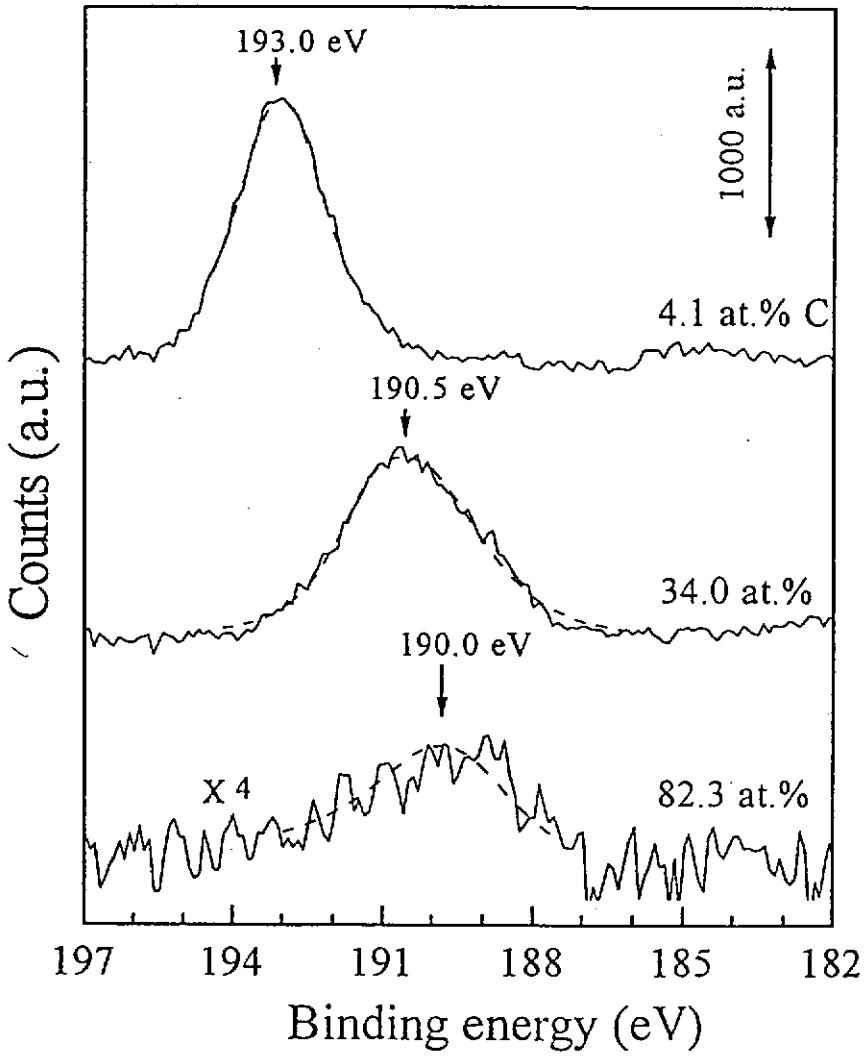

Fig. 6.5 b B 1*s* spectra of the B-C-N-O films with various C contents

From the structural analyses, it is concluded that when the C content in films drops, the film structure is first mainly graphitic, and then a h-BN phase grows, and finally a B-O phase dominates. With these changes, the values of H and E of the film with 82.3 at. % C content are equal to 10 and 93 GPa respectively (Fig. 6.6 a and b), lying below those ranges of DLC (12 - 40 and 140 - 300 GPa) prepared using various techniques [69-70].

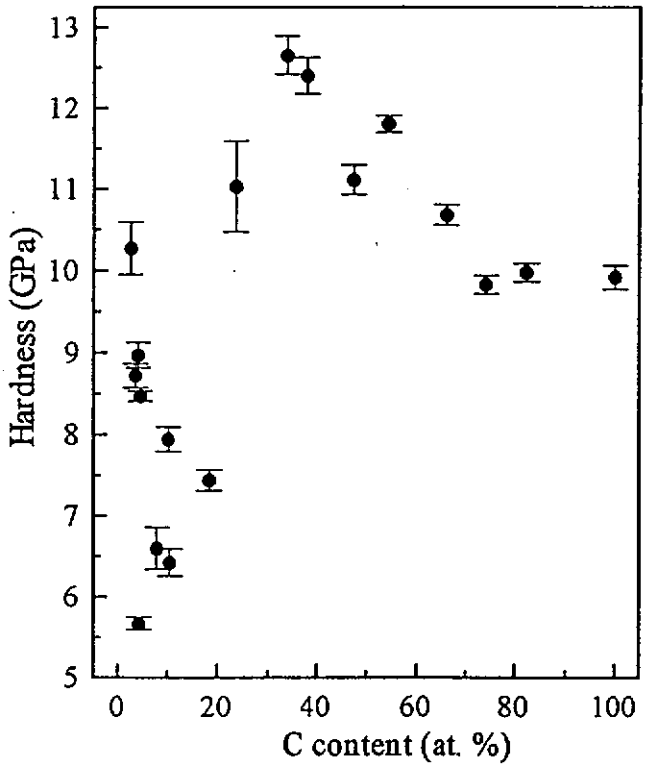

Fig. 6.6a Hardness of B-C-N-O films as a function of C content.

In particular E of this film is the lowest among those of other samples. Such a moderate value of H and low value of E are closely related to the graphitic structure of the film as detected. When the C content drops from 82.3 to 33.9 at. %, H and E rise gradually and reach peak values of 12.7 and 127 GPa, respectively.

This change is associated with the B and N contents, and the growth of the volume fraction of the h-BN phase. It is noted that the peak values of H and E are comparable with those of h-BN films at 17 and 111 GPa respectively (refer to Fig 6.3 a and b). For further decrease in the C content from 33.9 to 10 at. %, both H and E reduce prominently from the peaks and eventually reach dip values of 6.4 and 113 GPa. These trends occurred possibly because the O content is still low, such that the B-O phase has not been formed and the films are still in the h-BN structure and are soft. Finally, when the C content < 10 at. %, the B-O phase is formed and significantly influences the film properties, such that H and E rose again from the dips, and finally approach the values of 10.3 GPa and 132.5 GPa respectively.

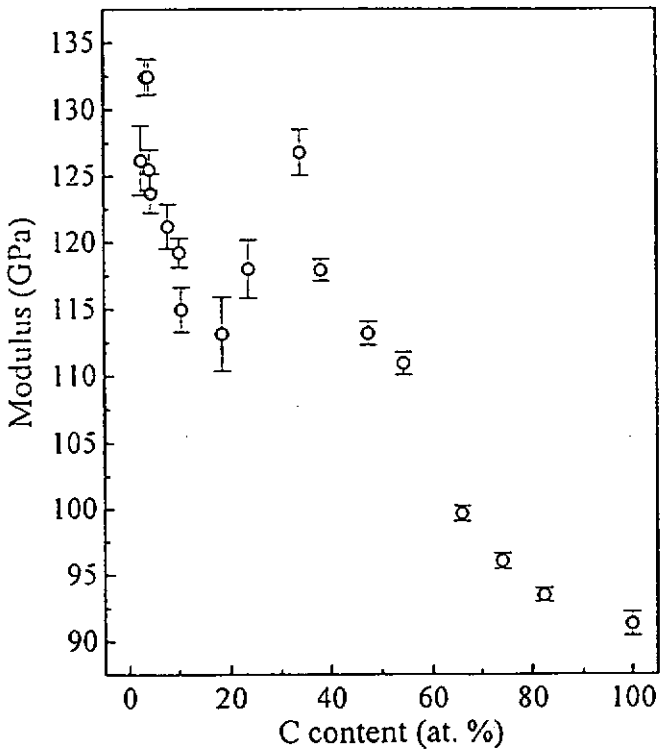

Fig. 6.6b Elastic modulus of B-C-N-O films as a function of C content.

This result leaves a problem of why the films contain up to about 60 at% O, although it was not intentionally added. An explanation for high O content was proposed. As the ultimate pressure, P, in our chamber reaches 1×10^{-6} Torr, the residual oxygen molecules from the background ambient impinge the substrate surface with a rate $\phi = P/(2\ \pi m k_B T)^{1/2}$, where T is the temperature (about 300 K), m is the mass of oxygen molecule (about 5.3×10^{-26} kg) and k_B is Boltzmann's constant. ϕ is determined to be 3.54×10^{14} molecules cm^{-2} s^{-1}. For close packing, there are $N_s = 8.6 \times 10^{14}$ oxygen molecules for each layer, if the effective diameter of an oxygen is set at 36.4 Å. Assuming that the sticking probability of the impinging oxygen molecules is about 1 when the C content in a film is low, there will be $\phi / N_s \approx 0.4$ layers of O incorporated into the growing films, giving a growth rate of 1.5 $Å s^{-1}$ which is comparable with the maximum overall coating rate (0.7 $Å s^{-1}$) among the film samples in the series.

6.6 Discussions about other films as overcoats on magnetic heads

Some data of the mechanical properrties of various hard coating materials such as CN_x/TiN multilayers, c-BN, B-Si-N, B-C-N and B-C-N-O were discussed above. Are they suitable for protective overcoats on recording heads? Even the cubic boron nitride (c-BN), boron-silicon-nitrogen (B-Si-N), boron-carbon-nitrogen (B-C-N) are very hard, there are still some difficulties in applying them as hard coating materials. It is becuase films with high hardness were synthesized at 620 °C, while at such a high temperature the heads would be damaged. Moreover they need buffer-layer to achieve good adhesion to substrate, so the total film thickness must not be less than thickness of overcoats currently deposited on magnetic recording head (≈ 8 nm). The B-C-N-O films were deposited at room temperature, but they have much lower hardness (6-13 GPa) comparing with that of the B-C-N films deposited at 620 °C . The CN_x/TiN multilayers, though exhibit good mechanical properties, consist of many layers and so cannot be thin enough to suit the requirements as protective coatings on heads and disks.

Chapter 7. Conclusions

The protective overcoats on recording devices are essential for highly reliable memory storage. For the demand of higher storage density, the head/disk separation is minimized, such that accidental collisions between them occur more frequently. Furthermore, when the drive starts and stops, the head-slider must be in contact with the disk so wear is induced. Therefore hard protective overcoats are generally prepared on head-slider is to prolong the lifetime of the head which is usually made of soft magnetic material.

Hydrogenated diamondlike carbon (DLC) discussed in chapter 5 is presently the most important protective coating material on head in industrial production. Recently, a new coating material carbon nitrate (CN_x) has been suggested for replacing DLC. In this study, the most interesting objective is to know how the structure and the mechanical properties of CN_x depend on the N content in the material.

The preparation parameters of the CN_x film were kept as constants, and the fractional flow rate of nitrogen $[N_2]/([Ar]+[N_2])$ in assist ion gun only was varied from 0 to 1, such that the fraction of the nitrogen ion species in the assist beam was controlled systematically from 0 to 100 %. Accordingly, the N content in the films increased from about 0 to 22.8 at.%.

It is verified that the increase of the N content in the dual-ion-beam deposited CN_x films induces a diamondlike-to-polymeric structural transition. As consequences, the films with higher N content have lower conductivity (σ), lower hardness (*H*), lower damage threshold (*DT*), weaker adhesion to Si substrate, and possibly have high toughness and ductility.

These results have important practical meaning, because the film properties can be tailored by controlling the level of N incorporation. σ of the coating material on a head-slider should lie in a suitable range. If σ is too high, the coating cannot electrically isolate the head (e.g. magnetoresistive head) and disk, leading to failure in signals. If σ is too low, some static charges may be accumulated on head/disk surfaces, causing dielectric bread down.

Although a higher *H* facilities to suppress wear of the surfaces sliding against each other, however, if one surface has a lower *H*, it will be worn much faster. Therefore, it is important for hardness of CN_x films to be adjustable, and the range of *H* (24.3 - 11.7 GPa) is found to be appropriate for the application in protective coatings on magnetic heads. Furthermore, CN_x films with higher N content are less brittle, consequently suppress the formation of debris, and prolong the lifetime of the head. The friction of all the CN_x films is as lower as that of the hydrogenated DLC films. Low friction favors the reduction of stiction, which is the resistant applying of the medium by the head during starting the drive. In the future,

more work has to be done to investigate the performance of the drives with CN_x as protective coatings, such that the advantages of using CN_x films can be compared with that of DLC films, which are commonly used at present.

In addition, some other hard coating materials were discussed to be protective overcoats on recording head (in the chapter 6). Although the cubic boron nitride (c-BN), boron-silicon-nitrogen (B-Si-N), boron-carbon-nitrogen (B-C-N) are very hard, there are still some difficulties in applying them as hard coating materials. The reason is that the films with high hardness were synthesized at 620 °C, while at such a high temperature the heads would be damaged. Moreover they need buffer-layer to achieve good adhesion to substrate, so the total thickness must not be less than current thickness in production (≈ 8 nm) . The CN_x/TiN multilayers, though exhibits good mechanical properties, consist of many layers and so cannot be to thin to suit the application in magnetic heads and medium causes film too thick.

List of publications

C.W. Ong, X.-A. Zhao, Y.M. Ng, K.F. Chan, Y.C. Tsang, C.L. Choy
and P.W. Chan
'Structural and mechanical properties of $(B_{0.5-X}Si_X)\ N_{0.5}$ films synthesized by dual-ion-beam deposited'
Appl. Phys. Lett., 69 (1996) 3501.

X.-A. Zhao, C.W. Ong, K.F. Chan, Y.M. Ng, Y.C. Tsang, C.L. Choy
and P.W. Chan
'Physical properties of dual ion beam deposited $(B_{0.5-X}Si_X)\ N_{0.5}$ films'
J. Vac. Sci. Technol. A, 15 (1997) 2297.

C.W. Ong, X.-A. Zhao, K.F. Chan, Y.M. Ng, C.L. Choy, P.W. Chan
and R.W.M. Kowk
'Effects of the carbon incorporation on the structure and mechanical properties of cubic boron nitride films'
Thin Solid Films 307 (1997) 152-155.

X.-A. Zhao, C.W. Ong, Y.M. Ng, K.F. Chan, C.L. Choy, P.W. Chan
and R.W.M. Kowk
'Structure of ion-beam deposited B-C-N-O films and the role of oxygen'
J. Mater. Sci. Lett. 16 (1997) 1910-1913.

Y.M. Ng, C.W. Ong, X.-A. Zhao and C.L. Choy
'Evidence of the diamondlike-to-polymeric transition for ion beam deposited CN_x films with increasing N content'
(preparing)

References

1. B. Bhushan, *Tribology and Mechanics of Magnetic Storage Devices* (1990)

2. B. Bhushan, *Handbook of Mico/Nano Tribology* (1995).

3. B. Bhushan and V.N. Koinkar, *Surf. Coat. Technol.*, 76/77 (1995) 655.

4. A.Y. Liu and M.L. Cohen, *Science, 245* (1981) 841.

5. D. Marton, K.J. Boyd, A.H. Al-Bayati, S.S. Todorov and J.W. Rabalais, *Phys. Rev. Lett., 73* (1994) 118.

6. D. Marton, A.H. Al-Bayati, S.S. Todorov, K.J. Boyd and J.W. Rabalais, *Nucl. Instrum. Methods B, 90* (1994) 277.

7. H.W. Song, F.Z. Cui, X.M. He, W.Z. Li and H.D. Li, *J. Phys.: Condens. Matter, 6* (1994) 6125.

8. X.-A. Zhao, C.W. Ong, Y.C. Tsang, Y.W. Wong, P.W. Chan and C.L. Choy, *Appl. Phys. Lett., 66* (1995) 2652.

9. Z.M. Ren, Y.C. Du, Z.F. Ying, Y.X. Qui, X.X. Xiong, J.D. Wu and F.M. Li, *Appl. Phys. Lett., 65* (1994) 1361.

10. Z.M. Ren, Y.C. Du, Y.X. Qui, J.D. Wu, Z.F. Ying, X.X. Xiong and F.M. Li, *Phys. Rev. B, 51* (1995) 5274.

11. C. Niu, Y.Z. Lu and C.M. Lieber, *Science, 261* (1993) 334.

12. S. Kumar and T.L. Tansley, *J. Appl. Phys., 76* (1994) 4390.

13. K.M. Yu, M.L. Cohen, E.E. Haller, W.L. Hansen, A.Y. Liu and I.C. Wu, *Phys. Rev. B, 49* (1994) 5034.

14. N. Nakayama, Y. Tsuchiya, S. Tamada, K. Kosuge, S. Nagata, K. Takahiro and S. Yamaguchi, *Jpn. J. Appl. Phys., 32* (1993) L1465.

15. J.H. Kaufman, S. Metin and D.D. Saperstein, *Phys. Rev. B, 39* (1989) 13053.

16. A. Bousetta, M. Lu, A. Bensaoula and A. Schultz, *Appl. Phys. Lett., 65* (1994) 696.

17. Z.J. Zhang, S. Fan, J. Huang and C.M. Lieber, *Appl. Phys. Lett., 68* (1996) 2639.

18. G. Wang, J.M. Silversten, J.H. Judy and G.L. Chen, *J. Appl. Phys., 79* (1996) 5782.

19. E.C. Cutiongco, D. Li, Y.W. Chung and C.S. Bhatia, *J. Tribol., 118* (1996) 543.

20. P. Hammer, M.A. Baker, C. Lenardi and W. Gissler, *J. Vac. Sci. Technol. A, 15* (1997) 107.

21. D. Li, E. Cutiongco, Y.W. Chung, M.S. Wong and W.D. Sproul, *Surf. Coat. Technol., 68/69*, (1994) 611.

22. P. Hammer, M.A. Baker, C. Lenardi and W. Gissler, *Thin Solid Films, 290/291* (1996) 107.

23. F.L. Freire Jr., G. Mariotto, C.A. Achete and D.F. Franceschini, *Surf. Coat. Technol., 74/75* (1995) 382.

24. E.H.A. Dekempeneer, J. Meneve, J. Smeets, S. Kuypers, L. Eersels and R. Jacobs, *Surf. Coat. Technol., 68/69*, 621 (1994).

25. F.-R. Weber and H. Oechsner, *Surf. Coat. Technol., 74/75* (1995) 704 .

26. B.W. Cook, and K. Jones, *A programmed introduction to infrared spectroscopy,* (1972) 57.

27. G. Socrates, *Infrared characteristic group frequencies,* (1994) 1-2.

28. H.-C. Tsai and D.B. Bogy, *J. Vac. Sci. Technol. A, 5* (1987) 3287

29. W. C. Oliver and G. M. Pharr, *J. Mater. Res., 7,* (1992) 1564.

30. W. C. Oliver, C. J. McHARGUE and S. J. Zinkle. *Thin Solid Films, 153* (1987) 185-196.

31. G. M. Pharr and W. C. Oliver, *Mrs Bulletin*, (1992) 33.

32. M.F. Doerner and W.D. Nix *J. Mater. Res., 1* (1986), 601.

33. M.O. Watanable, S. Itoh, K. Mitzushima and T. Sasski, *Appl. Phys. Lett., 68* (1996) 2962.

34. F. Fujimoto and K. Ogata, *Jpn. J. Appl. Phys., 32* (1993) 420.

35. G. Johansson, J. Hedman, A. Berndtson, M.Klasson, and R. Nilsson, *J. Electron Spectrosc. Relat. Phenom., 2* (1973) 295.

36. S. Kumar and T. L. Tansley, *Solid State Commun., 88* (1993) 803.

37. T. Mori and Y. Namba, *J. Appl. Phys., 55* (1984) 3276.

38. X.-A. Zhao, C.W. Ong, Y.C. Tsang, C.L. Choy and P.W. Chan, *J.Vac. Sci Technol A, 15* (1997) 99.

39. M. Barber, J.A. Connor, M.F. Guest, I.H. Hiller, M. Schwarz and M.Stacey, *J. Chem Soc. Faraday Trans. II, 69* (1973) 551.

40. B.J. Lindberg and J. Hedman, *Chem. Scr., 7* (1975) 155.

41. R. Larsson and B. Folkesson, *Chem Scr., 9* (1976) 148.

42. P. Brand and R.D. Feltham, *J. Organometal. Chem., C35* (1976) 120.

43. A. Khurshudov, K. Kato and S. Daisuke, *J. Vac. Sci. Technol. A, 14* (1996) 2935.

44. R.J. Nemanich and S.A. Solin, *Phys. Rev. B, 20* (1979) 392.

45. H.C. Hofsäss, C. Ronning, U. Griesmeier and M. Gross, *Mater. Res. Soc. Symp. Pro., 354* (1995) 93.

46. C.W. Ong, X.-A. Zhao, J.T. Cheung, S.K. Lam, Y. Liu, C.L. Choy and P.W. Chan, *Thin Solid Films, 258* (1995) 34.

47. G. Socrates, *Infrared characteristic group frequencies*, (1994) 61.

48. H.X. Han and B.J. Feldman, *Solid State Commun., 65* (1988) 921.

49. K.-R. Lee, K. Y. Eun and J.-S. Rhee, *Mat. Res. Soc. Symp., 356* (1995) 223.

50. J. Schwan, W. Doworschak, K. Jung and H. Ehrhardt, *Diamond Relat. Mater., 3* (1990) 10727.

51. J. Tauc, *Amorphous and Liquid Semiconductors,* (1974) 159.

52. X. Wang, P.J. Martin and T.J. Kinder, *Thin Solid Films, 256* (1995) 148.

53. E.C. Cutiongco, D. Li, Y.-W. Chung and S.C. Bhatia, *American Society of Mechanical Engineers (Paper) ASME, New York, NY, USA, 6* (1995) 95.

54. T.Y. Tsui, G.M. Pharr, W.C. Oliver, Y.W. Chung, *Mat. Res. Soc. Symop. Proc.,356* (1995) 767.

55. R.L. White, S.S Bhatia, M.C Friedenberg, *Tribology of Contact/Near-Contact Recording for Ultra High Density Magnetic Storage American Society of Mechanical Engineers, Tribology Division,. ASME, New York, NY, USA, 6* (1996) 33.

56. H. Sjöström, I. Ivanov, M. Johansson, , L. Hultman, J.-E. Sunggren, S.V. Hainsworth, T.F. Page, and L.R. Wallenberg, *Thin Solid Films, 246* (1994) 103.

57. P. Zou, Scherge, Matthias, Lambeth and N. David, *IEEE Transactions on Magnetics, 31* (1995) 2985.

58. A. Khurshudov, K. Kato and S. Daisuke, *J.Vac. Sci. Technol. A,14* (1996) 2935.

59. N. Axen, G.A. Botton, H.Q. Lou, R.E. Somekh, and I.M. Hutchings, Surf. Coat. Technol. 81, No. 2-3, pp. 262-268, Jun (1996).

60. M.E. O'Hern, R.H. Parrish, and W.C. Oliver,*Thin Solid Films, 181* (1989) 357.

61. M. Lu, A. Bousetta, R. Sukach, A. Bensaoula, K. Walters, K. Eipers-Smith and A. Schultz, *Appl. Phys. Lett. 64* (1994) 1514.

62. J.C. Angrus and C.C. Hayman, *Science, 241* (1988) 931.

63. D.R. McKenzie, W.D. McFall, W.G. Sainty, C.A. Davis and R.E. Collins, *Diamond Relat. Mater., 2* (1993) 970.

64. I. Endler, A. Leonhardt, M. Schönherr and E. Wolf, *J. Mater. Sic. 26* (1991) 782.

65. L. Maya and L.A. Harris, *J. Am. Ceram. Soc., 73* (1990) 1912.

66. K. Montasser, S. Hattori and S. Mortia, *J. Appl. Phys., 58* (1985) 3185.

67. F. Saugnac, F. Teyssandier and A. Marchand, J. *Am. Ceram. Soc., 75* (1992) 161.

68. V.I. Nefedov, D. Gati,B.F. Dzhurinskii, N.P. Sergushin, Y.V. Salyn, *Zh. Neorg. Khim., 20* (1975) 2307.

69. B.K. Gupta and B. Bhushan, *Thin Solid Film, 270* (1995) 398.

70. R. Riedel,
Av. Mater., 6 (1994) 549.